



**Titre:** Foundations of plasma enhanced chemical vapor deposition of functional coatings

**Auteurs:** R. Snyders, D. Hegemann, D. Thiry, O. Zabeida, Jolanta-Ewa Sapieha, & Ludvik Martinu

**Date:** 2023

**Type:** Article de revue / Article

**Référence:** Snyders, R., Hegemann, D., Thiry, D., Zabeida, O., Sapieha, J.-E., & Martinu, L. (2023). Foundations of plasma enhanced chemical vapor deposition of functional coatings. Plasma Sources Science and Technology, 32(7), 36 pages.  
Citation: <https://doi.org/10.1088/1361-6595/acdabc>

 **Document en libre accès dans PolyPublie**  
Open Access document in PolyPublie

**URL de PolyPublie:** <https://publications.polymtl.ca/54798/>  
PolyPublie URL:

**Version:** Révisé par les pairs / Refereed

**Conditions d'utilisation:** CC BY  
Terms of Use:

 **Document publié chez l'éditeur officiel**  
Document issued by the official publisher

**Titre de la revue:** Plasma Sources Science and Technology (vol. 32, no. 7)  
Journal Title:

**Maison d'édition:** IOP Publishing Ltd  
Publisher:

**URL officiel:** <https://doi.org/10.1088/1361-6595/acdabc>  
Official URL:

**Mention légale:** Original content from this work may be used under the terms of the Creative Commons Attribution 4.0 licence. Any further distribution of this work must maintain attribution to the author(s) and the title of the work, journal citation and DOI.  
Legal notice:

PAPER • OPEN ACCESS

## Foundations of plasma enhanced chemical vapor deposition of functional coatings

To cite this article: R Snyders *et al* 2023 *Plasma Sources Sci. Technol.* **32** 074001

View the [article online](#) for updates and enhancements.

You may also like

- [Plasma diagnostic approach for high rate nanocrystalline Si synthesis in RF/UHF hybrid plasmas using a PECVD process](#)  
B B Sahu, Jeon G Han, Kyung S Shin et al.
- [Experimental and theoretical analysis of tool life between plasma enhanced CVD and PVD multilayer nanocoated cutting tools](#)  
Y Carlin Calaph, K Manikanda Subramanian, P Michael Joseph Stalin et al.
- [Highly efficient shrinkage of inverted-pyramid silicon nanopores by plasma-enhanced chemical vapor deposition technology](#)  
Yifan Wang, Tao Deng, Qi Chen et al.



# Analysis Solutions for your Plasma Research

- Knowledge
- Experience ■ Expertise

[Click to view our product catalogue](#)

Contact Hiden Analytical for further details:  
[www.HidenAnalytical.com](http://www.HidenAnalytical.com)  
[info@hiden.co.uk](mailto:info@hiden.co.uk)



### Surface Science

- ▶ Surface Analysis
- ▶ SIMS



### Surface Science

- ▶ 3D depth Profiling
- ▶ Nanometre depth resolution



### Plasma Diagnostics






- ▶ Plasma characterisation
- ▶ Customised systems to suit plasma Configuration



### Plasma Diagnostics

- ▶ Mass and energy analysis of plasma ions
- ▶ Characterisation of neutrals and radicals

# Foundations of plasma enhanced chemical vapor deposition of functional coatings

R Snyders<sup>1,2,\*</sup> , D Hegemann<sup>3</sup> , D Thiry<sup>1</sup>, O Zabeida<sup>4</sup> , J Klemberg-Sapieha<sup>4</sup>   
and L Martinu<sup>4</sup> 

<sup>1</sup> Plasma-Surface Interaction Chemistry (ChIPS), Materials Institute, University of Mons, 23 Place du Parc, Mons, 7000, Belgium

<sup>2</sup> Materia Nova Research Center, Parc Initialis, 7000 Mons, Belgium

<sup>3</sup> Plasma & Coating Group, Empa—Swiss Federal Laboratories for Materials Science and Technology, Lerchenfeldstrasse 5, 9014 St. Gallen, Switzerland

<sup>4</sup> Department of Engineering Physics, Polytechnique Montreal, Montreal, QC H3T 1J4, Canada

E-mail: [Rony.SNYDERS@umons.ac.be](mailto:Rony.SNYDERS@umons.ac.be)

Received 25 November 2022, revised 27 March 2023

Accepted for publication 1 June 2023

Published 6 July 2023



CrossMark

## Abstract

Since decades, the PECVD ('plasma enhanced chemical vapor deposition') processes have emerged as one of the most convenient and versatile approaches to synthesize either organic or inorganic thin films on many types of substrates, including complex shapes. As a consequence, PECVD is today utilized in many fields of application ranging from microelectronic circuit fabrication to optics/photonics, biotechnology, energy, smart textiles, and many others. Nevertheless, owing to the complexity of the process including numerous gas phase and surface reactions, the fabrication of tailor-made materials for a given application is still a major challenge in the field making it obvious that mastery of the technique can only be achieved through the fundamental understanding of the chemical and physical phenomena involved in the film formation. In this context, the aim of this foundation paper is to share with the readers our perception and understanding of the basic principles behind the formation of PECVD layers considering the co-existence of different reaction pathways that can be tailored by controlling the energy dissipated in the gas phase and/or at the growing surface. We demonstrate that the key parameters controlling the functional properties of the PECVD films are similar whether they are inorganic- or organic-like (plasma polymers) in nature, thus supporting a unified description of the PECVD process. Several concrete examples of the gas phase processes and the film behavior illustrate our vision. To complete the document, we also discuss the present and future trends in the development of the PECVD processes and provide examples of important industrial applications using this powerful and versatile technology.

**Keywords:** plasma enhanced chemical vapor deposition, plasma polymerization, plasma diagnostics, thin films, energy per molecule, energy per deposited particle, mechanical and other functional properties

(Some figures may appear in colour only in the online journal)

\* Author to whom any correspondence should be addressed.



Original content from this work may be used under the terms of the [Creative Commons Attribution 4.0 licence](https://creativecommons.org/licenses/by/4.0/). Any further distribution of this work must maintain attribution to the author(s) and the title of the work, journal citation and DOI.

## 1. Introduction and scope of the paper

In the modern world, the utilization of thin films and coatings has become essential for a multitude of applications in various technological domains ranging from microelectronics, solar cells, and wearable electronics to optics/photonics, biotechnologies, manufacturing, aerospace, energy, textiles, and many others. Among the plethora of techniques developed for assuring the increasingly demanding characteristics and functions of high-quality thin films, plasma- and vapor-based technologies appear to be amongst the most convenient and suitable approaches. Film fabrication methods encompass numerous processes that are often classified as physical vapor deposition (PVD) or chemical vapor deposition (CVD), depending on the physical/solid or chemical/gas-vapor nature of the initial source material. For both families of processes, a plasma can be added to the process, allowing one to initiate and propagate the reactions and control the microstructure and composition of the deposited films. By adding plasma to the conventional deposition processes allows for several key advantages. The most important ones are as follows: (i) the process temperature can be significantly lowered enabling a reduction of the energy cost and the treatment of a wide range of materials including polymers, (ii) solvents are avoided making these processes more environmentally friendly, and (iii) specific features of the plasma allows for the deposition of materials that could not be synthesized by conventional methods. All these attractive properties justify the popularity gained by plasma technologies and their important development in numerous industrial fields such as automotive, aeronautics and microelectronics. Even if these industrial applications are already very well advanced, there are still numerous industrial sectors that could benefit from plasma technologies (energy, biomedical, chemistry, textile...). Until now, a frequent limitation for the acceptance has been a certain reluctance of industries to invest into technologies that would strongly impact their actual processes. Nevertheless, because of the global energy crisis and of the climate-related issues that strongly push toward the electrification of the industrial process, it is almost sure that these barriers would disappear.

In this paper, we specifically focus on plasma enhanced chemical vapor deposition (PECVD) technologies. The PECVD processes can further be categorized depending on the nature of the resulting coating. When depositing inorganic materials, one mostly refers to the ‘PECVD process’, while when considering the deposition of organic material, the community frequently refers to the so-called ‘plasma polymerization (PP)’ process. As long as only vapor deposition processes are considered, the two terms are often used as synonyms. The PVD film fabrication techniques are very complementary and they also use plasmas and plasma-surface interactions, while the source material originates from a solid state and enters the gas phase by approaches such as magnetron sputtering and arc, thermal, and e-beam evaporation in the presence of inert or reactive gases. The PVD processes are, however, out of the scope of this paper and the reader is referred to references such as [1] as well as other complementary ‘foundations papers’ [2, 3].

The present foundation paper aims at presenting and describing the basic knowledge associated with fundamental mechanisms responsible for the film growth and evolution of the microstructure when using the PECVD processes including PP. Specifically, we focus on the description of the main gas-phase processes and related plasma-surface interactions, their advantages and limitations. We share our view on a variety of promising scientific and technological approaches that have been developed to overcome these limitations and that can provide enhanced film and coating performances. Our goal is to reveal a practical foundation for the scientifically substantiated understanding of the PECVD processes that would help to make judicious choices for specific applications; as such, this review addresses both experienced colleagues as well as ‘newcomers’.

In section 2, after a short history of the field, we first describe the fundamental physics and chemistry behind the PECVD processes and the most common plasma sources that have been developed. This part specifically focuses on the various PECVD-related effects in the gas phase concerning the interactions of electrons with the atoms and molecules, and the transport of molecular fragments toward the surface, resulting in film deposition. From the fundamental perspective, we show that the concepts and physical mechanisms behind the growth of thin films in PECVD are very similar whenever the plasma-assisted synthesis of plasma polymerized organic or inorganic materials is considered.

Although presenting many common features in terms of basic mechanisms, the two families of PECVD processes also reveal important specificities. Therefore, sections 3 and 4 are dedicated to the processes applied to the synthesis of organic or polymer-like (section 3) and inorganic (section 4) materials, while keeping in mind very close relationships; in fact, we point to new developments such as the hybrid (organic/inorganic) films and coatings (section 5).

Section 3 addresses the PP process which is defined as a PECVD process generating organic/polymer-like coatings obtained at a relatively low-energy impact on the growing film. Although plasma polymer films (PPFs) have been known and applied for decades, better control of their properties (chemical composition, stability, surface energy, retention of the initial molecular nature, etc...) is still necessary to facilitate their further implementation in practical day-to-day applications. Two complementary approaches addressing the associated challenges are described. The first one can be seen as the natural evolution of the early works on the topic (Yasuda’s work) that can be considered as a macroscopic analysis of the process. This is based on the correlation between the process conditions and the output such as the film growth rate, as well as chemical and physical features of the deposited PPFs through the utilization of a single process parameter, namely the plasma-induced ‘energy input per monomer molecule— $E_{pl}$ ’ in the gas phase. In fact,  $E_{pl}$  resumes the effect of several major process variables such as the flow, pressure, power density, ...; as such, this approach thus considers plasma chemical processes initiated in the gas volume.

The second approach provides a journey within the intimacy of the plasma by implementing a thorough diagnostics of

the plasma phase to identify the film-forming species (neutral and ionic) and to measure their flux and energy delivered to the surface. This information can ultimately allow one to unravel the different contributions to the ‘deposited energy per arriving film-forming particle— $E_p$ ’ that is the key parameter in the considered process. Both  $E_{pl}$  and  $E_p$  thus represent the energy input by the plasma to the gas phase and surface processes, respectively, enabling the control of the highly non-equilibrium plasma conditions, and control of the film growth and evolution of its microstructure. These sets of data are used to better understand the fundamental mechanisms occurring at the plasma-growing film interface.

The aspect of energy dissipation during film deposition becomes particularly important when PECVD is applied to the growth of inorganic materials (section 4). We specifically focus on the variable allowing one to control the plasma-surface interactions in terms of the energy and flux of different species to the surface, including free radicals and mainly ions. We underline that the film microstructure and hence the film properties significantly depend on the key parameter,  $E_p$ , and we describe the methods of how to quantitatively assess it. Different plasma systems and plasma source configurations are discussed that allow one to tune  $E_p$  to obtain desirable coating performance; this includes different reactor geometries, plasma excitation frequency, plasma pulsing, substrate biasing strategies, etc. These approaches are illustrated by specific examples of the synthesis of inorganic functional films and systems including optical coatings, hard protective coatings, tribological coatings, barrier coatings, and coatings on flat and curved substrates, the latter one considering highly curved convex and concave surfaces and particulates.

Finally, the last part of the paper (section 5) addresses present and future perspectives related to the PECVD technologies. Specifically, we briefly describe the new trends including more recent techniques such as ion beam enhanced chemical vapor deposition (applied, for example, for the synthesis of hybrid organic-inorganic films), plasma enhanced atomic layer deposition (PE-ALD) and PECVD at atmospheric pressure (AP), and the current state, challenges, and opportunities associated with industrial applications of the PECVD processes.

## 2. PECVD

### 2.1. History of PECVD at a glance

Even if the first observations have been reported during the 18th century, it can be considered that CVD began to be developed in the late 1800s in the context of improving light bulb filaments by coating them with carbon or nickel [4, 5]. Following these pioneering works, CVD has penetrated the industry with applications in the tool and later (thanks to the development of low pressure processes), in the semiconductor industry. In parallel, CVD processes assisted by plasma, called in the early times ‘glow discharge deposition’ or ‘plasma deposition’, have been developed to reduce the process temperature thanks to the activation of the precursor by the plasma phase. Today, these deposition processes are known as PECVD or plasma-assisted chemical vapor deposition.

Already in 1911, the PECVD of diamond crystal from acetylene in the presence of Hg vapors has been reported [6–8], followed by the observation of amorphous carbon-based films on the walls of discharge reactors containing hydrocarbon molecules [9–11] or by the first depositions of diamond-like carbon (DLC) in 1953 [12, 13]. In the subsequent decades, the PECVD processes have started to be studied in detail allowing one to better understand the growth mechanisms of technologically important compounds such as silicon and silicon oxide from silane discharges [14]. Between the second half of the 60s and the early 70s, major technological improvements to the process have been implemented. On the one hand, the development of an RF (radio-frequency)-driven parallel-plate PECVD reactor enabled further reduction of the process temperature [15–18] and made it possible to synthesize optical coatings [19]. On the other hand, by strongly decreasing the process pressure (i.e. 1–5 Pa) and by simultaneously applying a negative bias to the substrate, Mattox invented the ‘ion plating’ process [20] used to grow metallic and carbide films. In the nineties, pulsed plasma sources (DC and bipolar) began to be used in PECVD processes allowing for even higher flexibility and control of the process [21].

When specifically considering the PECVD of organic-like coatings or PPFs, the first observations of solid deposits from organic compounds were reported at the end of the 18th century [22]. At that time, they were considered a nuisance until it has been shown that a 1  $\mu\text{m}$  thick plasma-polymerized styrene film made a satisfactory dielectric for a nuclear battery [23]. Initially and for decades afterward, PPFs have been studied as pinhole-free physical barriers with applications in the field of corrosion protection [24, 25] and food packaging [26, 27], since the dry, vacuum-based deposition avoids entrapment of moisture, air, solvents or other fluids as often observed in paints and wet-chemical coatings [28]. Nevertheless, since the 1980s, PP has been further developed in the search for PPFs with controlled and tailored chemistry for hi-tech applications, particularly in the biomedical field such as for the development of platforms for biomolecules immobilization [29–36] or cell growth [37–39], or antibacterial [40, 41], or controlled drug release coatings [42–45].

### 2.2. Basic principles

Considering the PECVD process, the first step of the synthesis for either organic or inorganic thin film material requires the vaporization of a molecule named precursor (or monomer) in a deposition reactor where a plasma is ignited. Based on the variability and the role of the initial gas-phase processes and plasma-surface interactions (involving atoms and molecular fragments—radicals, ions, and energetic photons), materials processing using ‘cold’ (thermodynamically non-equilibrium) plasma can be divided into three categories, according to the choice of the working gases or vapors and the discharge conditions [46]:

- (i) The PECVD of inorganic (such as oxides, nitrides, and carbides of metals or semiconductors, DLC films) or organic thin films (such as soft materials, PPFs, and



others). Here, it is useful to specify our understanding of what are ‘organic’ and ‘inorganic’ thin film material. As generally accepted, the PECVD community considers that organic compounds comprise a main chain formed by carbon atoms containing other atoms such as hydrogen, oxygen or nitrogen. Due to densification and  $sp^3$  hybridization during film growth, DLC thin films lost their organic character and are most of the time considered as inorganic materials. For both inorganic or organic material PECVD synthesis, during deposition, the bulk plasma parameters generally control the rate at which chemically active precursor species (molecular fragments—free radicals) and energetic species (electrons, ions, photons) are created. In combination with the selected gases, gas-phase chemical processes are largely responsible for the chemical composition of the deposited films, along with plasma-surface interactions and substrate surface conditions, which control film microstructure and surface morphology.

- (ii) Plasma etching or chemical etching (dry removal of materials), forming volatile products resulting from the chemical reactions of the plasma-generated free radicals and surface atoms, which are frequently ablated with additional ion bombardment assistance—e.g. see [47, 48].
- (iii) Surface modification, during which material is neither added nor removed in significant amounts, but the composition and structure of the surface and/or of the near-surface region are modified by plasma exposure allowing one to ‘engineer’ the surface and interface properties (improve adhesion, control roughness, wettability, biocompatibility, sterility, dye uptake, and other forms of activation)—e.g. see [3, 47, 49–51].

Frequently, the above mentioned processes are in competition, and the prevalence of one of them can be controllably adjusted by the choice of the external plasma parameters such as in a system schematically illustrated in figure 1.

Despite the proliferation of low-pressure plasma processes already in use, and having potential for numerous industrial applications, there is still much ongoing research regarding the most efficient use of plasma and this is especially true for the PECVD processes for which the plasma chemistry is often more complex than for PVD processes [2]. The reasons are the relative novelty of plasma processing in certain sectors of application and its inherent complexity. To ensure high quality, reproducibility, and reliability of a given plasma process, numerous parameters must be controlled (figure 1): this includes ‘external’ parameters set by the operator such as pressure,  $p$ , gas flow,  $F$ , discharge excitation frequency,  $f$ , and power,  $W$ , and the resulting ‘internal’ (bulk) plasma characteristics, particularly the electron (plasma) density,  $n_e$ , and the electron energy distribution function,  $f_e(E)$  or EEDF, as well as the fluxes of depositing species.

In a confined plasma, the electrons tend to leave the plasma readily due to their low mass and high mobility. This effect results in the formation of sheaths separating the quasi-neutral plasma from surfaces accompanied by a potential difference

to reach an equilibrium where the ion and electron losses to the confining surfaces balance each other. Hence, energy need to be delivered for ionization processes to sustain the plasma. Since the threshold energy for ionization is in the order of 10 eV, i.e. higher than the threshold for excitation and dissociation, the plasma is a highly energetic medium able to break any chemical bond. External electric (or electromagnetic) energy is provided via collisions to ‘hot’ electrons gaining mean energies according to an equivalent temperature,  $T_e$ , in the order of eV, whereas the heavy gas particles, including ions, can remain ‘cold’ as long as thermalization is avoided as affected by pressure and residence time in the plasma zone. The resulting non-equilibrium conditions enable plasma-chemical activation in the gas phase as well as energetic plasma-surface interactions, still able to treat temperature-sensitive materials.

Furthermore, a wide range of monomers (or precursors) can be ‘polymerized’ via formation of radicals in the plasma including saturated and unsaturated hydrocarbons, fluorocarbons, silanes, siloxanes, hydrocarbons containing further elements such as O, N, S, B, P, Cl, and metals (organometallics that can even be converted to inorganic coatings) as well as mixtures with various non-polymerizing gases—many compounds that would conventionally not polymerize. As a further consequence, specific to the PP process, the PPF does not polymerize in a regular way but forms highly branched and crosslinked deposits with a wide range of chemical compositions. As a consequence, appropriate control at the nano-scale enables unprecedented thin film properties ranging from polymer-like to multifunctional to hard coatings. The related high complexity of the involved process steps, however, complicates a detailed understanding of PP. Some of the underlying principles are thus rather discussed by introducing a ‘global model’. These principles are also valid when considering the synthesis of inorganic materials by PECVD.

Considering plasma activation of the precursor in the gas phase producing film-forming species of density,  $n_{\text{dep}}$ , via electron impact with a lumped rate coefficient,  $k_a$ , depending on  $T_e$ , a simple reaction rate can be written as

$$\frac{dn_{\text{dep}}}{dt} = n_e n_m k_a(T_e) \quad (1)$$

with electron density,  $n_e$ , and monomer density,  $n_m$  [52]. Here, the rate coefficient covers the full plasma-chemical reaction pathway [53]. This reaction pathway is most of the time unknown but can be, at least partly, evaluated by implementing detailed plasma diagnostics [54]. Activation occurs during the residence time of the precursor in the active gas phase (including the plasma and post-discharge regions),  $\tau_{\text{act}}$ , yielding the plasma-induced conversion of monomer into film-forming species:

$$c_a = \frac{\tau_{\text{act}}}{n_m} \frac{dn_{\text{dep}}}{dt} = \tau_{\text{act}} n_e k_a(T_e) \quad (2)$$

with  $c_a$  the conversion rate of the monomer into film-forming species. Microscopically, the gas phase processes are thus governed by the EEDF and the residence time in the plasma.

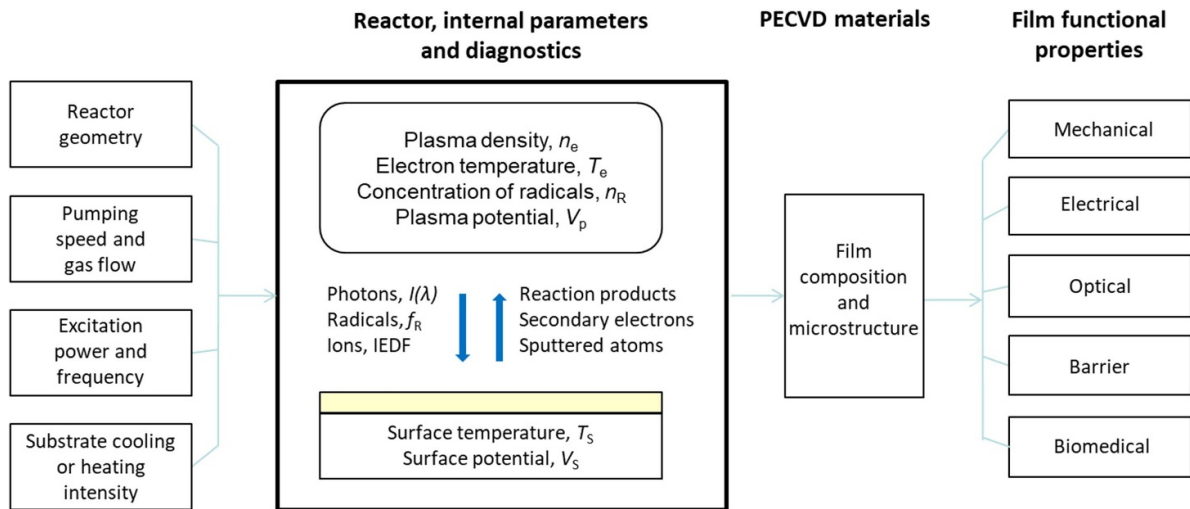


**Figure 1.** Schematic illustration of a deposition system and the relation between the internal and external process parameters, and the film characteristics. Reprinted from [46], Copyright (2010), with permission from Elsevier.

Furthermore, the flux of film-forming species,  $\Gamma_{\text{dep}}$ , as produced in the active plasma zone of volume  $V_{\text{pl}}$ , and contributing to deposition in the area  $A_{\text{dep}}$ , surrounding the plasma (figure 2), is given by

$$\Gamma_{\text{dep}} = \frac{V_{\text{pl}}}{A_{\text{dep}}} \frac{dn_{\text{dep}}}{dt} = \frac{V_{\text{pl}}}{A_{\text{dep}}} \frac{n_m}{\tau_{\text{act}}} c_a. \quad (3)$$

Considering that  $\tau_{\text{act}}$  is related to the monomer gas flow rate,  $F_m$ , by

$$\tau_{\text{act}} = n_m \frac{V_{\text{pl}}}{F_m} \frac{kT_0}{p_0}, \quad (4)$$

it follows that

$$\Gamma_{\text{dep}} = \frac{F_m}{A_{\text{dep}}} \frac{p_0}{kT_0} c_a \quad (5)$$

with Boltzmann constant,  $k$ , pressure,  $p_0$ , and temperature,  $T_0$ , both at standard conditions (101 325 Pa, 0 °C).

Aside from the highly reactive film-forming species, unreacted or low reactive (excited) species, stable side products, photons, and electrons as well as positively charged ions are leaving the active plasma zone. The latter ones are accelerated by the sheath voltage,  $V_{\text{sh}}$ , gaining the kinetic energy,  $E_i$ , and arriving with the flux,  $\Gamma_i$ , at the surface (depending on the Bohm criterion [58]). As can be seen in figure 2(d), Ar allows higher  $E_i$  and  $\Gamma_i$  mainly due to a larger mean free path length, whereas  $\text{C}_2\text{H}_x^+$  ions have the largest cross-section and undergo charge-exchange collisions. Furthermore, the pressure-dependent expansion of the plasma zones (sheath and presheath) contributes to collisions. Dilution in a non-polymerizing (non-deposition) gas such as Ar (but also  $\text{H}_2$  or  $\text{O}_2$  and  $\text{N}_2$  for inorganic coatings) can thus help to increase the energy flux. Despite low ionization degrees in the considered low-temperature plasmas, the accelerated ions also drag the neutral species toward the surface by elastic and charge-exchange collisions, even at AP (ionic wind) [59]. The

provided energy supports film formation by inducing surface diffusion, radical sites, crosslinking, and densification, but it can also result in ablation and re-sputtering depending on the deposited (kinetic) energy per deposited atom/molecule (in eV), here defined as:

$$E_d = \frac{E_i \Gamma_i}{s \Gamma_{\text{dep}}}. \quad (6)$$

$E_d$  is equivalent to  $E_p$  but is defined by the flux of deposited species (according to the global model) that arrive at the surface rather than those that stay at it. Therefore, the parameter ‘ $s$ ’ is introduced in equation (6). For predominant deposition processes,  $s$  represents the sticking probability and the denominator is proportional to the deposition rate (deposited species per area and time) [58]. Note that this formula should be considered with care since ion implantation and forward sputtering might also occur at high  $E_i$  [60]. Moreover, when ablation processes noticeably reduce the deposition rate, the affected near-surface volume during the film growth needs to be considered for the total surface loss probability. At low energies,  $s$  may depend on  $E_d$ , when the formation of radical sites determines the thin film deposition [61]. For PP, this situation is described by the ion activated growth model (AGM, see section 3.1 for more details), known as plasma-induced polymerization—in contrast to plasma-state polymerization dominated by activation of the monomer in the gas phase yielding highly reactive species that polymerize at a surface [62]. Note that  $s$  also depends on substrate temperature,  $T_s$ , as well as on the nature and state of the substrate regarding initial growth conditions. Either way, surface processes can be controlled by knowing  $E_d$  and  $T_s$ , which in turn requires the use of plasma diagnostics. In general, to use PP as a high precision surface modification tool, both gas phase and surface processes need to be controlled. In this way, hard coatings, e.g. DLC, have been optimized (selection of hydrocarbon gas, the addition of hydrogen, and adjustment of  $E_d$ ) but also functional plasma polymers regarding the degree of

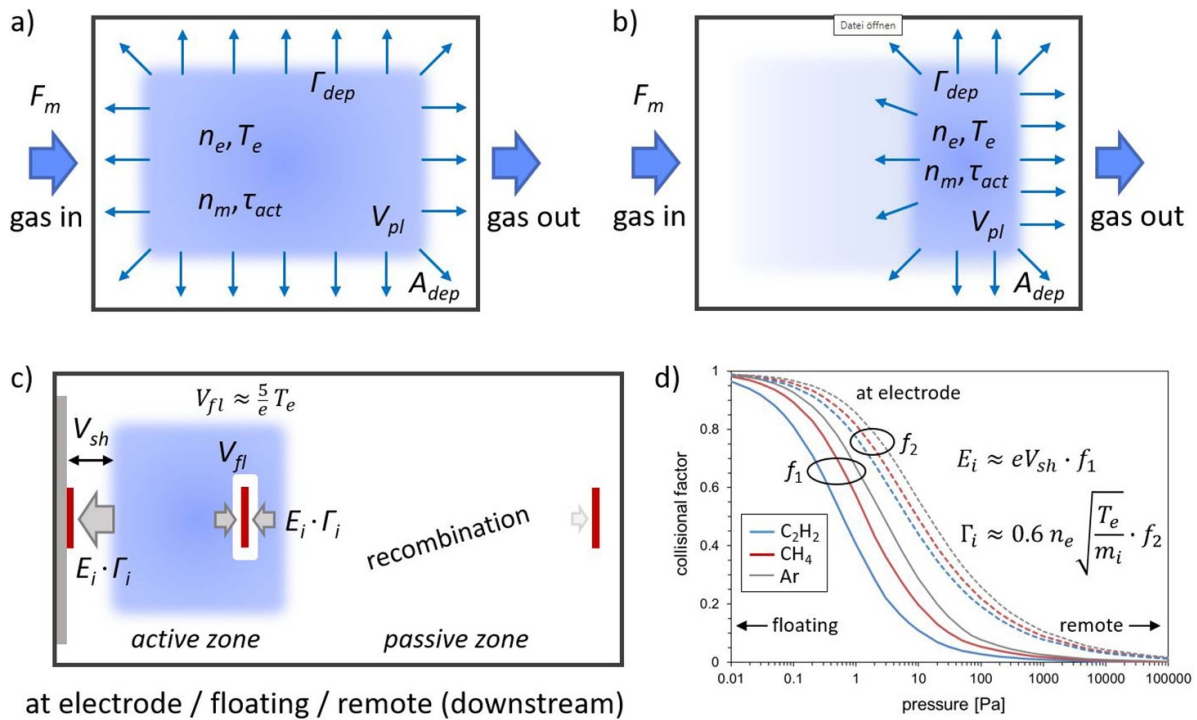


**Figure 2.** Schematic representation of conditions in a plasma reactor used for the global model: (a) symmetric plasma yielding a uniform flux of film-forming species to the walls, (b) asymmetric plasma with concentrated flux to one wall, (c) substrate positions exposed to different energy fluxes, and (d) collisions in the sheath (curves  $f_1$ ) and in the plasma (curves  $f_2$ ) that reduce the energy flux to the electrode, exemplarily shown for  $C_2H_x^+$ ,  $CH_x^+$ , and  $Ar^+$  ions in their parent gas. Data extracted from [55–57].

functionality and crosslinking [56, 63, 64]. The importance of the deposited energy for film microstructure and film properties is further discussed in section 4.1.

### 2.3. Which plasma for which process?

Among other parameters (pressure, power input, precursor flow, ...), an important factor influencing the processing plasma is the discharge electric field frequency,  $f = \omega/2\pi$ . Most often, high frequency plasmas ( $f > 1$  MHz) are used for PECVD processes (including PP), to avoid surface charging and plasma instabilities. These are, generally, the ITU (International Telecommunications Union) approved industrial, scientific, and medical frequencies (most frequently, 13.56 MHz—RF, or 2.45 GHz—microwave, MW). The choice of  $f$  also defines the type and construction of the PECVD reactor—see figure 3.

Plasma deposition equipment usually consists of several modules or functions: its main part is the reactor chamber, completed by the gas feeding and pumping system, power supply and power monitor, electrical matching network, process control and instrumentation, and process diagnostics. While most of the modules are similar for all PECVD processes, they principally differ by the reactor configuration and the power supply modules, depending on the range of plasma excitation frequency, the nature of the substrates, and film quality requirements.

Low-, medium-frequency and RF PECVD systems can all possess internal electrodes (capacitive coupling, figure 3(a)),

while the RF reactors can also use external plasma excitation using a coil or rings (inductive coupling, figure 3(b)). This allows one to distinguish them based on the level of control of the bulk plasma characteristics and ion bombardment effects on the substrate surface. The deposition rates on the grounded electrode are substantially lower than on the RF-powered electrode (usually 5–10 times), depending on the gas nature and composition. Typically,  $E_{i,max} = 25$  eV on the grounded electrode (see equation (8)), while on the RF-powered electrode,  $E_i$  values may reach several hundred electron volts due to high substrate bias voltage,  $V_B$ . In relation to the discussion in section 2.2, this asymmetry should be considered if the films are supposed to grow under high energy ion bombardment on the power-driven substrate holder leading to high packing density, or if such bombardment is to be avoided if higher film stress or possible defects cannot be tolerated.

Many successful deposition systems for functional (mostly dielectric) coatings are based on the use of MW discharges that generally provide high  $n_e$  and hence high  $\Gamma_i$  values (figures 3(c) and (d)). The substrate is placed on a grounded or electrically floating substrate holder, facing the MW (low water-content fused silica or alumina) window through which the MW power is supplied using different MW waveguides or applicators (see [49, 65]).

RF and MW discharges differ principally in their EEDFs (see figure 4), which can be determined by solving the Boltzmann equation; it has been shown that the population of electrons in the high-energy tail of the EEDF is higher in MW plasma than in its RF counterpart [66]. The number



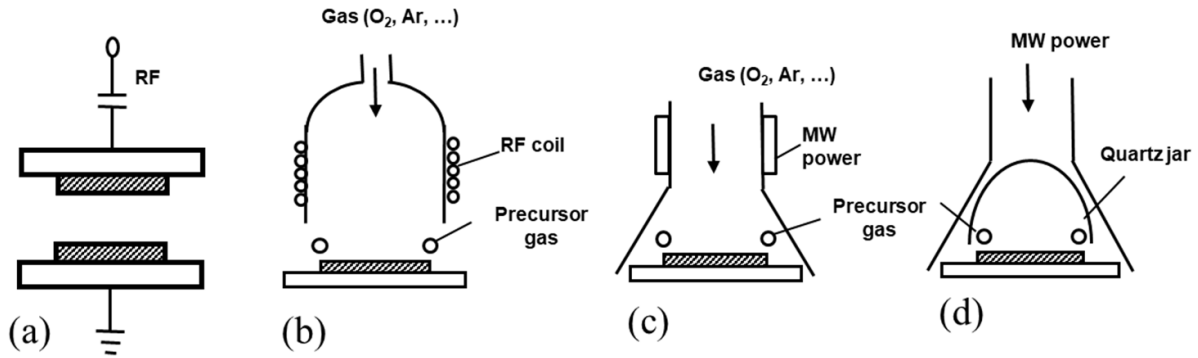


**Figure 3.** Schematic illustration of the reactor configurations of typical radiofrequency (a), (b) and microwave (c), (d) PECVD systems: (a) parallel plate capacitively coupled RF reactor, (b) downstream (remote) inductively coupled RF reactor, (c) remote MW excitation, (d) horn antenna MW excitation. Possible substrate positions are indicated. Reprinted from [46], Copyright (2010), with permission from Elsevier.

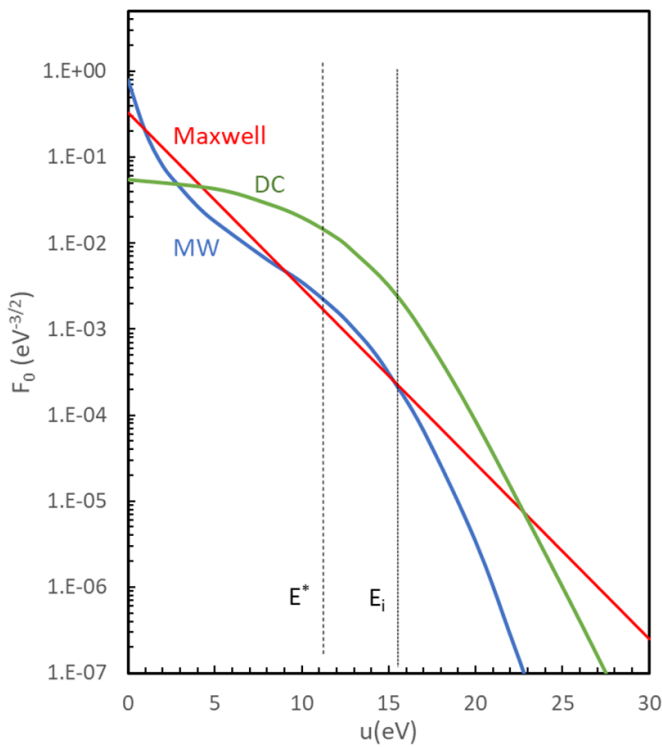


**Figure 4.** Electron energy distribution functions in high frequency plasmas—comparison of microwave (MW) and lower frequency (RF or DC) plasmas with the Maxwellian distribution [67].

of electron–ion pairs formed per unit of delivered energy is highest when the EEDF is Maxwellian such as in the MW plasma [67]. In addition, the MW plasma is controlled by ambipolar diffusion, i.e. electron–electron collisions prevail, while in the RF mobility-controlled discharge, the energy loss is due to a direct charged-particle impact on the walls. As a consequence, the ionization ( $n_e$ ) and dissociation rates are higher in the MW plasma, generally leading to higher process rates, and higher ion flux,  $\Gamma_i$ , toward the exposed surface [66]. On the other hand, RF plasma is more versatile, and it allows one to control the surface potential and hence the energy of bombarding ions,  $E_i$  [46]. These two approaches can be combined in the so-called ‘dual-mode MW-RF’ (or

‘dual-frequency’) process that helps to selectively tune the ion energy and ion flux [46, 68, 69].

Optimization of the PECVD processes generally involves the identification of discharge characteristics leading to the formation of large densities of free radicals ( $n_R$ ) that diffuse toward the surface (contributing to the flux of the film-forming species,  $\Gamma_{dep}$ ), as well as to high concentrations of ions (due to high  $n_e$ ) favoring high  $\Gamma_i$ , as will be discussed below.

As mentioned above, the choice of  $f$  defines the deposition reactor, and it influences the fundamental plasma properties such as the EEDF; however, it also has an important effect on how the plasma interacts with the exposed surface. At a surface in contact with plasma is an interface medium, the plasma sheath, which is electrically non-neutral, in contrast to the plasma itself. An electrically isolated surface is at a floating potential,  $V_{fl}$ , with respect to the plasma potential,  $V_p$ . Since  $V_{fl} < V_p$ , positive ions are accelerated from the plasma to the surface, while some of the electrons are repelled. Under steady-state conditions, no net current flows, since ion and electron fluxes are then equal. In this case, the thickness of the sheath,  $d_S$ , is a few times the Debye length,  $\lambda_D$ , and it grows with increasing average electron energy and decreasing  $n_e$  [46].

Assuming, for simplicity, that the EEDF is Maxwellian, and that the surface immersed in the plasma is a plane, the potential difference across the sheath can be approximated by [70]:

$$V_p - V_{fl} = (kT_e/2e) \ln(m_i/2\pi m_e), \quad (7)$$

where  $k$  is the Boltzmann constant,  $T_e$  is the electron temperature,  $e$  is the electron charge, and  $m_i$  and  $m_e$  are the masses of ions and electrons. We note that on floating potential surfaces, the ion energy  $E_i = e(V_p - V_{fl})$  is typically a few times  $T_e$  expressed in electron volts (e.g. around five times  $T_e$  for Ar-based plasma). The ions always acquire some additional energy as they pass through the sheath on their way to the surface.

The energy of the charged particles impinging on a substrate can be adjusted by biasing it at a potential  $V_B$  with respect to  $V_p$ . In the case of an insulating material, it can only be biased by applying a periodic voltage. The substrate

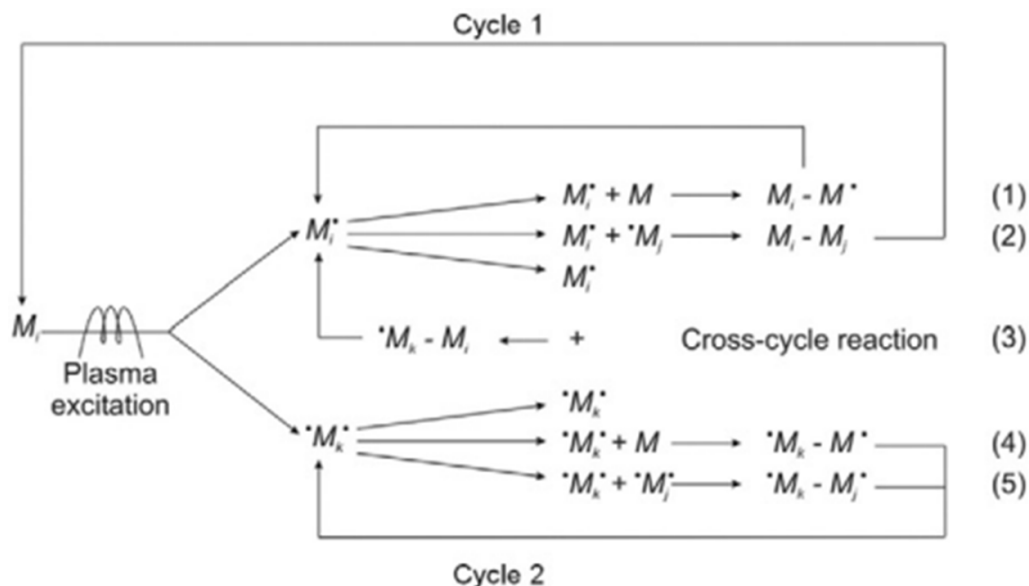


**Figure 5.** Schematic description of the rapid step-growth polymerization mechanism. Reprinted from [54], Copyright (2016), with permission from Elsevier.

surface exposed to the plasma is then capacitively charged, that is, electrically polarized, providing a mean DC voltage component,  $V_B$ . If the frequency of the applied periodic voltage,  $f$ , is greater than  $f_{ci}$ , the critical ion plasma frequency [(such as at  $f = 13.56$  MHz)], the sheath is not influenced by the periodic variation of the biasing voltage [46, 67]. When a positive ion diffuses from the plasma bulk into the sheath region, it will then be accelerated toward the substrate, which it strikes with a maximum kinetic energy  $E_{i,max}$  [71, 72]:

$$E_{i,max} = e|V_p - V_B| = eV_{sh}. \quad (8)$$

In the pressure range generally used for plasma processing, however, the ions lose part of their energy due to elastic, inelastic, and charge transfer collisions in the sheath (see figure 2(d)) and exhibit a broad ion energy distribution function (IEDF) by transferring energy to the flux of neutral particles.

Finally, the processes leading to the deposition of thin films in the plasma environment include reactions in the gas phase, transport toward the surface involving specific energetic considerations, and reactions at the surface, giving rise to film formation and microstructural evolution, providing specific film functional properties. Energetic aspects of plasma-surface interactions and the importance and ranges of ion and photon energies (particularly of the ultraviolet, UV, and vacuum ultraviolet, VUV, radiation) are discussed in the next sections.

### 3. Plasma Polymerization (PP)

#### 3.1. State of the art and current limitations

The PPFs are generated from the activation of an organic precursor in a plasma. This process gives rise to thin film materials that, despite their name, strongly differ from conventional

polymers except for their organic nature. Indeed, because of the PP process, the PPF is not characterized by repeating units but mostly by a random network often presenting a high level of crosslinking which confers to this family of organic materials' unusual mechanical or chemical properties. Their unique characteristics make PPFs very attractive, while strongly stimulating the curiosity of surface scientists who have devoted strong efforts to understand their growth mechanism. As already mentioned, the overall PP process involves both gas phase and surface reactions [73–75]. The first step consists of introducing (e.g. by vaporization) an organic (organometallic) precursor to the deposition chamber. The activation takes place in the plasma phase through collisional processes between energetic electrons/metastables (depending on the pressure) and precursor molecules. Because of the energetic conditions, the most probable reaction consists of precursor dissociation reactions resulting in the formation of radicals. Historically, it was assumed that the growth of the layer mainly occurs through either radical–radical or radical–molecule reactions. Indeed, the radicals possess an unpaired electron and therefore are highly reactive toward the termination reactions with other radicals, or toward addition reactions with unsaturated molecules (i.e. with double or triple bonds) [76].

Some of the processes involved in the synthesis of a PPF are summarized in the ‘Rapid Step Growth Polymerization’ (RSGP) model proposed by Yasuda in 1985. The model, schematically shown in figure 5, is built on the concept of recombination of reactive species and the subsequent reactivation of the resulting products [77, 78]. In this figure, cycle 1 involves the reaction of monoradicals (species with one radical site), whereas cycle 2 concerns biradical species (with two radical sites), both originating from the interaction of the precursor with the plasma. It is worth noting that owing to the similarity between the energy of the organic chemical bonds, numerous fragmentation pathways are possible [79]. As a

consequence, a great variety of radicals is generally produced in the plasma whatever the chemical nature of the organic precursor, hence contributing to the irregular structure of PPFs.

Steps (1), (3), (4), and (5) correspond to addition reactions between the reactive species and (i) a stable molecule (which can be the precursor molecule) containing a reactive site such as a double or triple bond (steps (1) and (4)) or (ii) other reactive species including radicals and biradicals (steps (3) and (5)). In both cases, the generated products can undergo other propagation reactions.

During the PP process, the molecules formed through the recombination between two radicals (step (2), termination reaction) can be reactivated via electron impact or interaction with excited species, in contrast with the situation encountered in conventional polymerization. Consequently, the RSGP mechanism can be viewed as a succession of termination reactions followed by the reactivation of the products. When a surface is exposed to such a plasma, a solid organic thin film is deposited on the substrate, arising from the condensation of reactive species produced in the plasma. However, further 'polymerization' reactions (initiation, addition, termination, reactivation) can still occur at the plasma growing-film interface. The reaction of the reactive species at the growing film surface resulting in the ablation of the deposited layer is included through the 'Competitive ablation and polymerization' principle, namely the simultaneous occurrence of film etching and deposition processes [77, 80, 81]. Note that the reactivity of the radicals, that is, their probability to contribute to film growth, is a key parameter. While some radicals might be abundant in the plasma state but reflected at surfaces, others with high sticking probability determine the film growth, which are thus difficult to assess using plasma diagnostics. The evaluation of deposition rates as used by Yasuda is thus a suitable way.

Initially, the RSGP model has been developed for explaining the mechanism of PP operated at low pressure, however, this model can also be applied when considering the synthesis of PPFs at higher pressure despite some specificities [82]. One difference lies in the activation step. Indeed, when increasing the pressure, the formation of radicals/ions as a result of collisions involving metastable atoms or molecules have also to be considered in addition of the already discussed mechanisms. On the other hand, the extent of addition reactions in the gas phase also depends on the pressure. For instance, at high pressure conditions, characterized by a very small mean free path of the particles, numerous propagation (steps (1), (3), (4), and (5) in the RSGP, see figure 5) and recombination (step (2) in the RSGP, see figure 5) reactions could take place giving rise to polymerization and/or nucleation events in the gas phase which ultimately may lead to the formation of solid particles (so-called dust). For the fabrication of stable and dense coatings, this phenomenon has to be avoided. The most common strategy to overcome such an issue for thin film deposition consists in diluting the precursor in a carrier gas. However, nucleation in the gas phase can also be exploited for the synthesis of plasma polymer nanoparticles as recently reviewed by Choukourov *et al* [83].

In the Yasuda model, the ions have been excluded from the reaction paths owing to their relatively low abundance in the discharge compared to radicals and neutrals. However, in plasma processing, a surface facing the discharge is continuously bombarded by positive ions with kinetic energy ranging from 5 to 30 eV even in the absence of external bias, specifically driven by the difference between the plasma potential and the surface potential (see equation (8)). This supply of energy is sufficient to 'activate' the surface through surface chemical bond breaking resulting in the formation of surface dangling bonds acting as preferential adsorption sites for the reactive species of the plasma [84–86]. The occurrence of these reactions is included in the ion-AGM proposed by d'Agostino in which the formation of surface defects through ion interaction is considered [85, 87]. Based on the AGM, the incorporation of the precursor into the growing film is possible via a surface reaction with a radical site through, for example, the opening of a double bond. Such reaction is referred to as *induced PP* in contrast to *plasma-state polymerization* for which the activation of the molecule in the plasma is an essential step. Unlike radical polymerization, that is, grafting non-activated molecules to an activated polymer surface, however, the plasma allows to activate both the molecules and the surface, thus enabling also the use of generally non-reactive (e.g. saturated) molecules. Regarding the activation step in the AGM, increasing the working pressure significantly decreases the kinetic energy of the bombarding ions, and hence the efficiency of the formation of surface defects for further grafting. In this context, with respect to a debate on the subject [88, 89], d'Agostino and Palumbo have concluded that for a working pressure higher than 47 Pa, the activation of the surface by ionic impact is prevented but might still contribute to surface mobility, mixing and branching [89]. Therefore, plasma-chemical processes have to be considered.

Initially, the AGM was developed for the growth of fluorine-based coatings, but it can also be applied to other PPF families [84]. In addition, the impinging ions can also be responsible for other phenomena such as ion-assisted etching or coating densification as will be described below. For the sake of completeness, it has to be mentioned that, though not considered in the AGM, surface reactive sites can also be created through UV photons irradiation of the growing film interface or through hydrogen surface abstraction reactions [62, 80].

While considering ions as active species in the growth of PPF, the AGM still implies that the density of ions is so low that any mass deposited by ions would be insignificant [62]. Nevertheless, recent studies pointed out that under certain experimental conditions, e.g. favoring the formation of heavy ionic molecules undergoing soft landing, the contribution of condensing ions cannot be neglected [76, 90–95]. In some cases, some authors even claim that the ions are the main species responsible for PPF growth [93]. The origin of this potentially important contribution of ions in the PPF formation is justified by several factors. One of them is that the 'Bohm Sheath Criterion' results in an increase in the ion flux toward the surface, significantly higher than the thermal flux

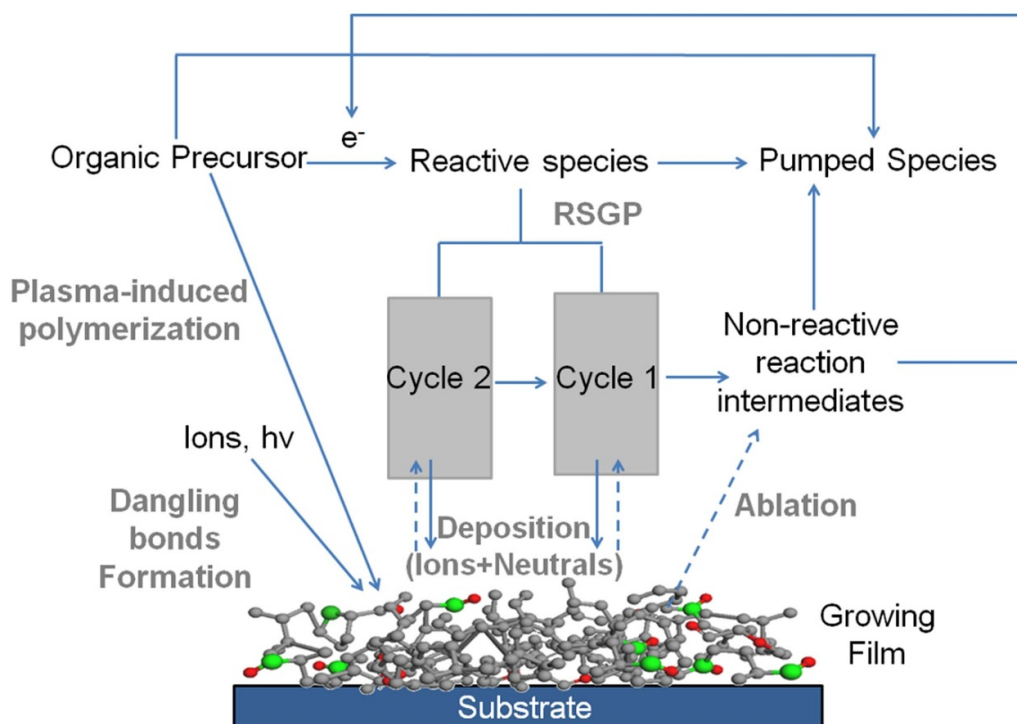


**Figure 6.** Overall mechanism of plasma polymerization. Reprinted from [54], Copyright (2016), with permission from Elsevier.

(by a factor of  $\sim 15$ ) [96]. In addition, it has been suggested that the sticking coefficient associated with some ionic species can be very high, significantly increasing their probability of incorporation in the growing film [91, 97, 98]. Considering these elements, it clearly appears that establishing the correlation between a particular species density in the plasma (i.e. the one of ionic species but it is also true for radicals) and their relative importance for film growth is a very tricky problem.

The exact role played by the ions in the mechanistic formation of PPFs has already been debated in the 1960–1970s [80], and this debate was further revisited in 2010 [99]. Nevertheless, up to now, there is no consensus about the contribution of ions to the overall deposited mass, which might strongly depend on the selected plasma conditions.

The different models described in this section are summarized in figure 6 providing a global overview of the PP mechanism and allowing one to understand the irregular structure of the plasma polymer including the absence of repeating units, the great diversity of chemical functions, branched/cross-linked network, presence of trapped radicals responsible for post-deposition reactions, etc [80, 102]. Nevertheless, due to the complexity of the overall mechanism, it does not allow the assessment of each reaction as well as the prediction of the film properties.

Another factor to consider is the high dependence of the PP process on the synthesis conditions (pressure, energy density, distance from the plasma source, precursor flow rate, ...) as illustrated in figure 7, and also the plasma reactor geometry itself. Depending on the operating parameters, some specific reactions can predominate while directly influencing

the chemical composition, cross-linking degree, mechanical properties, stability of the coatings, etc [80, 103]. In this context, numerous efforts have been made to deeply understand the mechanistic formation of PPF. From these works, two main approaches have emerged, namely the *microscopic* and the *macroscopic* approach. The former relates to a deep insight into the molecular intimacy of the plasma, while the latter is based on a global chemical pathway governed by apparent activation energy.

### 3.2. Into the intimacy of PP

As already mentioned, the plasma chemistry associated with the PECVD processes and singularly with PP is most of the time very complex because of the numerous chemical reactions that occur in the plasma phase. Therefore, to better control the film forming process, one of the strategies is to implement experiments allowing one to obtain a precise picture of the plasma chemistry including the identification/quantification of the involved species (i.e. ionic and neutral), as well as the determination of the flux and the energy of ions reaching the surface. The idea is to correlate the plasma and film chemistries to unravel the mechanisms governing film growth at the molecular level. It should be noted that theoretical tools are also frequently employed to support the interpretation of the experimental data.

In the context of PP, several diagnostic methods have been developed and employed during the past 30 years; this includes mass spectrometry (MS), optical emission spectroscopy, *in-situ* Fourier transform infrared spectroscopy (FTIR), and ion probes. A detailed description of each technique and



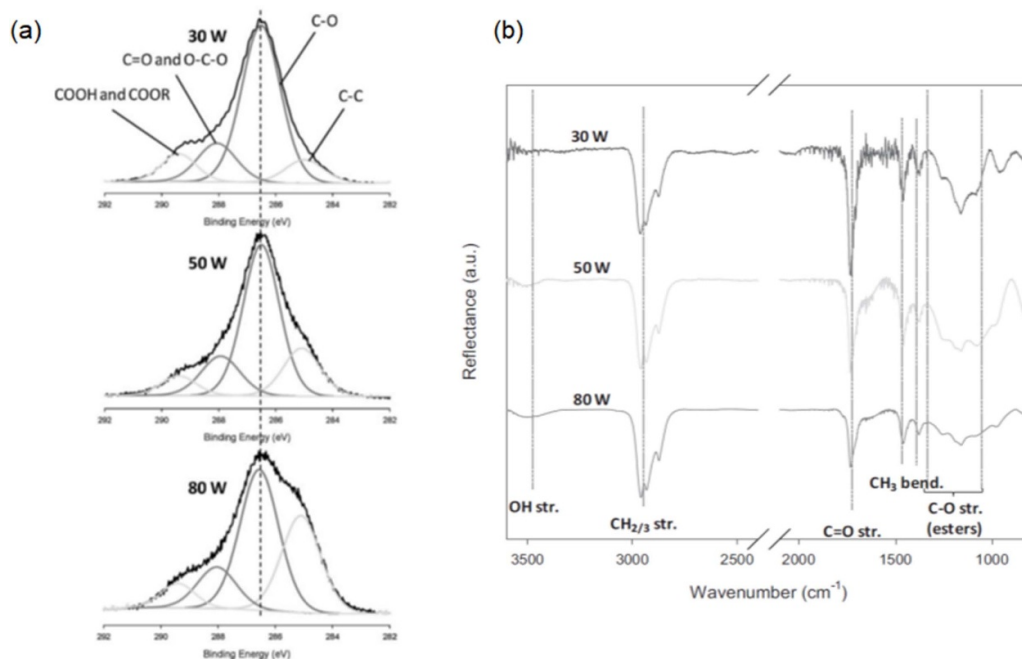


**Figure 7.** (a) Atmospheric plasma polymerization of polyethylene glycol: influence of the plasma power on the high resolution C1s spectra revealing the increase in the C–C component shoulder with power. [100] John Wiley & Sons. [Copyright © 2010 WILEY-VCH Verlag GmbH & Co. KGaA, Weinheim]. (b) FTIR spectra of atmospheric plasma polymerized propylisobuturate coatings showing the change in the relative intensities of the C=O to CH<sub>2</sub>/CH<sub>3</sub> bonds when increasing power. [101] John Wiley & Sons. [© 2013 WILEY-VCH Verlag GmbH & Co. KGaA, Weinheim]. In both cases, a loss of the precursor functionality (C–O–C for PEG, and COO for PiB) occurs.

its advantages and disadvantages can be found in the review of Thiry *et al* [54]. Specifically, in this context, MS has particularly been favored since it enables the identification of both neutral and ionic species as well as their relative quantification. Besides, for ions, their energy distribution can also be measured.

As an example, the mass spectra of acrylic acid plasma are depicted in figure 8. The peaks can be assigned as follows [104, 105]:  $m/z = 72$  for the acrylic acid precursor;  $m/z = 55$  for  $\text{CH}_2\text{CHCO}^+$ ;  $m/z = 44$  for  $\text{C}_2\text{H}_4\text{O}^+$ ,  $\text{C}_3\text{H}_8^+$  and  $\text{CO}_2^+$ ;  $m/z = 28$  to  $\text{C}_2\text{H}_4^+$  and  $\text{CO}^+$ ;  $m/z = 27$  to  $\text{C}_2\text{H}_3^+$ ;  $m/z = 26$  to  $\text{C}_2\text{H}_2^+$ ;  $m/z = 18$  to  $\text{H}_2\text{O}^+$ ;  $m/z = 2$  to  $\text{H}_2^+$ ; and  $m/z = 1$  to  $\text{H}^+$ . It is worth noting the presence of numerous peaks in the mass spectrum indicating the expected complex plasma chemistry even at low power as also reported for other plasma polymer families [79, 95, 106–109]. Although traces of molecules with  $m/z$  higher than the precursor have sometimes been observed, no ‘dimer’ or ‘trimer’ have been identified in contrast to positive ions (see hereafter) [79, 95, 110]. One exception is the PP of methylisobutyrate for which a neutral dimer has been observed [111].

A closer look at the mass spectrum in figure 8 also reveals the production of stable hydrocarbon-based molecules (e.g.  $\text{C}_2\text{H}_2$ ,  $\text{C}_2\text{H}_4$ ), as frequently encountered by whatever precursor is employed [95, 104, 106, 107, 112, 113]. As proposed by Thiry *et al* and supported by theoretical calculations, these hydrocarbon molecules result from rearrangement reactions of the radicals generated by dissociation reactions in the gas phase [79]. In addition to stable hydrocarbon-based

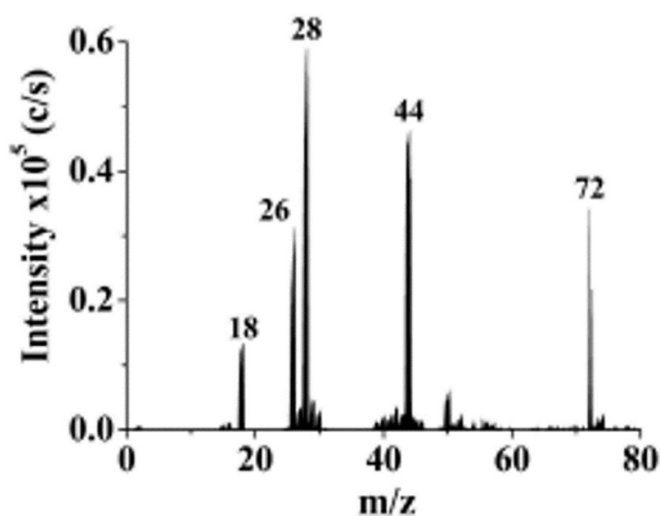


**Figure 8.** Neutral mass spectra of acrylic acid plasma (mean RF power of 50 W, pulsed mode) for a working pressure of 1.3 Pa. Note that the fragmentation of the acrylic acid precursor in the ionization source has been subtracted. Reprinted with permission from [122]. Copyright (2007) American Chemical Society.

molecules, stable molecules containing a hetero-element ( $\text{CO}$ ,  $\text{CO}_2$ , and  $\text{H}_2\text{O}$  in the present example) are also formed [104, 110, 112]. Similarly,  $\text{NH}_3$  and  $\text{N}_2$  species are identified in nitrogen-based discharges [95, 106, 108, 114, 115] as well as  $\text{H}_2\text{S}$  and  $\text{CS}_2$  in sulfur-containing organic plasmas [79,



[116–120]. The concentration of such molecules in the gas phase is generally inversely correlated to the hetero-element concentration in the films [121]. Indeed, considering the low reactivity of the stable molecules, they do not take part in the film growth. This reduces the amount of hetero-elements available for the deposit.

The last example illustrates the high complexity of MS data. Therefore, to better understand plasma chemistry, MS data can be combined with density functional theory (DFT) calculations allowing one to theoretically determine the different chemical fragmentations pathways of the considered precursors [79, 86, 113, 123]. Other theoretical tools (i.e. molecular dynamics, particle-in-cell Monte Carlo) have also been employed for simulating the film growth [124–129]. These methods were mainly applied to a-C:H layers likely because of ‘simpler’ plasma chemistry rather than for functionalized PPF (containing a hetero-element). To the best of our knowledge, only two studies have addressed the simulation of the growth of functionalized PPF, both from the cyclopropylamine precursor [124, 130]. Compared with experimental data, these studies shed light on the role of ions and radicals in the global surface reaction scheme, the ultimate goal being to predict the film properties. Nevertheless, although promising, the plasma modeling for simulating PPF growth still needs to be developed to better support the experimental data.

As already mentioned, it has been concluded that ions play a major role in the PPF growth process. The ionic gas phase chemistry has therefore also been extensively investigated by MS, especially at low pressure. Figure 9 shows a typical example of the chemical composition of positive ions in an acrylic acid discharge. It is important to underline that ions do not suffer additional fragmentation before their detection during their transport in the mass spectrometer (no additional ionization step). Therefore, all peaks appearing in the spectrum correspond to ions originating from the plasma. The peak at  $m/z = 73$  is ascribed to the protonated monomer ( $[M + H]^+$ ) while the most prominent fragments are observed at  $m/z = 39$  ( $C_3H_3^+$ ), 55 ( $CH_2CHCO^+$ ) and 57 ( $CH_3CH_2CO^+$ ).

A relevant observation is the detection of oligomeric ions of the form  $(2M + H)^+$  at  $m/z = 145$  and  $(3M + H)^+$  at  $m/z = 217$ , where  $M$  corresponds to the molecular weight of the starting material as also observed in other works [90, 111, 112, 131]. Oligomer ions corresponding to  $[4M + H]^+$  have been identified in [104]. The dimer and trimer ions can lose  $H_2O$  giving rise to additional signals separated by a value of 18. Such oligomer ions formed through gas-phase neutral/ion reactions have also been identified in propanoic acid [111, 131], allyl alcohol [109], propanol [109], allylamine [95, 108], hexamethyldisiloxane (HMDSO) [91, 132, 133], methyl isobutyrate, methyl methacrylate, *n*-butyl methacrylate [134], ethanol [135, 136],  $\gamma$ -terpinene [137] and thiophene [138] plasmas. Most of the time, the formation of these oligomeric ions involves the addition of a hydrogen ion to the neutral precursor followed by the successive additions of uncharged monomers. However, the exact mechanism remains unclear in some aspects. For example, gas-phase oligomerization reactions do not require the presence of a double bond in the organic precursor marking a clear difference

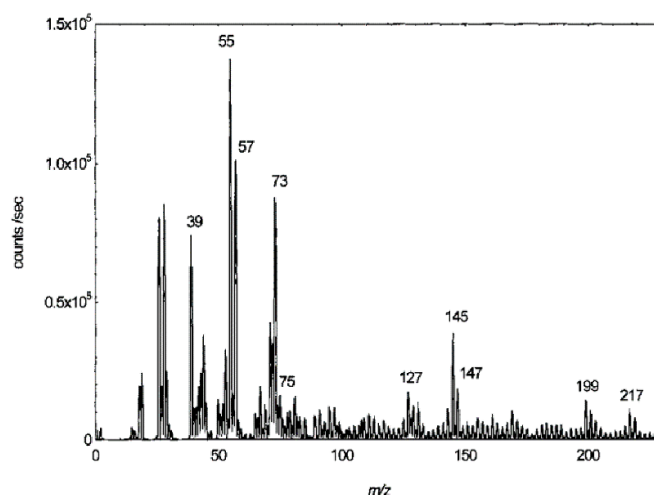


**Figure 9.** Positive-ion mass spectrum of acrylic acid plasma sustained at a RF power of 1 W and a working pressure of 2.5 Pa. Reprinted with permission from [104]. Copyright (2000) American Chemical Society.

from classical ionic polymerization [111, 134]. The reason why neutral/radical addition reactions in the gas phase are ruled out lies in the kinetics of the reactions as proposed by Benedikt [139]. Indeed, ion-neutral reactions are typically ten times faster than reactions between neutral particles due to the attractive potential created by the induced dipole moment in the neutral particle. More details about the role of ions at low pressure in the PP process can be found elsewhere [54, 76, 96, 98]. Oligomeric ions (cations and anions) have also been observed considering PP of acrylic acid at AP using a pulsed plasma jet as an excitation source [140].

Using the MS technique, although all ions constituting the plasma can be identified, the absolute ion flow toward the growing film cannot be deduced since MS measurements do not give access to the absolute density of ions. This aspect is, however, of crucial importance to measure the contribution of ions in the total energy flux reaching the growing film. This can be achieved by using an ionic probe especially dedicated to operating in organic discharges and developed by Braithwaite *et al* in 1996 [141]. Readers interested in the working principle of the probe are invited to consult the following [76, 91, 141].

An example of the evolution of the ion flux toward the substrate as a function of power is shown in figure 10 for the PP of allylamine in an inductive RF plasma. The ion flux was found to increase from  $6.6 \times 10^{16} \text{ m}^{-2} \text{ s}^{-1}$  ions at 1 W to  $1.4 \times 10^{18} \text{ ions m}^{-2} \text{ s}^{-1}$  at 14 W. The observed trend is attributed to the increase in the electron density and, in turn, in the ion density in the plasma volume upon increasing the power [142]. The calculation of the average ion mass based on the ionic mass spectra combined with ion flux measurements allows us to deduce the ion mass flux toward the growing film. To evaluate the contribution of ions in the deposited mass, the latter is compared with the mass deposition rate. At low power (i.e. 1 W), approximately 63% of ions could, in principle, contribute to film formation. Interestingly, at a power

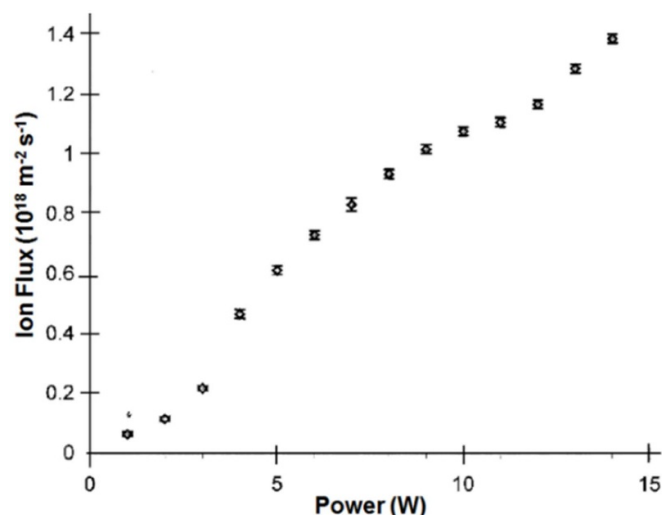


**Figure 10.** Evolution of the ion flux in allylamine plasmas as a function of RF power for a working pressure of 2.5 Pa in an inductive RF plasma. Reprinted with permission from [95]. Copyright (2001) American Chemical Society.

of 5 W, the ion flux is sufficient to account for all deposited mass. This provides a strong argument that ions significantly contribute to film formation. However, it is important here to stress that it does not mean that the film grows through a pure ionic mechanism and that neutral/radical surface reactions are ruled out. Estimation of the mass delivery to the film by ions by a comparison between the mass deposition rate and ion flux inherently implies that all ionic species which collide with the surface are incorporated in the growing film which is unrealistic. At the same time, an increase in the ion flux at the interface causes the formation of surface defects favoring the adsorption of radicals at the interface [86, 143]. Similar trends and ion flux values were reported for the PP of acrylic acid [94, 131], propionic acid [94, 131], hydrocarbons (*n*-hexane and 1,7-octadiene), diethylene glycol, diethylene glycol divinyl ether [94],  $\gamma$ -terpinene [137] and ethanol [136] plasmas.

Therefore, in summary, even if nowadays a considerable knowledge of plasma chemistry can be achieved with the combination of several plasma diagnostic techniques (sometimes supported by theoretical tools), there are still important questions related to the surface reactivity of the film-forming species, particularly those related to the sticking coefficient. The latter is defined as the ratio of particles absorbed or ‘stuck’ at the surface to the number of particles that impinge the surface during the same time. Although crucial for a complete understanding of the growth mechanism at the molecular level, the determination of the sticking coefficient has received little attention regarding the PP of functional precursors. This is likely due to the fact that to access such kind of information, it is necessary to determine absolute density values which is not possible with the MS approach.

The limitation of MS can be overcome by using *in situ* absorption FTIR spectroscopy to characterize the plasma phase as shown in the investigation of the growth mechanism

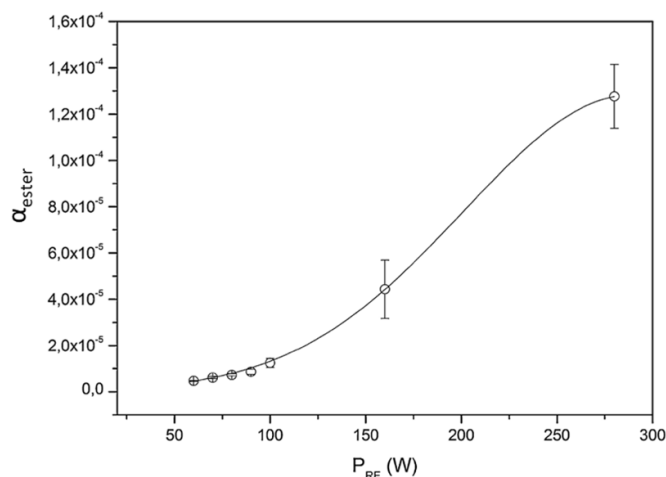


**Figure 11.** Evolution of  $\alpha_{ester}$  as a function of the RF power at a working pressure of 1.3 Pa for ethyl-lactate plasma polymerization in an inductive RF plasma. [86] John Wiley & Sons. [© 2015 WILEY-VCH Verlag GmbH & Co. KGaA, Weinheim].

of ethyl-lactate-based PPF in a inductive RF plasma [86]. In this case, the absolute density of reactive ester-based molecules in the plasma is measured allowing one to evaluate the ester flow reaching the growing film. Then, a comparison between these data with the ester content in the films, measured by x-ray photoelectron spectroscopy (XPS), enables one to estimate the surface reactivity of the considered condensing moieties ( $\alpha_{ester}$ ) as illustrated in figure 11. When the power dissipated in the plasma increases from 60 to 280 W,  $\alpha_{ester}$  evolves from  $2.6 \times 10^{-6}$  to  $1.3 \times 10^{-4}$ . This trend is explained by a higher ion bombardment at higher power resulting in the formation of more dangling bonds at the interface and hence a higher efficiency of grafting the ester functions according to the ion-AGM. This example again illustrates that both neutrals and ions are intertwined in the overall mechanism.

For the sake of completeness, it should be emphasized that, although directly related to the sticking coefficient of reactive ester-based species,  $\alpha_{ester}$  represents the probability of incorporating an ester group in the coating. Indeed, once grafted into the growing film, the ester functions can undergo further reactions activated by ions and photons, and be converted into other chemical groups. Therefore, considering the complex mechanistic formation of plasma polymers,  $\alpha_{ester}$  can be viewed as the grafting efficiency of the film-forming species bearing an ester function minus the extent of the degradation of the ester groups once incorporated in the growing film [86].

In this context, one should also consider the work related to the growth of a-C:H-based layers for which the surface reactivity of film-forming species has been studied by the so-called ‘cavity technique’ [144–147]. This strategy is based on the transport of reactive species, evaluated through plasma diagnostic methods, inside a cavity consisting of a closed volume with a small entrance through which film-forming species can enter (see figure 12(a)). Actually, what is determined by this method is the ‘surface reaction probability’ ( $\beta$ ) involving both sticking coefficient ( $s$ ) and the probability for the radical to

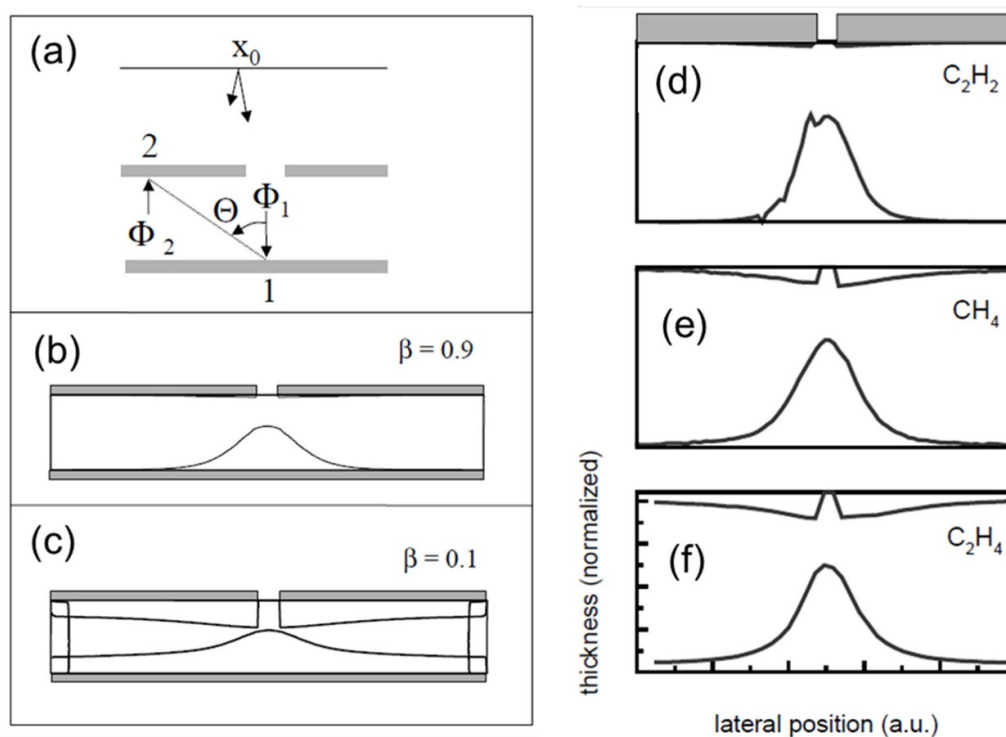


**Figure 12.** (a) Schematic diagram of the cavity made of silicon wafers. Particles from the discharge enter the cavity through a slit in the top wafer. Theoretical variation in film thickness inside the cavity for a surface loss probability (b)  $\beta = 0.9$  and (c)  $\beta = 0.1$ . Measured variation in film thickness at the top and bottom of the cavity after exposure to (d) a  $C_2H_2$ , (e)  $CH_4$ , and (f) a  $C_2H_4$  plasma discharge. Each deposition profile is normalized to the maximum of the bottom profile. Reproduced from [146]. © IOP Publishing Ltd. All rights reserved.

react and form, ultimately, a nonreactive volatile product from the surface reactions. In some specific cases, the latter can be estimated, and then the sticking coefficient is deduced [146]. If  $\beta$  is high, most of the entering species react after the first collision giving rise to a large film thickness at the bottom of the cavity opposite to the entrance slit (figure 12(b)). In contrast, a small  $\beta$  means that the reactive species will ‘survive’ many wall collisions resulting in a more uniform coating in terms of thickness (figure 12(c)). Practically, applying this methodology for  $C_2H_2$ ,  $CH_4$  and  $C_2H_4$  discharges helped to evaluate the main contributions of the film-forming species to the growth of the layer (see figure 12(d)). The analysis of the data in combination with MS experiments reveals that the sticking coefficients of hydrocarbon-based radicals scale with their hybridization state:  $\sim 0.8$  for  $C_2H$ , and  $\sim 0.3$  for  $C_2H_3/C_2H_5$ , explaining the higher deposition rate observed for unsaturated precursors [148]. It is important to mention that the cavity located in a remote plasma zone does not allow one to determine the influence of the ionic bombardment on the surface reactivity of radicals. Nevertheless, as already pointed out, this aspect has been considered. For instance, it has been shown for  $\cdot CH_3$  radicals that the sticking coefficient can vary in a wide range (i.e. from  $10^{-4}$  to  $10^{-2}$ ) depending on the density of dangling bonds at the interface [143, 149].

The concept of the ‘cavity technique’ has recently been applied to the growth of cyclopropylamine PPF [150]. In this case, the substrate consisted of Si micro trenches with an aspect ratio ranging from 2 to 40. The authors estimated an

effective sticking coefficient based on the experimental deposition profile compared with the expected step coverage (i.e. the ratio of the film thicknesses on the trench bottom and outside) in CVD driven by Knudsen diffusion (see [150] for more details). However, considering previous works on the cavity technique, this is most likely comparable to a surface reaction probability (i.e.  $\beta$ ). If  $\beta$  is high, the film-forming species are accumulating on the walls before reaching the bottom. In contrast, a more uniform layer is deposited for a lower  $\beta$  value. The analysis of the data reveals that  $\beta$  of the film-forming species are represented by a two-population model. The majority of the condensing moieties (i.e.  $\sim 76\%$ ) have a large  $\beta$  value (i.e.  $0.2 \pm 0.01$ ) while  $\sim 24\%$  possess a lower  $\beta$  (i.e.  $0.0015 \pm 0.0002$ ), thus explaining the difference in terms of surface chemical composition between the coating covering the bottom and the walls of the trench. Therefore, besides the significant improvement in the fundamental understanding of the plasma/surface interaction, this study also highlights the importance of the surface reactivity of reactive species on the chemical uniformity of covered 3D complex shape substrates as increasingly required for biological and other applications [151, 152].

It is expected that the combination of the microscopic approach with the empiric ‘cavity method’ for probing the surface reactivity of film-forming species could lead in the future to significant progress regarding the molecular growth mechanism of PPF. The collection of all these data could also serve as input for the simulation of the growth of the layers (i) to

improve the ‘match’ between the experiments and the theory, and (ii) potentially to reduce the time scale of the plasma modelling process, also representing a critical factor.

From the described works, it appears that to assure a reliable control of the PPF synthesis, it is necessary and efficient to shed light on the plasma chemistry to better understand the plasma-surface interactions during the film growth. Plasma diagnostics of such discharges is therefore very important but also often difficult to implement and, for certain techniques, quite expensive. Therefore, this strategy has to be complemented by other approaches allowing for easier access to some of the important features of the PP process. Such kind of complementary approaches is described in the next section.

### 3.3. A macroscopic view of PP

As for now, we understood that the plasma delivers the energy required to open chemical bonds in the precursor’s molecule to create reactive species as building blocks for film growth allowing high control on the nanoscale. We also pointed out that the plasma, however, may easily yield a surplus of energy during the film growth at highly non-equilibrium conditions resulting in damage, mixing, ablation, and radical trapping [153, 154]. The resulting layers may therefore remain in an unstable state and reorganize with time, showing so-called aging effects [155]. A high level of understanding of the energy transfer occurring in the complex gas phase and surface processes yielding plasma deposition is thus required. This can be obtained from a detailed characterization of the plasma phase as described in the previous section. Nevertheless, such a kind of approach is not always possible especially when considering industrial processes. In such a case, a more practical way has to be established.

Within the presented global model, the dependence of the conversion of the selected monomer into film-forming species on the internal plasma parameters, as given by equation (2), can be related to macroscopic parameters. The total absorbed power by the electrons in the plasma (per unit volume; in  $(\text{W cm}^{-3})$ ) equals the absorbed power density,  $W_{\text{abs}}/V_{\text{pl}}$ , in the plasma:

$$n_e \theta_{\text{abs}} = \frac{W_{\text{abs}}}{V_{\text{pl}}} \quad (9)$$

where  $\theta_{\text{abs}}$  is the average power absorbed per electron in the plasma (in  $(\text{W})$ ). With equations (2) and (4) it follows that

$$c_a = \frac{V_{\text{pl}} kT_0}{F_m p_0} \frac{n_m}{\theta_{\text{abs}}} \frac{W_{\text{abs}}}{V_{\text{pl}}} k_a(T_e) = \frac{W_{\text{abs}} kT_0}{F_m p_0} \frac{n_m}{\theta_{\text{abs}}} k_a(T_e) \quad (10)$$

evinced that the plasma-chemical conversion depends on the macroscopic reaction parameter,  $W_{\text{abs}}/F_m$ , which is related to the specific energy input (SEI) per monomer particle. The rate coefficient,  $k_a$ , and the normalized power per electron,  $\theta_{\text{abs}}/n_m$  (in  $(\text{W cm}^3)$ ) are often considered to solely depend on  $T_e$  for a Maxwellian electron energy distribution [156]. PP can macroscopically be described by externally accessible quantities (absorbed power, gas flow rate, and plasma expansion) and

operating parameters (gas composition, plasma source, frequency, and pressure) that define  $T_e$ . Note, however, that  $k_a$  has been introduced as a lumped rate coefficient, where different specific reaction pathways can contribute to varying degrees with respect to their threshold energies,  $E_{\text{th}}$ . Hence,  $k_a$  also depends on SEI, that is, the average energy available per monomer molecule in the plasma,  $E_{\text{pl}}$ , (in  $(\text{eV})$ ) as given by

$$E_{\text{pl}} = \frac{kT_0}{ep_0} \frac{W_{\text{abs}}}{F_m}, \quad (11)$$

finally yielding for the plasma-chemical conversion

$$c_a = eE_{\text{pl}} \frac{n_m}{\theta_{\text{abs}}} k_a \left( T_e, \frac{E_{\text{pl}}}{E_{\text{th}}} \right). \quad (12)$$

Here and in the following, SEI and  $E_{\text{pl}}$  are used synonymously. This macroscopic view of PP typically uses the measurement of mass deposition rates,  $R_m$  (in  $(\text{g cm}^{-2} \text{s}^{-1})$ ), obtained by weighing samples before and after deposition. The conversion in the gas phase can thus be assessed as:

$$R_m = \frac{M_{\text{dep}}}{N_A} s \Gamma_{\text{dep}} = \frac{M_{\text{dep}}}{N_A} s \frac{F_m}{A_{\text{dep}}} \frac{p_0}{kT_0} c_a \quad (13)$$

considering the molecular mass of the deposited species,  $M_{\text{dep}}$ , their sticking probability,  $s$ , and the Avogadro number,  $N_A$ . Note that  $M_{\text{dep}}$  and  $s$  can be affected by surface processes with respect to the delivered energy,  $E_d$ , during the film growth (equation (6)), as also discussed in section 3.2.

For plasma-chemical reaction pathways with one apparent  $E_{\text{th}}$  and dominant gas-phase reactions (as in plasma-state polymerization), normalized deposition rates (by  $A_{\text{dep}}/F_m$ ) were found to increase linearly with  $E_{\text{pl}}$  up to  $E_{\text{th}}$  before slowly reaching saturation following an Arrhenius-type curve (with  $E_{\text{pl}}$  replacing  $kT$ , due to the non-equilibrium conditions) as a consequence of the energy distribution in a plasma with the average value  $E_{\text{pl}}$  [157]. This situation can be described as

$$c_a \approx \begin{cases} \alpha(T_e) \cdot \frac{E_{\text{pl}}}{E_{\text{th}}}, & E_{\text{pl}} \leq E_{\text{th}} \\ \alpha(T_e) \cdot \exp\left(\frac{E_{\text{pl}} - E_{\text{th}}}{E_{\text{pl}}}\right), & E_{\text{pl}} > E_{\text{th}} \end{cases} \quad (14)$$

where  $\alpha$  is the fraction of the transferred energy in the plasma yielding activation reactions that contribute to PP which only depends on  $T_e$ . Since  $\alpha$  defines the conversion at  $E_{\text{pl}} = E_{\text{th}}$ , its maximum value is limited to 37% (i.e.  $\exp(-1)$ ) reached for a sufficiently high  $T_e$ , which also corresponds to the maximum energy conversion efficiency [158]. Note that a higher efficiency as pursued in plasma gas conversion governed by SEI might be obtained by additional ways of activation such as thermal effects or vibrational ladder-climbing [159, 160].

To illustrate this theoretical foundation, in the following, the deposition of hydrophobic PPFs from the organometallic compound HMDSO ( $(\text{CH}_3)_3\text{Si-O-Si-(CH}_3)_3$ ) is discussed regarding gas phase and surface processes. In particular, the transfer from a symmetric, capacitively coupled plasma (CCP) to an asymmetric CCP at different positions (at the electrode, floating, wall, and remote) is described. Note that PP



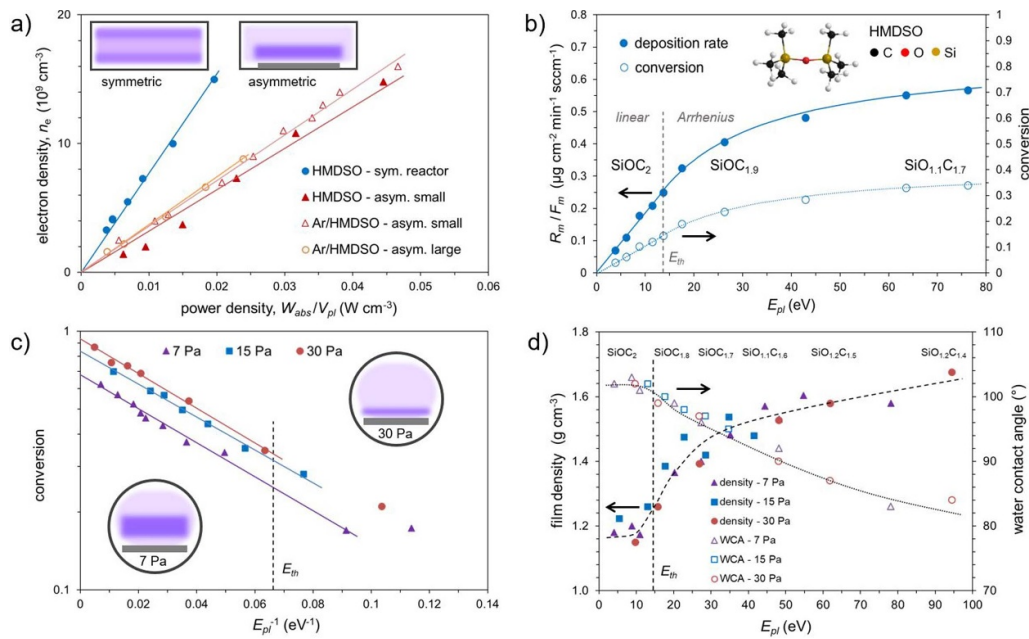


**Figure 13.** Plasma polymerization of HMDSO as monomer using RF excitation (13.56 MHz) at low pressure. (a) Electron densities for symmetric and asymmetric CCPs of different reactor size with pure HMDSO and mixtures with Ar, (b) deposition rates and conversion as observed in the symmetric reactor with pure HMDSO (at 10 Pa pressure) indicating  $E_{\text{th}}$  of 14 eV, (c) conversion in an asymmetric reactor (measured only at the RF electrode) with varying pressure while keeping Ar/HMDSO ratio 1:1 using an Arrhenius-type plot, and (d) hydrophobic film properties according to the plasma conditions given in (c). [53] John Wiley & Sons. [© 2020 Wiley-VCH GmbH].

of HMDSO can yield both (inorganic) silicon- and  $\text{SiO}_2$ -like films depending on the oxidation degree of Si, e.g. by adding  $\text{O}_2$  in the plasma, which is not considered here (see chapter 4).

A symmetric CCP with a uniform gas inlet into the plasma zone (as depicted in figure 2(a)) enables well-defined conditions to derive  $E_{\text{pl}}$  from the external power input,  $W$ , by

$$E_{\text{pl}} = \frac{kT_0}{ep_0} \frac{W_{\text{abs}}}{F_{\text{m}}} \approx \frac{kT_0}{ep_0} \frac{W}{F_{\text{m}}} \frac{d_{\text{act}}}{d} f_{\text{abs}} \quad (15)$$

where  $d_{\text{act}}$  is the length of the active plasma zone,  $d$  is the path of the gas traveling through the plasma (i.e. the gap between plane parallel electrodes with the uniform gas flow), and  $f_{\text{abs}}$  is the fraction of the absorbed power. While  $d_{\text{act}}$  generally varies with pressure and power, which need to be considered for asymmetric plasmas, it can be taken as constant in a confined symmetric discharge. Furthermore, the EEDF is different in a symmetric discharge due to two equal plasma-electrode interactions requiring a relatively higher  $n_e$  to sustain the plasma (figure 13(a)) with a high plasma potential and lower  $\theta_{\text{abs}}$  (and thus  $T_e$ ) compared to an asymmetric plasma with one dominant electrode developing a negative bias potential also reducing the plasma potential [57, 161]. By measuring  $n_e$ , for example using microwave interferometry for depositing plasmas,  $W_{\text{abs}}$  (e.g. using a  $V/I$  probe), as well as  $d_{\text{act}}$  and  $V_{\text{p}}$  (e.g. by optically detecting the plasma luminosity),  $\theta_{\text{abs}}$  and  $E_{\text{pl}}$  can be derived. Measuring  $c_a$ , that is, the overall deposited mass to the mass of the monomer gas inlet, the lump rate coefficient,  $k_a$ , can be determined according to equation (12) for varying  $E_{\text{pl}}$ . Plotting the normalized mass deposition rate,  $R_{\text{m}}/F_{\text{m}}$ , vs.  $E_{\text{pl}}$ , the linear and Arrhenius-type regimes can be

identified indicating an apparent  $E_{\text{th}}$  of around 14 eV for the HMDSO monomer (figure 13(b)). This agrees well with energies required for different reaction pathways yielding highly reactive  $(\text{CH}_3)_2\text{-Si-O}$  biradicals in the plasma (see cycle 2 in figure 5), the building blocks for hydrophobic polydimethylsiloxane (PDMS)-like ( $\text{SiOC}_2$ ) plasma polymers [53]. Note that this reaction pathway involves vibrational excitation and dissociation via different gas phase reactions requiring a sufficient residence time in the plasma as given for plasma-state polymerization. For special plasma conditions with very short residence times ( $\sim 1$  ms), on the contrary, larger ionized molecules have been identified as film-forming species based on single-step activation ( $\text{CH}_3$  abstraction by dissociative ionization) [162]. Higher energy input (above  $E_{\text{th}}$ ) promotes further H and  $\text{CH}_3$  abstraction in the plasma, yielding film compositions with lower CH and higher O contents due to post-plasma oxidation at trapped radical sites [163]. Hence, the most hydrophobic and stable PPFs have been observed for specific energies just around  $E_{\text{th}}$  [164]. Uniform and equal deposition rates on both electrodes in a symmetric plasma allow the calculation of the overall conversion (here  $\sim 15\%$  at  $E_{\text{pl}} = E_{\text{th}}$ , limited by  $T_e$ ).

Similarly, the PP of HMDSO in asymmetric reactors can be assessed, taking the varying plasma expansion into account. With increasing pressure, the plasma is more concentrated near the RF-driven electrode. For Ar/HMDSO mixtures of 1:1, a nearly 100% conversion of HMDSO molecules into film growth at the electrode was found at high  $E_{\text{pl}}$  and a pressure of 30 Pa (figure 13(c)). The  $s$  value of the film-forming species is thus assumed to be close to 1, independent of  $E_{\text{d}}$  at least for the range of 0.4–45 eV per deposited  $\text{SiOCH}$  species [53].



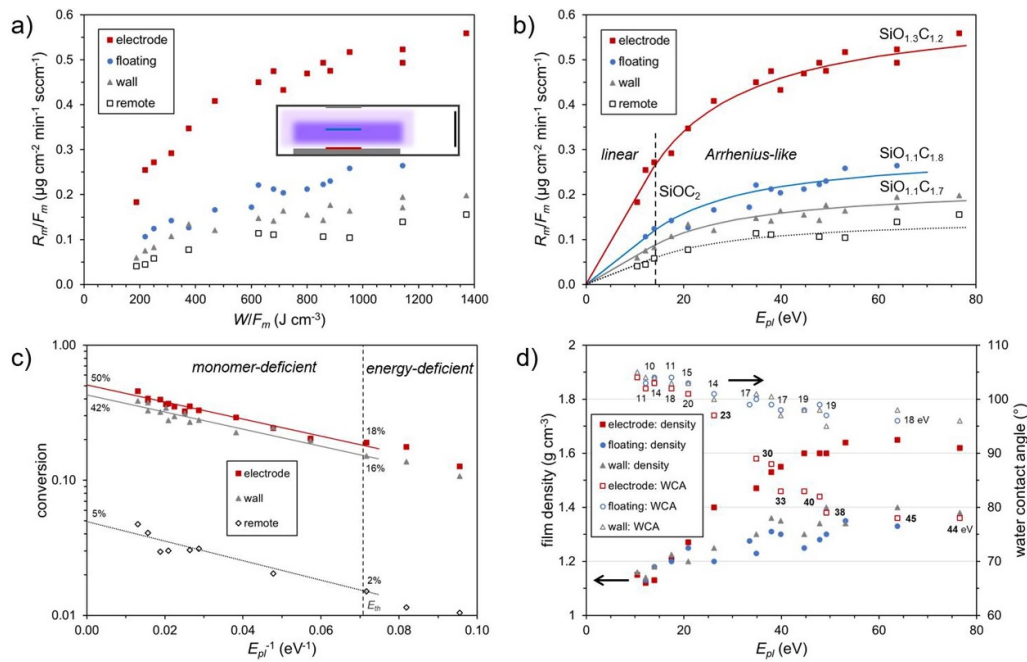


**Figure 14.** Plasma polymerization of HMDSO highly diluted in Ar in a large asymmetric CCP reactor (at 4 Pa pressure). (a) Normalized mass deposition rates plotted over  $W/F$  using external parameters. Samples were placed at different positions in the plasma reactor as indicated in the inset. (b) Same plot as in (a) after calculation of the energy invested per HMDSO molecule in the plasma,  $E_{pl}$ , with linear and Arrhenius-like fittings around  $E_{th}$ . Chemical compositions are indicated for different parameters. (c) Equal slopes of the Arrhenius-like fits (same  $E_{th}$ ) are observed at substrate positions close to the plasma albeit with different deposition rates yielding different fractions of the overall conversion. (d) Film density and hydrophobicity follow  $E_{pl}$  for deposited energies,  $E_d$ , up to around 20 eV (indicated by the added numbers). For higher  $E_d$  at the electrode, the ion bombardment causes additional densification and ablation of hydrocarbons.

In addition, film properties such as hydrophobicity, chemical composition, and film density were found to mainly depend on  $E_{pl}$  (figure 13(d)) despite the use of different pressures yielding largely varying  $E_d$  (see figure 2(d) for illustration). While this is clearly indicative of plasma-state polymerization, where hydrophobic film properties can be optimized by controlling  $E_{pl}/E_{th}$ , the role of surface processes in HMDSO plasmas needs to be further investigated.

To this end, the PP of HMDSO highly diluted in Ar plasmas was examined using an asymmetric, large reactor ( $21 \times 70 \text{ cm}^2$  electrode size) at a low pressure of 4 Pa ( $W$ : 35–100 W,  $F_m$ : 2–6 sccm,  $F_{Ar}$ : 45 sccm) [53]. Substrates were placed at different positions to enable large variation in  $E_d$ : directly at the electrode (with negative bias potential), immersed in the plasma (at floating potential), at the wall (grounded), and remote (20 cm downstream) as schematically displayed in figure 14(a). The macroscopic approach to describe PP will be illustrated in the following based on these conditions.

At first, mass deposition rates are measured by weighing and then plotted (normalized to  $F_m$ ) over  $W/F_m$  using the power input from the generator (figure 14(a)). Note that a (minor) energy uptake by the carrier gas should be taken into account [165]. Next,  $W/F_m$  can be converted to  $E_{pl}$  according to equation (15). Here, a power absorption,  $f_{abs}$ , of 60% (using  $VII$  probe) and a plasma expansion,  $d_{act}/d$ , of about 40% (based on luminosity distribution above the electrode) were determined for the fixed pressure of 4 Pa (figure 14(b)). The latter might also depend on  $W$  and  $F$ , however, it was

found to be rather constant due to the high Ar dilution. Fitting the data indicates the linear as well as the Arrhenius-like regime.

To calculate the conversion from HMDSO monomer into film-forming species deposited in different areas (electrode, wall, and remote) according to equation (13),  $M_{dep}$  can be estimated from the observed chemical composition, e.g. using XPS. At low  $E_{pl}$ ,  $M_{dep}$  is 74 amu based on  $\text{SiO}(\text{CH}_3)_2$  radicals yielding PDMS-like films, reducing to about 61 amu ( $\text{SiO}(\text{CH}_2/3)_{1.2}$ ) at the electrode, and about 69 amu ( $\text{SiO}(\text{CH}_2/3)_{1.7-1.8}$ ) at the floating or the wall positions at high  $E_{pl}$ . Note that the enhanced O incorporation results from post-plasma oxidation of trapped radicals, which is why  $R_m$  should be corrected as well. Since both corrections tend to balance each other, these effects might be neglected but were considered in figure 13(c). From the modified Arrhenius plot, again, threshold energy,  $E_{th}$ , of  $14 \pm 1 \text{ eV}$  was derived as required to activate PP of HMDSO, valid for all positions within the asymmetric plasma chamber. Vice versa, the accepted value for  $E_{th}$  of 14 eV for the considered reaction pathway could be used to determine the often unknown geometrical factor of a specific plasma reactor set-up. It is noteworthy that an almost complete conversion was observed for the discussed parameters adding to about 36% at  $E_{pl} = E_{th}$ , whereby half of the produced film-forming species are directed towards the RF electrode. The smaller electrode area thus results in the highest deposition rate followed by floating and wall positions (figure 14(a)). Note that by reaching maximum conversion, the

PP mechanism is no longer limited by  $T_e$  [53]. Interestingly, the deposition rates follow the same quasi-Arrhenius behavior even 20 cm remote from the active plasma zone. It can thus be inferred that PP of HMDSO at low pressure is mainly governed by gas phase activation, while possible recombination and oligomerization reactions in the downstream region do not affect the deposition mechanism [166]. This might be different at AP owing to an increased number of collisions, where a 20 cm path at 4 Pa corresponds to just about 8  $\mu\text{m}$  at AP conditions [167].

Reactions at the surface that influence film growth can be discussed by assessing film density and related wettability as presented in figure 14(d). To this end, excitation and bias voltage,  $n_e$ ,  $T_e$ , and plasma expansion were determined. The effect of collisions reducing the energy flux at the electrode was estimated as in Ar (see figure 2(d)) while floating conditions were assumed to be collision-free. For values of  $E_d$  up to around 20 eV per deposited SiOCH species, ion bombardment shows a minor influence on the film properties, whereas it causes increasing densification and ablation of hydrocarbons at the surface for higher values. Hence, a more inorganic film composition of  $\text{SiO}_{1.3}\text{C}_{1.2}$  was detected for the highest  $E_{pl}$  at the electrode, while PDMS-like PPFs can be obtained when  $E_{pl}$  is kept close to  $E_{th}$  independent of sample position. The resulting hydrophobic films were found to be highly stable containing a low number of defects, and well-suited to delay water intrusion taking place by a reaction-diffusion mechanism [168]. Such optimized plasma conditions can thus be used as diffusion-controlled barrier SiOCH layers in aqueous environments [169].

Owing to the well-understood plasma chemistry of HMDSO related to plasma-state polymerization, HMDSO might be used as a model monomer to investigate the characteristics of plasma reactors as illustrated above. Besides HMDSO, a variety of further monomers for PP can be evaluated based on the discussed macroscopic approach [150, 170–176]. A detailed analysis gives hints on the reaction mechanism and allows for the differentiation between the gas phase and surface processes. It thus contributes to the understanding of complex PP processes to design coatings with tailored properties, while upscaling and transfer to the industry are supported. Using model monomers such as HMDSO with determined  $E_{th}$  for the reaction pathway, the macroscopic approach can be used to link microscopic and macroscopic parameters and to assess parameters that might be difficult to measure otherwise.

## 4. PECVD for the synthesis of inorganic coatings

### 4.1. State of the art and current limitations

Key parameters that influence the film microstructure in low-pressure low-temperature deposition processes are the ion energy ( $E_i$ ) and ion flux ( $\Gamma_i$ ). In the PECVD process these are most frequently controlled by the choice of excitation frequency (e.g. RF or MW), or by applying pulsed DC or RF-induced negative substrate bias,  $V_B$  (see section 2.3). The IEDF can be evaluated in the process chamber using

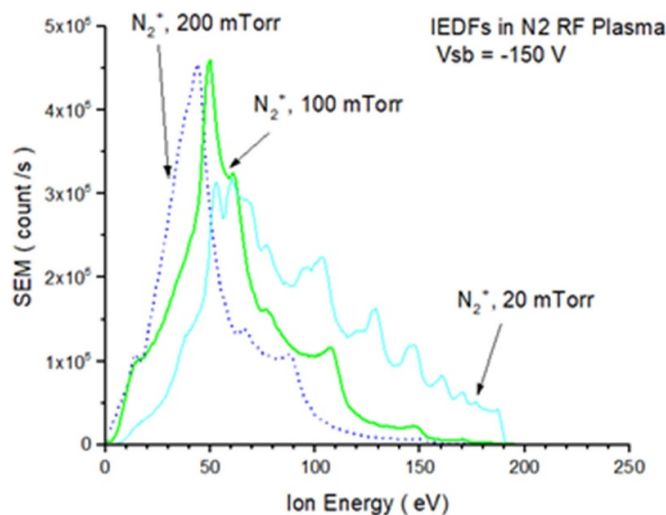


**Figure 15.** Examples of the IEDFs of  $\text{N}_2^+$  ions in RF plasma in nitrogen at three different pressures measured on the powered electrode in a reactor such as the one in figures 3(a) and (b).  $V_{sb}$  denotes the self-bias voltage ( $=V_B$ ).

a multigrid electrostatic ion energy analyzer (IEA) [177] or a quadrupole mass spectrometer integrated with an IEA [178, 179].

An example of the IEDFs on the powered electrode (frequently used as a substrate holder) in an RF CCP is shown in figure 15. As shown,  $E_i$  can reach several tens or several hundreds of eV. We note, that the IEDF is characterized by a peak  $E_i$  and a relatively long energy tail that increases with a decreasing pressure due to less inelastic collisions where the ions lose part of their energy. One can also see that the IEDFs are structured due to sheath modulation when the ions are accelerated and decelerated during their passage through the sheath [71, 177]—specifically, the sheath thickness increases with decreasing the pressure. It is also worth mentioning that the IEDFs,  $n_e$ ,  $V_B$ , and  $V_p$  values in PECVD are very similar to those encountered on the powered electrode in magnetron sputtering and reactive ion etching systems. Finally, the possibility of controlling  $E_i$  and  $\Gamma_i$  values is important for adjusting film microstructure and hence, specific properties and functional and device characteristics, as discussed below.

Appropriate control of ion bombardment energy ( $E_i < 1 \text{ keV}$ ) is particularly important in the context of the deposition of thin films at low substrate temperature,  $T_s$ . Film growth while under ion bombardment leads to growth-related effects such as interfacial atom mixing, high surface mobility (diffusion) of deposited species, re-sputtering of loosely bound species, and deeper penetration of ions below the surface ('sub-plantation'), leading to the displacement of atoms (forward sputtering or knock-in effects) [180, 181]. Such phenomena give rise to the disruption of growth nuclei, to the suppression of columnar structure, and hence to material densification. This is in agreement with the structure zone model (SZM) first proposed by Movchan and Demchichin [182], improved by Thornton [183] and Messier *et al* [184],

and finally refined by Anders [185] for PVD processes, but also valid for PECVD [46].

Various approaches to quantitatively describe the effect of ion bombardment have been developed. It appears that a key parameter for representing these effects is the energy  $E_p$  delivered to the growing film per deposited particle [186]:

$$E_{p(T_s=\text{const})} = (E_i\Gamma_i + E_m\Gamma_m)/(\Gamma_n + \Gamma_t) \sim E_i(\Gamma_i/\Gamma_n), \quad (16)$$

where  $E$  denotes energy,  $\Gamma$  the particle flux; and the indices  $i$ ,  $m$ ,  $n$ , and  $t$  refer to ions, condensing precursor (monomer) species (radicals), neutrals, and trapped inert gas, respectively.  $E_p$  is an equivalent of  $E_d$  (equation (6)) but is defined by the flux of neutrals that stay on the surface rather than those that arrive at it (by considering  $s$ , in addition). As a first approximation, one can neglect  $\Gamma_t$  compared to  $\Gamma_n$  and  $E_m\Gamma_m$  compared to  $E_i\Gamma_i$  and obtain the simplified relation in equation (16). Such an approximation is possible in a case when ions bring most of the energy to the surface, e.g. in ion beam experiments; however, the energy flux of neutral particles may become significant in PECVD because a certain fraction of the initially accelerated ions become neutral due to charge transfer collisions in the sheath region. Detection of neutral species and determination of their energy is difficult, requiring careful measurements, using MS combined with ion energy analysis [178, 179].

It has been proposed that there exist critical ion energies, and critical ion flux ratios [ $E_{i,c}$  and  $(\Gamma_i/\Gamma_n)_c$ ], which can be associated with transitions in the evolution of film microstructure and properties [66, 187]. Clearly,  $E_p$  in equation (16) can be adjusted to the same level by combining low and high  $E_i$  and  $\Gamma_i/\Gamma_n$  values. However, experience suggests that good-quality (dense, hard, chemically stable, low stress) films are obtained under conditions of low (10–50 eV) or intermediate (about 100 eV) ion energies, sufficient for densification ( $E_i \sim E_{i,c}$ ), but using high  $\Gamma_i$ . This reduces microstructural damage and gas entrapment, generally yielding low values of stress. High fluxes are highly advantageous, especially when one aims at achieving high deposition rates,  $r_D$  ( $>10 \text{ nm s}^{-1}$ ).

In figure 16 the  $E_{i,c}$  and  $(\Gamma_i/\Gamma_n)_c$  values for PECVD  $\text{SiO}_2$ ,  $\text{Si}_3\text{N}_4$ ,  $\text{TiO}_2$ , and a-C:H films have been compared with the compilation of literature data by Auciello and Kelly [187] who summarized examples of  $E_{i,c}$  and  $(\Gamma_i/\Gamma_n)_c$  values reported to be necessary for property modification in numerous materials deposited by different (non-PECVD) ion-assisted techniques. It was concluded that the  $E_{i,c}$  values are lower, and  $(\Gamma_i/\Gamma_n)_c$  values are higher for most of the PECVD processes than most of the other techniques. The energetic conditions leading to good-quality films obtained by the MW PECVD process (while the MW discharge can be continuous wave or pulsed) also fall within the same energy limits, that is low  $E_i$  ( $E_i < 10 \text{ eV}$ ) but high  $\Gamma_i/\Gamma_n$  ( $\sim 1$ – $10$ ) values, due to a high plasma density and ionization rate [188]. In this context, to derive appropriate relations between  $E_i$  and  $\Gamma_i/\Gamma_n$ , and to benefit from the availability of experimental data, one can apply the conversions for the experimentally measured ion current, where  $1 \text{ mA cm}^{-2}$  corresponds to  $6.25 \times 10^{15} \text{ ions cm}^{-2} \text{ s}$ , and a useful relation [189]:

$$\Gamma_n = r_d \rho N_A / m, \quad (17)$$

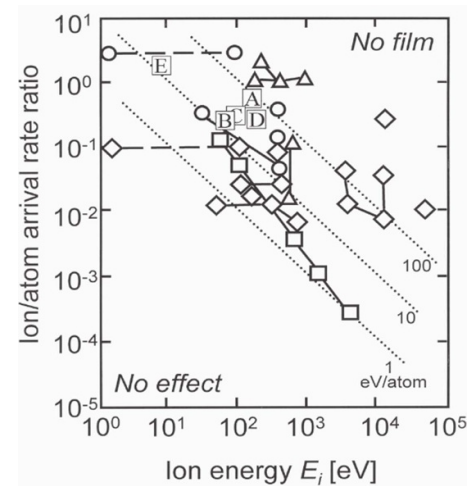


**Figure 16.** Plot of critical ion/condensing particle arrival rate ratios  $(\Gamma_i/\Gamma_n)_c$  vs critical ion energy  $(E_i)_c$ , required for film structural modification, particularly densification: (A)  $\text{SiN}_{1.3}\text{H}$ ; (B)  $\text{SiO}_2\text{H}$ ; (C) a-C:H; (D)  $\text{TiO}_2$ ; (E)  $\text{TiO}_2$  obtained in a MW/RF discharge (based on [188]). For comparison, other data points are from [187] for different materials obtained by PVD techniques: (O)  $\text{SiO}_2$ , ( $\Delta$ ) other dielectrics, ( $\square$ ) metals, and ( $\diamond$ ) semiconductors. Reproduced with permission from [19]. © 2000 American Vacuum Society.

where  $N_A$  is Avogadro's constant while  $\rho$  and  $m$  are the density and the molecular mass, respectively, of the film material.

We conclude from figure 16, that for most materials, energy may range from several to several hundreds of electron volts per film-forming particle [181]. These relatively high  $E_p$  values were obtained as a result of process and materials optimization, and point to the trend in recent deposition techniques, favoring lower  $E_i$  and high  $\Gamma_i$  [19, 189]. In addition,  $E_p$  appears to be higher for materials with a higher melting point, a result is in agreement with the SZM. This rather simplified approach does not take into account the fact that at a relatively high pressure considerable energy is also delivered to the growing surface by energetic neutrals as indicated in the full equation (16) [55].

As a complement to ion bombardment during the film growth, one should also consider another source of energetic plasma-surface interactions, namely photons in the entire range from infrared (IR) and visible to UV, VUV, and soft x-ray regions (for a review, see [190]). In particular, VUV photons play an important role in the interaction with organic (polymer) surfaces, since their energy of more than 10 eV can break any chemical bond. Of considerable importance in active plasmas is the radiation in discharges containing hydrogen with its strong Lyman line at 121 nm and intense molecular bands, oxygen with its strong resonant line at 130 nm, and helium (intense lines at 57 nm and above), which are particularly effective [49, 50]. In this context, intense VUV features due to the excitation of different discharge components including impurities (fragments of  $\text{H}_2$ ,  $\text{SiH}_4$ ,  $\text{CH}_4$ ,  $\text{H}_2\text{O}$ , hydrocarbons, and others) desorbed from chamber walls and polymer substrates may be very important and can participate in controlling the characteristics of polymer surfaces, of



coating-polymer interfaces, and contribute to photo-induced reactions, the latter one possibly giving rise to deposition. It should be mentioned, however, that the impact of VUV photons on metals is much less pronounced compared to covalent materials because the electronic excitation by photons quickly dissipates among the free electrons of the metal.

These principles and associated strategies have been successfully applied to grow many types of coatings for decades. Among these materials, optical and tribological coatings are very good examples of the flexibility and efficiency of the PECVD processes. These are described in more detail in the next sections.

#### 4.2. Synthesis and performance of PECVD optical coatings

Optical coatings represent a particularly important category of PECVD technology since it allows one to control the optical characteristics over a large range and tune their additional functional (multifunctional—e.g. gas/vapor permeation barrier, wear resistance, corrosion protection, etc) properties suitable for optical interference filters (OIF) and other optical applications. Optical properties are determined either from spectrophotometric (reflectance,  $R$ , and/or transmittance,  $T$ ) and/or ellipsometric measurements.

The basic optical properties, namely the refractive index  $n$  of the most frequently studied optically transparent PECVD films are summarized in figure 17, where they are compared with those of the most often used substrates. The optical applications require the availability of materials with low, high, and intermediate indices ( $n_L$ ,  $n_H$ ,  $n_M$ ) that are related to the composition as well as the microstructure (particularly the packing density) controlled by the fabrication conditions.

Regarding the optical characteristics, we can divide the materials into several categories: (i) silicon-based (inorganic) coatings, (ii) metal oxide PECVD coatings, and (iii) carbon-based coatings and related covalently bonded materials including PPFs.

**4.2.1. Silicon-based (inorganic) coatings.** Silicon compound films have been studied for many decades because of their use in microelectronics, microsystems (MEMS), optics and photonics, photovoltaics, and other areas. PECVD Si-based films are generally amorphous, and contain considerable amounts of hydrogen, due to the use of precursor gases such as silane ( $\text{SiH}_4$ ) and organosilicones (OS). The most frequently applied systems include silicon oxide ( $\text{SiO}_2$ ), silicon nitride ( $\text{SiN}_{1.3}$ ), silicon oxynitride ( $\text{SiO}_x\text{N}_y$ ), hydrogenated amorphous silicon (a-Si:H), and silicon carbide (a-SiC:H).

Among all dielectric and silicon-compound coatings, **silicon dioxide** ( $\text{SiO}_2$ ) is probably the most studied PECVD material, typically deposited from a mixture of  $\text{SiH}_4$  and  $\text{O}_2$  or  $\text{N}_2\text{O}$ . Both theoretical and experimental studies of the various phases of  $\text{SiO}_2$  underline the link of the film characteristics, such as  $n$ , optical gap,  $E_g$ , and others, to the microstructure, in particular, the Si–O–Si mean bonding angle,  $\theta$  [191, 192], density [193], and H incorporation. In amorphous  $\text{SiO}_2$ , changes in  $\theta$  values can be estimated experimentally from IR

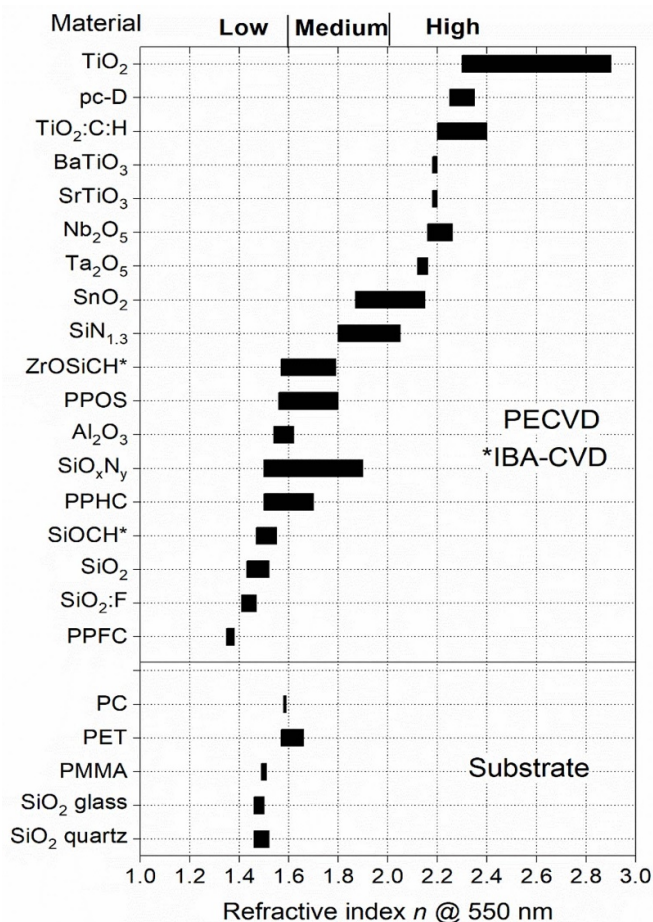


**Figure 17.** Typical refractive index values of transparent PECVD and \*IBA-CVD (ion beam assisted CVD) films. Reprinted from [46], Copyright (2010), with permission from Elsevier.

spectra of the Si–O–Si stretching mode at  $2260\text{ cm}^{-1}$ . A small  $\theta$  value is related to a stressed network in a dense structure.

Small-angle Si–O–Si bonds are unstable. They can be broken by an accumulation of stress and force the network to relax, leading to a more flexible structure, accompanied by the formation of defect centers, or by a reaction with water [194]. In the latter process, water absorption in pores may not necessarily be associated with aging, since not all types of pores give rise to water sorption, but the concept of ‘open’ and ‘closed’ pores and their size should be considered [195].

$\text{SiO}_2$  usually contains 5–15 at.% of hydrogen, mostly in the form of –OH, which affects the optical properties and stability. It has been shown that during deposition from a  $\text{SiH}_4/\text{O}_2$  mixture, the surface of the growing oxide is initially covered with silanol ( $\text{SiOH}$ ) [196], due to the instant oxidation of  $\text{SiH}_x$  by atomic oxygen. The  $\text{SiH}_x$  groups react further with  $\text{SiOH}$  and Si–O–Si to yield  $\text{H}_2\text{O}$  and Si–O– $\text{SiH}_x$ , which are oxidized by neutral O, leading to superficial –SiOH terminations.

$\text{O}_2^+$  bombardment seems to be particularly efficient for reducing [H] in the film [196]. When the dissociation of  $\text{SiH}_4$  is high, Si exists on the surface, and it is easily oxidized, compared with  $\text{SiH}_2$  and  $\text{SiH}_3$  groups, for which several reactions with oxygen are needed to release all the H atoms. This means

that high  $n_e$  (high discharge power) can reduce H concentration, such as in the MW plasmas [66, 197].

An important issue with silane as a precursor is the formation of particles due to the radicals from silane that can react rapidly in the gas phase. This results in nodules and large voids in the films. Several steps can help to solve such problems, namely: (i) reduced operating pressure; (ii) dilution of  $\text{SiH}_4$  in Ar or He; (iii) heating the electrode; and (iv) use of a pulsed discharge [198]. Frequently, organosilicon precursors are used to replace  $\text{SiH}_4$  to avoid hazards (it is strongly pyrophoric) and to increase surface coverage. Therefore, the deposition of  $\text{SiO}_2$  from HMDSO and tetra ethoxysilane (TEOS) is widely used.

It should be mentioned at this point that there exist numerous activities trying to deposit high-quality  $\text{SiO}_2$  coatings at AP—this, however, leads to limited success because the densification by ion impact is almost absent (see further comments in section 5.1).

Work on **fluorinated  $\text{SiO}_2$**  ( $\text{SiO}_2\text{:F}$  or  $\text{SiOF}$ ) has been stimulated by the search for low index and low permittivity (low- $k$ ) materials for optics and photonics, to reduce the parasitic capacitance in multilevel interconnects in microelectronic devices [199]. In such a case,  $n$  could be reduced to 1.41–1.43 (@550 nm), compared to 1.45–1.48 for non-fluorinated  $\text{SiO}_2$  (figure 17).

Fluorine was chosen due to the low- $k$  properties of fluoropolymers, and the properties of fluorine-doped amorphous silicon (a-Si:F), in which fluorine plays a stabilizing role, while passivating dangling bonds and reducing [H]. Many methods involving plasma have been applied to fabricate  $\text{SiOF}$ , using different organic and inorganic precursors, most frequently  $\text{TEOS}/\text{O}_2/\text{CF}_4$ ,  $\text{TEOS}/\text{O}_2/\text{C}_2\text{F}_6$ , and  $\text{SiH}_4/\text{O}_2/\text{CF}_4$  mixtures (for a review see [19]).

Among possible  $n_H$  materials, **silicon nitride** ( $\text{SiN}_{1.3}$ ) has been widely used because of its transparency, hardness, impermeability, and other advantageous functional properties. It can be deposited using  $\text{SiH}_4$  mixed with nitrogen ( $\text{N}_2$ ) or ammonia ( $\text{NH}_3$ ). The use of OS precursors is limited by the presence of carbon in the final product. When deposited at low temperatures and low energy conditions,  $\text{SiN}_{1.3}$  exhibits a columnar structure; therefore, more energy must be brought to the surface by ion bombardment or substrate heating to achieve high packing density. The residual gas concentration in the PECVD reactor must also be kept very low, as  $\text{SiN}_{1.3}$  can react rapidly with traces of  $\text{O}_2$  or  $\text{H}_2\text{O}$  [200].

The main ‘impurity’ in  $\text{SiN}_{1.3}$  is hydrogen, which significantly affects the electronic and optical properties. Replacing Si–N with Si–H has little effect on the gap ( $E_g = 5.3$  eV for H-free  $\text{SiN}_{1.3}$ ) [201], but N–H bonds considerably reduce the value of  $n$ . One way to avoid H incorporation is to use silicon halide precursors, such as  $\text{SiCl}_4$  or  $\text{SiF}_4$  [202]. Attempts have been reported to deposit ‘nitride-like’  $\text{SiN}_{1.3}$  films using OS precursors, using, for example, hexamethyl disilazane, and hexamethyl cyclosilazane, [203] mixed with  $\text{N}_2$  or  $\text{NH}_3$ .

Coatings with an intermediate refractive index,  $n_M$ , can be obtained by adjusting the gas composition [204, 205] or by controlling the film density [205, 206]. The most extensively used  $n_M$  material is **silicon oxy-nitride**,  $\text{SiON}$ , obtained from gas mixtures with  $\text{SiH}_4$  using varying nitriding versus

oxidizing gas ratios (e.g.  $\text{NH}_3/\text{N}_2\text{O}$  or  $\text{N}_2/\text{O}_2$ ). Since O has more affinity to Si than N, one can choose to control only the  $\text{O}_2$  flow [207].  $\text{SiON}$  films exhibit homogeneous and amorphous microstructures, close to those of a solid solution [208], and no crystal formation has been observed up to a temperature of 900 °C. The use of  $\text{SiON}$  films allows one to benefit from the advantages of the specific characteristics of individual  $\text{SiO}_2$  and  $\text{SiN}_{1.3}$  layers and, besides controlling  $n$ , it is also possible to adjust the film stress and charge trapping suitable for electret microphones, electret-enhanced solar cells, etc [209].

**4.2.2. Metal oxide optical coatings.** Fabrication of metal oxide films has been stimulated by the prospect of obtaining high  $n$ , high hardness, advantageous tribological properties, and numerous other functional characteristics. The films are generally prepared from halocarbons or from metal-organic compounds which exhibit specific requirements for handling low vapor pressure sources and/or corrosive products [210]. Among  $n_H$  materials, **titanium dioxide** ( $\text{TiO}_2$ ) attracts much attention due to its large bandgap, high  $n$  (exceeding 2.4 @ 550 nm), and its photocatalytic properties. Its high  $n$  is due to the high ionic character of the  $\text{TiO}_6$  octahedral structure, the building block of rutile, and anatase.

The deposition of transition metal oxides such as  $\text{TiO}_2$  is complicated by the fact that they can take different forms and stoichiometries (e.g.  $\text{TiO}$  or  $\text{Ti}_2\text{O}_3$ ) [211]. In addition, in the case of  $\text{TiO}_2$ , three stable crystalline phases are possible: rutile, anatase, and brookite. Rutile, with the highest density, is the most desired phase in terms of transparency and index, but also has the highest birefringence, with  $n_{\text{ord}} = 2.9$  and  $n_{\text{ext}} = 2.6$ , and is often unwelcome because of light scattering. Anatase, which differs from rutile in the coordination number of its  $\text{TiO}_6$  octahedra (10 in the case of rutile, 8 for anatase), is less birefringent and has  $n = 2.5$ . Brookite, an unstable rhombohedral structure, is rarely observed in thin films.

The most frequently used precursors for plasma deposition of Ti-compounds are  $\text{TiCl}_4$  (mixed with  $\text{O}_2$ ), TIPT, TEOT,  $\text{Ti}(\text{O}-i\text{-C}_3\text{H}_7)_4$ , and  $\text{Ti}[\text{OCH}(\text{CH}_3)_2]_4$  [19]. The use of metal-organic precursors has been stimulated by two considerations: (i)  $\text{TiCl}_4$  is hazardous, highly corrosive, and requires special installations; and (ii) Cl can be a major contaminant in  $\text{TiO}_2$ , increasing its absorption coefficient and decreasing long term stability.

Both rutile and anatase are tetragonal and often coexist in films. High temperatures and  $E_i$  may be needed during growth to control the rutile/anatase concentration ratio. At temperatures below 200 °C, anatase is frequently observed, lowering  $n$ . Using a  $\text{TiCl}_4/\text{He}/\text{O}_2$  mixture [212], it was observed that rutile is usually formed above 600 °C and that it is the only phase observed above 900 °C. Room temperature-deposited films generally possess a low concentration of Cl (~5%), which further decreases with increasing  $T_s$  and  $V_B$ , accompanied by an increase of  $n$  from 2.25 to 2.50. The films often exhibit excess oxygen ( $\text{O}/\text{Ti} > 2$ ), related to hydroxyl groups and to film density, which affects the  $n$  value.

**Tantalum oxide** and **niobium oxide** have been deposited by PECVD using a mixture of metal isopropoxide



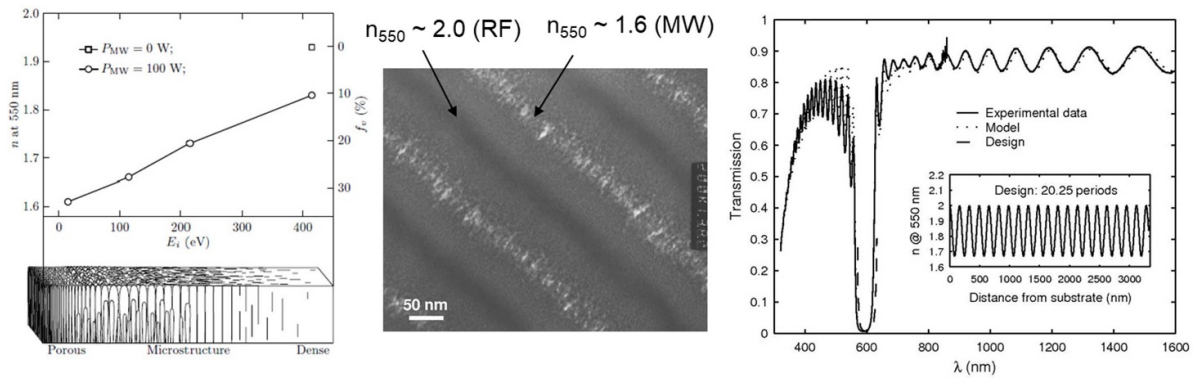


**Figure 18.** Single-material optical coatings based on the control of porosity in  $\text{SiN}_{1.3}$  films: (a) variation of the refractive index and the void volume fraction as a function of  $E_i$  in the discharge; (b) transmission electron microscopy (TEM) micrograph of the filter cross-section with continuously varied  $n$ , and (c) optical transmission of a dense/porous graded ('rugate') filter based on the continuous variation of  $n$  (see insert). Reprinted with permission from [206] © The Optical Society (b, c). Reproduced with permission from [222] (a).

( $\text{Ta}(\text{OC}_2\text{H}_5)_5$  or  $\text{Nb}(\text{OC}_2\text{H}_5)_5$ ) and  $\text{O}_2$  with Ar and an RF plasma under intense ion bombardment. Their  $n$  values were found between 2.12 and 2.16, and 2.26, respectively [213]. In comparison, medium index **aluminum oxide** ( $\text{Al}_2\text{O}_3$ ) ( $n = 1.62$ ) has been prepared from  $\text{AlBr}_3$ ,  $\text{AlCl}_3$ , trimethylaluminum (TMA), or trimethylamine alane (TMAA) precursors [19, 210, 214].

Studies of numerous other PECVD optical coatings have been stimulated by an attempt to combine optical properties, conductivity, color, and other effects. These include transparent conductors such as **tin-oxide** ( $\text{SnO}_2$ ) [215] and **indium-tin-oxide** [216], high-permittivity **barium titanate** ( $\text{BaTiO}_3$ ), **strontium titanate** ( $\text{SrTiO}_3$ ), and electrochromic **tungsten oxide** ( $\text{WO}_3$ ) [217–219].

PECVD can provide  $n_H$ ,  $n_L$ , and  $n_M$  materials for any simple or complex OIF. The design strategies can be based on three types of approaches [19]: (i) multilayer (step index) design, using two or more materials with different indices, (ii) inhomogeneous [graded index depth profile,  $n(z)$ ] design, and (iii) quasi-inhomogeneous design when very thin layers with varied composition are consecutively applied, providing properties close to that of an inhomogeneous design. Specifically, inhomogeneous filters (approach (ii)) offer an optical advantage of suppressing harmonics and sidelobes in the filter performance, while the absence of sharp interfaces helps to decrease residual stress and increase coating mechanical durability [19, 220]. In such approaches, at each instant of the deposition process, the  $n(\lambda)$  dispersion and  $r_D$  value must be known and controlled.

Typically, the  $n$  value is continuously varied between  $n_H$  and  $n_L$  during the deposition process, mostly by changing the gas composition [19]: materials such as  $\text{SiON}$  and  $\text{TiO}_2/\text{SiO}_2$  have been tested with success [220]. An interesting approach well illustrating the importance of plasma-surface interactions, is the fabrication of a single-material porous/dense system in which the variation of  $n$  as a function of depth is achieved by changing  $E_i$ , specifically the substrate bias potential for the control of film microstructure (packing density—porosity) [206] illustrated in figure 18. Controlling the ion bombardment characteristics in the growth of  $\text{SiN}_{1.3}$  films allows one to vary

$n$  from 1.50 to 1.90 by tailoring the film porosity (pore volume fraction, figure 18(a)) in agreement with the SZM, making it possible to fabricate (discrete) multilayer as well as inhomogeneous filters with one single material. Such filters have been designed and fabricated, and examples of the corresponding  $n(z)$  profile, optical transmission spectrum, and TEM micrograph are shown in figures 18(b) and (c) [221, 222]. In this case, a shift of the peak in reflection due to the sorption of gases or vapors in the pores has been proposed for all-optical gas or vapor sensors [223].

**4.2.3. Carbon-based coatings.** Optical applications of carbon-based materials have been stimulated by a combination of their advantageous functional properties ranging from optical transparency in the IR to high hardness and low friction, high corrosion resistance, high heat conductivity, and biocompatibility. They can be categorized, depending on the  $sp^1$ ,  $sp^2$ , and  $sp^3$  hybridizations, level of structural order, as well as by hydrogen concentration [149, 224–226] (see figure 19). We distinguish among the most frequent forms of carbon-based films, namely (i) PECVD DLC or hydrogenated amorphous carbon (a-C:H); (ii) polycrystalline diamond, pc-D; and (iii) soft organic carbonaceous coatings (plasma polymers) obtained under 'mild' plasma conditions. The latter one defines its own family of coatings (PPFs) and has been extensively discussed in section 3 above.

In this context, several categories of organic amorphous PECVD films prepared from hydrocarbon precursors under controlled ion bombardment can be distinguished based on  $E_i$ : (a) plasma polymers,  $E_i < 30$  eV ( $[\text{H}] = 35$  at.%, and  $n = 1.6$ ); (b) soft ('polymer-like') DLC,  $E_i = 30$ –60 eV ( $[\text{H}] = 30$  at.%, and  $n = 1.6$ –1.8); and (c) hard DLC,  $60$  eV  $< E_i < 1$  keV ( $[\text{H}] = 20$  at.%,  $n = 1.8$ –2.2, and  $E_g = 1.3$ –2.0 eV). The presence of hydrogen contributes to the formation of C–H  $\sigma$  bonds at the expense of  $\pi$  bonds ( $sp^2$  hybridization). A detailed study of the effect of  $E_i$  and  $\Gamma_i$  values on the film growth has revealed that a significant amount of hydrogen is not chemically bonded, but it is trapped as molecular hydrogen inside the material [227].

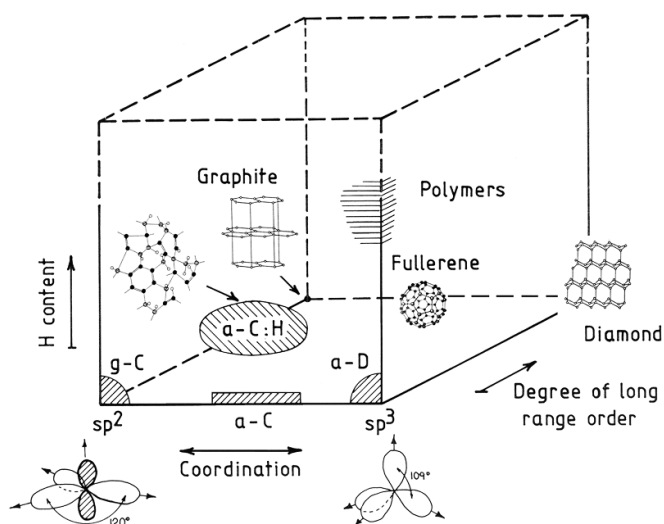


**Figure 19.** Schematic representation of different phases of carbon distinguished by the carbon coordination, degree of range order, and hydrogen content. In the literature, the different carbon hybridizations in the DLC have also been indicated using a triangular diagram with  $sp^2$ ,  $sp^3$  and H in its corners at first introduced by Robertson [149]. See also for instance [46]. Reproduced with permission from [228].

**Polycrystalline diamond** (pc-D) films typically deposited from  $CH_4/H_2$  mixtures in high frequency (MW) plasma at temperatures above  $700^\circ C$  have a high refractive index ( $n = 2.35$ ) and transparency over a large wavelength range ( $0.2\text{--}20\ \mu m$ ) and have attracted much attention due to their extreme hardness ( $H = 90\text{--}100\ GPa$ , see figure 20), heat conductivity and chemical inertness. Their unique properties have stimulated considerable interest in numerous applications, ranging from infrared optics to electronics, biomedical engineering, manufacturing, and numerous other sectors (for reviews, see [229–231]).

Research on plasma polymers has frequently focused on **plasma polymerized fluorocarbons** (PPFC), stimulated by the prospect of obtaining low  $n$  and low  $\epsilon$  values, similar to those of bulk polytetrafluoroethylene (for example, Dupont Teflon, with  $n = 1.35$ ) or for amorphous fluorocarbons, such as Dupont Teflon AF2400 ( $n = 1.29$ ) or Teflon AF1600 ( $n = 1.31$ ) [47, 232, 233]. There is now abundant literature on the use of fluorocarbon plasmas for film deposition and anisotropic etching of silicon and silicon dioxide [48, 234]. By suitably adjusting the experimental parameters, one can shift the plasma conditions from etching to deposition [74]. Various precursors have been explored for deposition, including  $C_2F_4$ ,  $C_2F_6$ ,  $C_4F_8$ ,  $C_3F_6$ ,  $C_2H_2F_4$ , and  $CH_2F_4$  [47, 235, 236]. The low dispersion and low  $n$  which are frequently observed, are generally attributed to a high concentration of  $CF_2$  groups in the films.

**Amorphous hydrogenated silicon carbide** (a-SiC:H or SiC) coatings are attractive due to their optical, electronic, and mechanical properties [191, 237, 238]. Using PECVD, SiC is usually obtained from varying mixtures of  $SiH_4$  and  $CH_4$  at relatively low substrates temperatures ( $T_S = 200^\circ C\text{--}400^\circ C$ )

[237, 239]. Ternary Si compound coatings, such as SiCN, have become increasingly attractive since they can combine the advantages of the individual binary materials and their intrinsic properties, specifically of  $SiN_{1.3}$ , SiC, and CN when considering the infrared and tribological properties [240].

**Graphene and other 2D materials:** Graphene is a two-dimensional material composed of carbon atoms forming a hexagonal crystal lattice. Since graphene was properly isolated and characterized in 2004, it attracted great attention due to its unique electrical, optical and mechanical properties. The synthesis of high-quality large-surface graphene is still a challenge despite the great effort to fabricate this material through different techniques including exfoliation, epitaxial growth, and thermal CVD [241]. As in many other cases, PECVD allows one to lower the deposition temperature of graphene films. In addition, one can produce such films without the use of a catalyst, making this technique attractive for many applications including optoelectronics, flexible displays, sensors, drug delivery, etc. Both, the low-pressure [242] and the AP [243] PECVD were successfully used for the deposition of high-quality graphene films. In addition, other 2D materials such as  $BC_xN$  and hexagonal boron nitride (h-BN) were also produced by PECVD. It is worth noting that plasma activation has been explored to modify the graphene properties by doping it with nitrogen, oxygen, fluorine, and other molecules [244].

#### 4.3. Synthesis and performance of protective and tribological coatings

**Metal nitride and carbide** (MeN, MeC), **carbonaceous and nanostructured PECVD** protective and functional coatings have been successfully used due to their excellent mechanical [245–247] properties such as high hardness ( $H$ ), adhesion, and wear- and corrosion resistance, which makes them attractive for tribological and biomedical applications. In addition, such materials frequently provide attractive colors [248] as a consequence of mixed covalent and metallic bonding [249].

In general, for tribological coatings,  $H$  and coefficient of friction,  $C_f$ , have usually been considered primary properties affecting wear resistance. However, it has been recognized that energy dissipation when two bodies are in relative motion is of primary importance [250, 251]. This allows one to link the tribological properties with two important elasto-plastic characteristics: (i) the  $H/E$  ratio representing the elastic strain to failure, and (ii) the  $H^3/E^2$  ratio known as resistance to plastic deformation that is key for predicting the tribological behavior [252] as well as the toughness [251, 253].

Measurements of  $H$  and  $E$  are performed by depth-sensing indentation and analyzed using the Oliver and Pharr method [254] and allowing one to also determine the elastic rebound. The  $H$  values of the most frequently studied PECVD films are summarized in figure 20, where they are compared with those of the most often used substrates. Each of the characteristics exhibits a certain range of values, related to the fabrication conditions, and hence to the microstructure and composition. One can observe that the typical hardness of transition MeN and MeC is between 20 and 40 GPa, while ‘super-hardness’

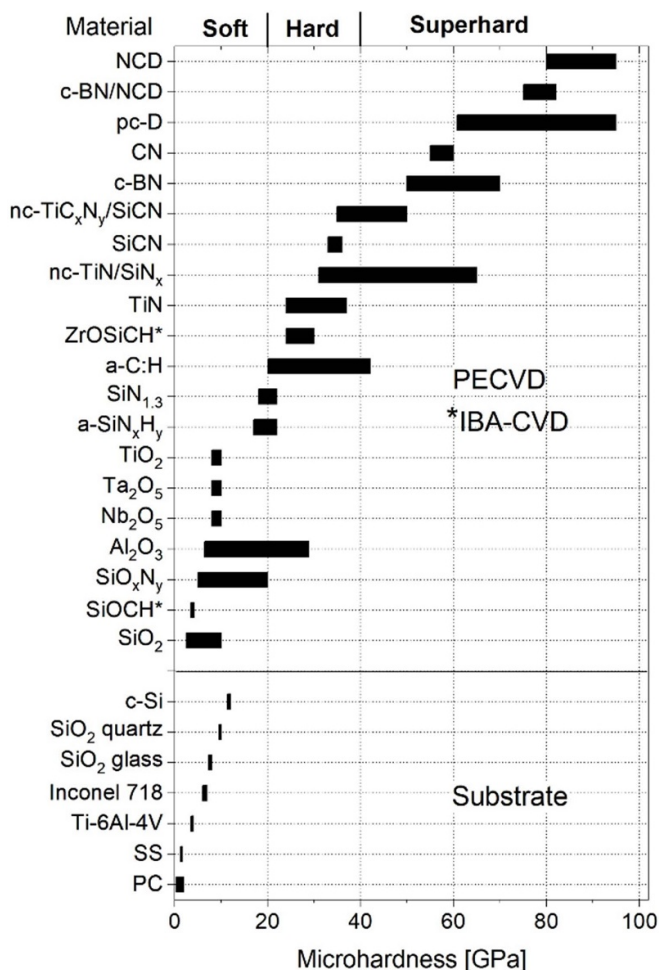


**Figure 20.** Typical microhardness values of PECVD films; often used substrates are shown for comparison. Reprinted from [46], Copyright (2010), with permission from Elsevier.

of  $H > 40$  GPa is generally reported for nanocomposite (nc) and covalently bonded coatings obtained at high temperatures above  $600^\circ\text{C}$  (the latter ones including pc-D and cubic BN).

MeN and MeC are obtained by PECVD when organometallic or chelate precursors are decomposed in mixtures containing  $\text{N}_2$  or  $\text{CH}_4$ , Ar, and  $\text{H}_2$ . The film microstructure can be selectively controlled by adjusting chemical reactions in the gas phase and at the growing surface, and by an appropriate choice of  $E_i$ ,  $\Gamma_i$ , and  $\Gamma_n$  values, which affect the development of crystals, their size, shape, and orientation [240, 245–247, 255–257]. One of the important difficulties is handling frequently hazardous and/or corrosive precursors including metal chlorides and others. Typical materials in this respect are TiN or TiC obtained from  $\text{TiCl}_4/\text{N}_2/\text{H}_2$  or  $\text{TiCl}_4/\text{CH}_4/\text{H}_2$  mixtures in an RF or pulsed DC discharges at temperatures between  $300^\circ\text{C}$  and  $500^\circ\text{C}$ , and a substrate bias voltage of 50–200 V [240, 257].

**Nanocomposite**, nc, and superhard coatings ( $H > 40$  GPa) formed by nanometer-size particles in an amorphous or crystalline matrix are of considerable interest. Formation of such nanostructure is based on the thermodynamically driven

segregation in binary, ternary, or quaternary systems, which leads to spontaneous self-organization of a stable nanoscale structure [245–247, 249, 258–260]. The properties are related to the difficulty of forming dislocations in the grains of about 10 nm in size and by the reduction of intergranular sliding due to the thinness of the grain boundary region. The most frequently investigated superhard nc PECVD coatings are the ones formed by TiN, TiC, or TiCN nanoparticles imbedded in a  $\text{SiN}_{1.3}$ , a-C, or SiCN matrix, while the boundary between grains is about one or two monolayers thick [245, 255, 256, 259, 261].

The need to assure high durability including good adhesion to numerous technological substrates has stimulated much research exploring different interface engineering approaches to further improve the tribological characteristics. This frequently involves so-called duplex or triplex treatments to stabilize the interface by affecting its composition, and frequently introducing property gradients such as hardness. The commonly used methods consist of two or three of the following independent steps: (i) surface treatment in an active (non-deposition) plasma containing nitrogen, carbon, boron, or other gases leading to surface nitriding, boriding, or carburizing generally giving rise to surface hardening; (ii) deposition of an intermediate layer, usually metal or metal compounds; and (iii) deposition of the final hard protective tribological coating.

Examples of the wear properties of TiN-based coatings deposited onto martensitic 410 stainless steel are shown in figure 21. To enhance adhesion, the hardness of the steel ( $H = 5.5$  GPa) has been gradually increased by nitriding to a depth of several  $\mu\text{m}$  ( $H = 12$  GPa), followed by the deposition of 1  $\mu\text{m}$  thick TiN ( $H = 25$  GPa), on which 4  $\mu\text{m}$  thick nc-TiN/SiN and nc-TiCN/SiCN coatings have been subsequently prepared ( $H = 35$ – $42$  GPa; triplex process) [262]. The nc-TiCN/SiCN system exhibits superior tribological performance compared to TiN and even nc-TiN/SiN, such as low friction ( $C_f = 0.17$ ) and low wear rate ( $K = 1.6 \times 10^{-7} \text{ mm}^3 \text{ Nm}^{-1}$ ), allowing one to reduce wear by a factor of  $\sim 600$  compared to bare SS410. One can conclude that this performance is due to higher hardness, higher elastic rebound, and low  $C_f$  due to the presence of carbon-containing, flexible, Si–C and C–N bonds in the tribo-layer [262]. In addition, the presence of carbon also leads to interesting color shifts complementary to nc-TiN/SiN and the traditional gold color of TiN [248].

A significant effect of applying nc coatings onto aerospace components has also been found by evaluating the solid particle erosion resistance, ER, following the ASTM G76 standard. As illustrated in figure 22, gradually applying a sequence of PECVD TiN, nc-TiN/SiN and nc-TiCN/SiCN coatings resulted in an increase of ER by a factor of about 50 compared to uncoated Ti-6Al-4V substrates. It is interesting to note that such substantial improvement of the film tribological behavior (erosion and wear resistance, for example) occurs for  $H^3/E^2 > 0.5$  GPa (or  $H/E > 0.15$ – $0.20$ ) [46] in agreement with finite element calculations using a model considering tensile and shear stress, and yielding criteria for failure upon particle impact [263].



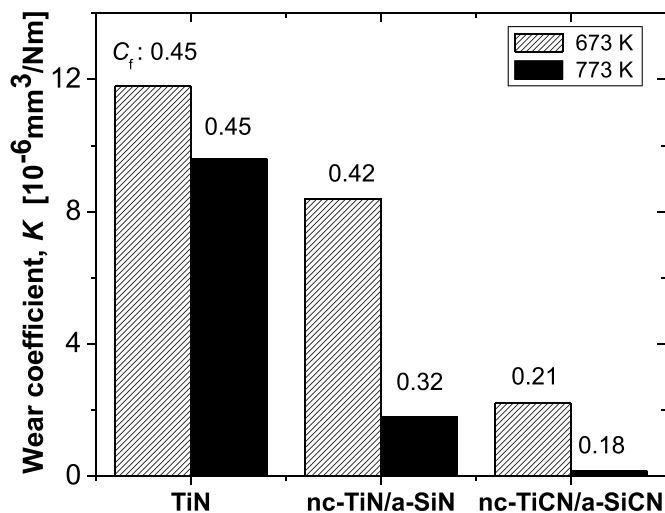


**Figure 21.** Wear coefficient,  $K$ , and the coefficient of friction,  $C_f$ , of TiN and nanocomposite ncTiN/SiN<sub>1.3</sub> and ncTiCN/SiCN films deposited at  $T_s$  of 673 K and 773 K. Reprinted from [262], Copyright (2009), with permission from Elsevier.

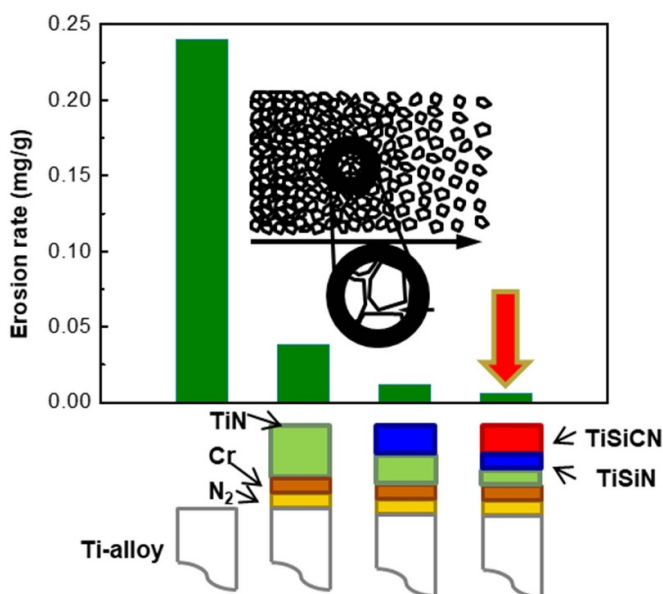


**Figure 22.** Solid particle erosion rate of TiN, nanocomposite ncTiN/SiN<sub>1.3</sub> and ncTiCN/SiCN films deposited on Ti-6Al-4 V substrates and eroded by Al<sub>2</sub>O<sub>3</sub> particles, 50  $\mu\text{m}$  in diameter, at a speed of 80  $\text{m s}^{-1}$ .

## 5. Perspectives and applications of PECVD

### 5.1. Complementary processes and new developments

Understanding of the physical and chemical reactions behind various processes involved in PECVD is now very well advanced. In the above sections, we have underlined the key factors affecting the control of the film compositional and microstructural evolutions, namely the choice of the precursor, and adjustment of the plasma density ( $n_e$ ) related to the EEDF, and plasma-surface interactions strongly affected by the ion energy and ion flux. With this knowledge, the final choice

of the appropriate process will be determined by the need to develop specific functional coating characteristics or by additional factors such as those related to different scale-up issues and economic aspects. In some cases, new and novel PECVD-based techniques benefit from a combination of different and complementary plasma-related effects and technologies as described by several representative examples below (see figure 23).

The **ion beam assisted chemical vapor deposition (IBA-CVD)** method has been proposed for the synthesis of hybrid (organic-inorganic) optical coatings that allow one to control and increase the hardness and the elasticity (high elastic rebound of 80% and more), while well controlling the refractive index [264, 265]. This technique is based on using an ion beam source in combination with an organic precursor injection (see figure 23(a)) that can be applied to retain the advantages of both the organic as well as inorganic characteristics, expressed by the ‘hybridicity parameter’ (the carbon-to-silicon ratio,  $C/Si$ ). The latter parameter allows one to obtain a high  $H/E$  ratio, and compatibility of the coatings with plastic substrates, while enhancing the limits of thermal excursion and environmental stability suitable for ophthalmic lenses, flexible electronics, and other applications. In addition, since this process runs at a much lower pressure ( $<0.13$  Pa) than conventional PECVD, it is fully compatible with existing industrial evaporation systems such as box coaters.

Analysis of the discharge characteristics pointed out that the initiation of radicals from the monomer molecules could be induced by ions and electrons, while the former species may play an important role due to much higher energy. This feature represents a peculiar difference between the IBA-CVD process in comparison with a ‘standard’ PECVD, where the electrons are considered the most critical species. In addition, detailed process diagnostics demonstrated that both gas phase and surface processes can be controlled by the  $W/F$  parameter, however, the  $W/F$  ratio is not a universal variable, but many other factors such as reactor geometry, type of the ion source, gas flow dynamic inside the chamber, IEDF, discharge geometry, and surface reactions play an important role in the process mechanism [266].

**Hollow cathode discharges** appear very suitable for the PECVD inside hollow objects such as tubes, making this **non-line-of-sight** approach suitable for providing protective coatings on surfaces that are difficult to reach. This method is based on the specific feature of the hollow cathode that is usually electrically powered, thus representing a cathode, in which the electrons follow a ‘pendulum’ movement giving rise to multiple inelastic collisions leading to a high plasma density [267] (see figure 23(b)). This technique has been initially applied for the growth of DLC films for protection against corrosion [268]. Recent work on **immersion hollow cathode PECVD** has shown that the fabrication of hard coatings such as TiN from halogenated precursors (e.g. TiCl<sub>4</sub>) requires appropriate plasma pulsing in terms of frequency (typically kHz range) and duty cycle. Specifically, high hardness (25 GPa) and good uniformity of thickness and microstructure inside narrow tubes ( $<10$  mm) have been demonstrated for TiN coatings, together with high solid particle ER (improvement factor of 15) [269].



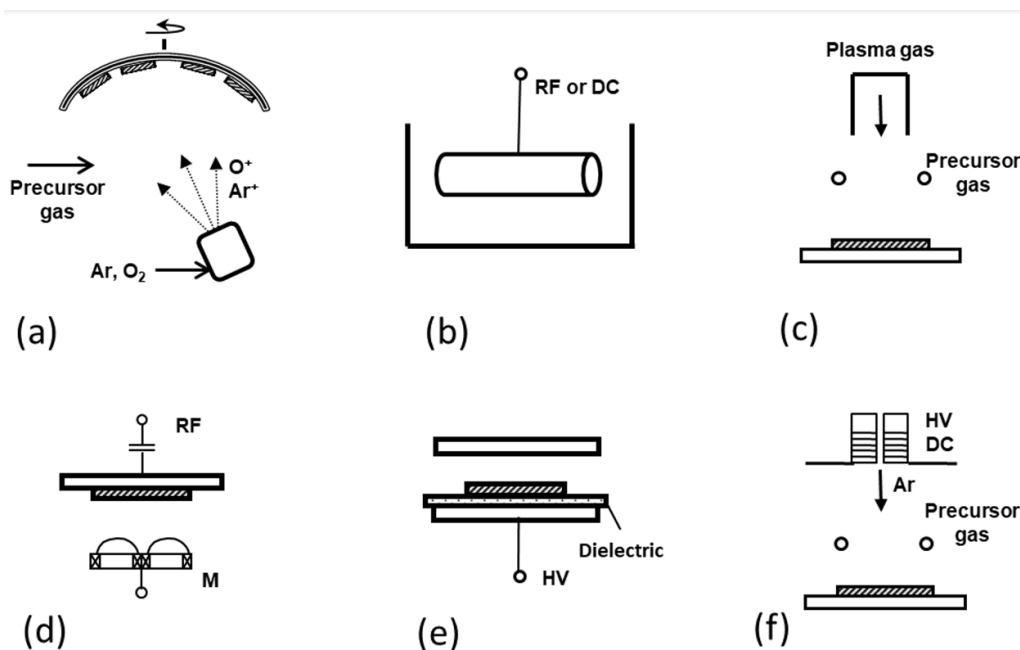


**Figure 23.** Schematic illustration of complementary PECVD-based reactors: (a) ion beam assisted chemical vapor deposition (IBA-CVD), (b) imbedded hollow cathode PECVD, (c) plasma assisted ALD, (d) simultaneous PECVD/PVD (co-sputtering), (e) atmospheric pressure AP PECVD in a dielectric barrier discharge (DBD), and (f) AP PECVD using a plasma jet.

This technique is well suited for the protection of aerospace, manufacturing, and other critical components with complex shapes of inner surfaces.

**ALD** has become increasingly important and well explored during the last two decades because of its ability to fabricate highly conformal surface layers due to a control of the sequential surface reactions. The use of plasma has been widely applied as a possibility to enable certain reactions and obtain some materials that cannot be easily prepared by simple thermal activation. In such a case, **plasma ALD** has been introduced to supply active species to facilitate and enhance surface reactions while most frequently using inductive plasma or, more recently, also hollow cathode plasma excitation (figure 23(c)). There presently exists a wide range of plasma ALD reactor designs, demonstrating many methods by which plasma species can be applied in ALD processes (for more detail, see comprehensive reviews—[270, 271]).

The work on **nanocomposite** materials, formed by nanometer size (typically about 1–50 nm, mostly metal) conductive particles embedded in dielectric matrices, has mainly been stimulated by the plasmonic effects leading to optical selectivity suitable for absorption filters, colored/decorative coatings, photothermal energy conversion, photon energy harvesting in solar cells, optical nonlinearity, and others [272]. Such structures can be effectively fabricated by a combination of **simultaneous PECVD and PVD** processes, the former one to form a dielectric matrix (plasma polymerized fluorocarbons (PPFC), plasma polymerized organosilicons (PPOS),  $\text{SiO}_2$ ,  $\text{Al}_2\text{O}_3$ ,  $\text{SiN}_{1.3}$ ), the latter one (sputtering or evaporation) to incorporate metallic or other conductive nanoparticles (Au, Ag, Cu, and others) [19, 272] (see figure 23(d)). Precipitation of plasmonic nanoparticles by PECVD directly from the gas phase (such as TiN) has also been demonstrated [273].

During the past one or two decades, we have witnessed an increasing interest in performing **PECVD at AP** [274, 275]. Principally motivated by the prospects of decreasing the complexity of the vacuum systems, the AP plasma reactors usually use the concept of a dielectric barrier discharge with parallel electrodes with the powered one covered by a dielectric (fused silica or other ceramic (figure 23(e))), or a tubular plasma jet, while the precursor is injected in the stream of the emanating plasma stream (figure 23(f)). Such concepts have most frequently explored the fabrication of functional coatings from organosilicon precursors aimed at films providing corrosion resistance, gas permeation barrier, hydro- or ice-phobicity, and other characteristics [275].

## 5.2. Application of PECVD technologies

Given the advantages of the PECVD methods compared to other deposition techniques, including PVD methods, such as a high deposition rate and the possibility to coat complex substrate geometry, this technology has been increasingly considered for industrial applications in numerous sectors for which advanced and high-performance materials are needed. As a consequence, nowadays, the application areas of the PECVD coatings encompass numerous industrial sectors ranging from the initial microelectronics to textile, food, optics, automotive, aircraft, biomaterial, and energy fields to name a few. Here are some examples of today's industrial applications of PECVD-deposited thin films.

The historical application field of PECVD coatings is the microelectronics/semiconductors industry in which PECVD coatings have been utilized for decades for the fabrication of integrated circuits [276], solar cells [277], transistors [278] etc.

For example, silicon-based PECVD coatings including hydrogenated amorphous silicon or silicon-based compound materials such as SiON or SiC are nowadays spread in this industrial sector. Some applications in this field include SiON and SiN as insulating layers for metal–insulator–metal capacitors [279] or the utilization of SiC coatings in MEMS devices [280]. These coatings are also commonly used as barrier coatings to encapsulate devices to protect them from outside contaminants and humidity.

Another important field of applications of the PECVD coatings is related to the tribo-mechanical properties that can be obtained. As a good example, DLC coatings are especially useful where a combination of wear and friction reduction as well as corrosion resistance are required [281]. This is why, today, they are implemented, at the industrial level, in automotive (piston rings and pins, rocker's arms), medical (surgical tools, prosthetic applications), or jewelry (wrist watch parts) applications. Another field of application benefiting from the excellent wear-resistance properties of coatings is the design of forming tools (aluminum die casting, plastic injection molding, or sheet metal forming), for which transition metal-nitride PECVD coatings, such as Ti(C,N), are typically used to strongly increase the life-time of the expensive components [282].

For more than two decades, both atmospheric and low-pressure PECVD technologies have also been considered an alternative to wet chemical processes for the surface modification of fabrics or fibers [283]. In this context, and depending on the applications (hydro-, ice- or oleo-phobicity, adhesion improvement, biocompatibility, etc), different families of PECVD coatings can be applied ranging from organic-like films, including PPF, to ceramic-type of coatings. Even if industrial-scale processes are already used for coating webs and fibers, the process rates still constitute a challenge to fully integrate this technology into existing conventional treatment lines. This seems to have recently been overcome particularly in other web-based production in which PECVD coatings are utilized, such as in food packaging [284]. Technically, low-pressure PECVD allows homogeneous deposition conditions over large areas and good process control by adjusting the supplied energy during film growth, e.g. converting hydrocarbon molecules into DLC coatings. AP PECVD, on the contrary, might be more limited regarding plasma-surface interaction, but is more flexible with respect to local deposition and use of a wider range of molecules, e.g. introduced as aerosol. Economically, low pressure enables resource-saving processes at low running costs, while AP PECVD requires high gas flow rates to limit temperature rise but avoids vacuum technology. The foundations given here might guide the selection of the best available technology regarding PECVD of functional coatings that depends on the particular requirements for a specific application.

Finally, by producing very dense, inert coatings with an extremely high degree of purity, PECVD also offers numerous biomedical applications. This is especially true for the PPF for which good control and tuning of the surface chemistry can nowadays be reached allowing for their utilization in applications such as antimicrobial/antifouling coatings

[285], tissue engineering [286], implants design [287], bio-electronics [288], and others.

Not surprisingly, the fields of application of the PECVD coatings are significantly increasing, especially due to technology transfer from the lab/pilot scale to large-scale industrial tools. As an example of recent developments, the novel large scale (3.2 m × 6 m) glass PECVD deposition system (PlasmaMAX™) has recently been commercialized by AGC/Interpane® which utilizes linear hollow cathode plasmas for various field of applications such as the display industry. Such a kind of tool will for sure allow for an even stronger spreading of the PECVD technologies in the industrial world.

### 5.3. Challenges

Even if the field has largely developed since decades, important challenges and key questions are still open and would justify the development of new research directions. As a good example, in the field of PP, a better understanding of the correlation between chemistry and the mechanical properties of the material is still necessary to fully access future applications of the coatings in the biomedical field [289]. From the fundamental point of view, the concept of glass transition of PPFs needs to be better understood to access the fabrication of mechanically responsive PPF, finding application in flexible electronics, stretchable solar cells, bio-inspired devices, and others [74, 103]. Furthermore, there is still an important quest for ways to minimize trapped radicals and defects during film growth to avoid or minimize aging effects and to enhance the quality of PPFs.

The PECVD technologies clearly require an appropriate choice of suitable precursors that would provide films and coatings with the desired functional and multifunctional properties. Indeed, these choices are made based on the precursor molecules composition, but one should carefully take into consideration other factors such as the precursor partial pressure (most of them are in a gaseous form, but some may be liquid or solid) and gas or vapor handling. Besides the frequently used benign precursors such as hydrocarbons or organosilicons, some may have different levels of hazards (toxicity, flammability, etc). In some cases, this may require specific hardware including anticorrosive protection of the vacuum equipment, heating of the gas distribution lines, scrubbers for scavenging any inappropriate products, or installation of suitable sensors. However, much experience has been accumulated over the past decades, especially in the microelectronics and other industries using CVD, and relevant information can easily be reached.

As mentioned throughout this article, PECVD of organic and inorganic coatings is relatively complex given the interplay between physical and chemical phenomena in the gas phase and at the exposed surfaces. To assure further progress it is very important to advance the modelling approaches both at the molecular scale of the gas phase reactions and film growth with respect to the chemical pathways and energetic interactions, as well as of the complete reactors in terms of the gas and power/energy distributions. Further development

of the diagnostic tools with appropriate species-, time- and space-resolved characteristics as well as machine learning approaches are expected to particularly benefit this fast advancing field.

## 6. Concluding remarks

The present paper summarizes our perception and understanding of the PECVD processes; it was motivated by our goal to help newcomers and/or experienced students, academics, or industrial researchers and engineers to appreciate the main principles defining this technology which encompasses numerous families of processes including reactions at low and APs leading to the deposition of inorganic or organic thin films. One of our aims was to convince the readers that different reaction pathways in the PECVD technology can exist or co-exist, but their prevalence is strongly dependent on the energy dissipated in the gas phase for the reaction initiation, but the final coating performance and characteristics would strongly depend on the energy dissipated during the film growth. Therefore, tailoring the film functional properties is achieved by appropriate control of the energy provided to the system per depositing material quantity. Good control of such a parameter can be obtained through a thorough plasma diagnostics of the system, namely the determination of the fluxes and energy distribution of the depositing species (neutrals, radicals, ions).

Although powerful, the PECVD approach is often rather technically complex, relatively expensive, and not readily adapted to different process geometries, especially in an industrial context (particularly outside of microelectronics). Therefore, a complementary macroscopic description of the PECVD processes has been implemented to overcome these limitations allowing one to access important features of the process, including basic parameters such as injected power, power density, monomer flow and partial pressure, and energy and flux of the bombarding ions. We have shown through a discussion of the major PECVD process families, namely PECVD for inorganic coatings and PP, that such knowledge allows one, depending on the situation, to tune the properties such as chemical composition and crosslinking of PPFs or crystalline structure of inorganic thin films.

This discussion and associated references illustrate our vision, and it is ultimately intended to help the reader to better tune their existing PECVD process or to guide them towards new ones. Finally, we discuss state-of-the-art and innovative concepts for PECVD technology and we illustrate the increasingly important integration of the PECVD processes in various industrial sectors such as microelectronics, textile, food, optics, automotive, aerospace, biomedical, and energy thanks to a generally intrinsically high deposition rate (in comparison to the PVD methods), a possibility to form new nanostructures, implement new functionalities, coat complex substrate geometries, and further develop and improve industrial-scale deposition systems. Further advances in PECVD as a clean, non-polluting technology, will also strongly contribute to sustainable development.

## Data availability statement

All data that support the findings of this study are included within the article (and any supplementary files).

## ORCID iDs

R Snyders  <https://orcid.org/0000-0001-8164-346X>

D Hegemann  <https://orcid.org/0000-0003-4226-9326>

O Zabeida  <https://orcid.org/0000-0001-8103-9852>

J Klemberg-Sapieha  <https://orcid.org/0000-0001-6051-1978>

L Martinu  <https://orcid.org/0000-0003-2630-4048>

## References

- [1] Martin P M (ed) 2010 *Handbook of deposition technologies for films and coatings : science, applications and technology* 3rd edn (Oxford: William Andrew Publishing)
- [2] Gudmundsson J T, Anders A and von Keudell A 2022 Foundations of physical vapor deposition with plasma assistance *Plasma Sources Sci. Technol.* **31** 083001
- [3] Booth J-P, Mozetič M, Nikiforov A and Oehr C 2022 Foundations of plasma surface functionalization of polymers for industrial and biological applications *Plasma Sources Sci. Technol.* **31** 103001
- [4] Sawyer W E and Man A 1880 *Carbon for electric lights* US Patent No. 229,335
- [5] Mond L Process of depositing nickel US Patent No. 455,230
- [6] von Bolton W 1911 Über die Ausscheidung von Kohlenstoff in Form von Diamant *Z. Elektrochem.* **17** 971
- [7] Ruff O 1917 Über die Bildung von Diamanten *Z. Anorg. Allg. Chem.* **99** 73–104
- [8] Tammann G 1921 Über Kohlenstoff, der bei der Einwirkung von Quecksilber auf CCl<sub>4</sub>, CBr<sub>4</sub> und CJ<sub>4</sub> entsteht *Z. Anorg. Allg. Chem.* **115** 145–58
- [9] Stewart R L 1934 Insulating films formed under electron and ion bombardment *Phys. Rev.* **45** 488
- [10] König H and Helwig G 1951 Über dünne aus Kohlenwasserstoffen durch Elektronen-oder Ionenbeschuß gebildete Schichten *Z. Phys.* **129** 491–503
- [11] Holland L and Ojha S M 1976 Deposition of hard and insulating carbonaceous films on an r.f. target in a butane plasma *Thin Solid Films* **38** L17–L19
- [12] Schmellenmeier H 1953 Die Beeinflussung von festen Oberflächen durch eine ionisierte Gasatmosphäre *Exp. Tech. Phys.* **1** 49–68
- [13] Spitsyn B, Bouilov L and Derjaguin B 1981 Vapor growth of diamond on diamond and other surfaces *J. Cryst. Growth* **52** 219–26
- [14] Verprek S and Heintze M 1990 The mechanism of plasma-induced deposition of amorphous silicon from silane *Plasma Chem. Plasma Process* **10** 3–26
- [15] Reinberg A R 1973 Radial flow reactor US Patent No. 3,757,733
- [16] Rosler R, Benzing W C and Baldo J 1976 A production reactor for low temperature plasma-enhanced silicon nitride deposition *Solid State Technol.* **19** 45
- [17] Reinberg A R 1979 Plasma deposition of inorganic thin films *Annu. Rev. Mater. Sci.* **9** 341–72
- [18] Rand M J 1979 Plasma-promoted deposition of thin inorganic films *J. Vac. Sci. Technol.* **16** 420–7
- [19] Martinu L and Poitras D 2000 Plasma deposition of optical films and coatings: a review *J. Vac. Sci. Technol. A* **18** 2619–45

- [20] Mattox D M 1967 Apparatus for coating a cathodically biased substrate from plasma of ionized coating material Patent No 3,329,601
- [21] Beer T A, Laimer J and Störi H 2000 Study of the ignition behavior of a pulsed dc discharge used for plasma-assisted chemical-vapor deposition *J. Vac. Sci. Technol. A* **18** 423–34
- [22] Bondt N, Deimann J R and Trostwijk A P V 1796 *J. Fourcroy Ann. Chem.* **21** 58
- [23] Goodman J 1960 The formation of thin polymer films in the gas discharge *J. Polym. Sci.* **44** 551–2
- [24] Barranco V, Carpentier J and Grundmeier G 2004 Correlation of morphology and barrier properties of thin microwave plasma polymer films on metal substrate *Electrochim. Acta* **49** 1999–2013
- [25] Grundmeier G, Thiemann P, Carpentier J and Barranco V 2003 Tailored thin plasma polymers for the corrosion protection of metals *Surf. Coat. Technol.* **174–175** 996–1001
- [26] Deilmann M, Theiß S and Awakowicz P 2008 Pulsed microwave plasma polymerization of silicon oxide films: application of efficient permeation barriers on polyethylene terephthalate *Surf. Coat. Technol.* **202** 1911–7
- [27] Schneider J, Kiesler D, Leins M, Schulz A, Walker M, Schumacher U and Stroth U 2007 Development of plasma polymerised SiO<sub>x</sub> barriers on polymer films for food packaging applications *Plasma Process. Polym.* **4** S155–9
- [28] Jin X, Bi W, Wang L and Qian H 2020 Root cause analysis of pinhole defects on painted galvanized steel panel *Eng. Fail. Anal.* **115** 104598
- [29] Liu S, Vareiro M M L M, Fraser S and Jenkins A T A 2005 Control of attachment of bovine serum albumin to pulse plasma-polymerized maleic anhydride by variation of pulse conditions *Langmuir* **21** 8572–5
- [30] Siow K S, Britcher L, Kumar S and Griesser H J 2006 Plasma methods for the generation of chemically reactive surfaces for biomolecule immobilization and cell colonization—a review *Plasma Process. Polym.* **3** 392–418
- [31] Macgregor-Ramiasa M N, Cavallaro A A and Vasilev K 2015 Properties and reactivity of polyoxazoline plasma polymer films *J. Mater. Chem. B* **3** 6327–37
- [32] Qi P, Yan W, Yang Y, Li Y, Fan Y, Chen J, Yang Z, Tu Q and Huang N 2015 Immobilization of DNA aptamers via plasma polymerized allylamine film to construct an endothelial progenitor cell-capture surface *Colloids Surf. B* **126** 70–79
- [33] Coad B R, Jasieniak M, Griesser S S and Griesser H J 2013 Controlled covalent surface immobilisation of proteins and peptides using plasma methods *Surf. Coat. Technol.* **233** 169–77
- [34] Manakhov A, Skládal P, Nečas D, Čechal J, Polčák J, Eliáš M and Zajíčková L 2014 Cyclopropylamine plasma polymers deposited onto quartz crystal microbalance for biosensing application *Phys. status solidi a* **211** 2801–8
- [35] Bazaka K, Jacob M, Chrzanowski W and Ostrikov K 2015 Anti-bacterial surfaces: natural agents, mechanisms of action, and plasma surface modification *RSC Adv.* **5** 48739–59
- [36] Thiry D, Pouyanne M, Cossement D, Hemberg A and Snyders R 2018 Surface engineering of bromine-based plasma polymer films: a step toward high thiol density-containing organic coatings *Langmuir* **34** 7655–62
- [37] Bhatt S, Pulpytel J and Arefi-Khonsari F 2015 Low and atmospheric plasma polymerisation of nanocoatings for bio-applications *Surf. Innov.* **3** 63–83
- [38] Qi P, Yang Y, Xiong K-Q, Tu Q, Yang Z, Wang J, Wang J, Chen J and Huang N 2015 Multifunctional plasma polymerized film: towards better anti-corrosion property, enhanced cellular growth ability, attenuated inflammatory and histological responses *ACS Biomater. Sci. Eng.* **1** 513–24
- [39] Haycock J W 2011 3D cell culture: a review of current approaches and techniques *3D Cell Culture: Methods and Protocols* ed J W Haycock (*Methods in Molecular Biology*) vol 695 (Totowa, NJ: Humana Press) pp 1–15
- [40] Vasilev K, Cook J and Griesser H J 2009 Antibacterial surfaces for biomedical devices *Expert Rev. Med. Devices* **6** 553–67
- [41] Taheri S, Cavallaro A, Christo S, Majewski P J, Barton M, Hayball J D and Vasilev K 2015 Antibacterial plasma polymer films conjugated with phospholipid encapsulated silver nanoparticles *ACS Biomater. Sci. Eng.* **1** 1278–86
- [42] Bhatt S, Pulpytel J, Mirshahi M and Arefi-Khonsari F 2013 Plasma co-polymerized nano coatings—as a biodegradable solid carrier for tunable drug delivery applications *Polymer* **54** 4820–9
- [43] Vasilev K, Poulter N, Martinek P and Griesser H J 2011 Controlled release of levofloxacin sandwiched between two plasma polymerized layers on a solid carrier *ACS Appl. Mater. Interfaces* **3** 4831–6
- [44] Vasilev K, Poh Z, Kant K, Chan J, Michelmor A and Losic D 2010 Tailoring the surface functionalities of titania nanotube arrays *Biomaterials* **31** 532–40
- [45] Simovic S, Losic D and Vasilev K 2010 Controlled drug release from porous materials by plasma polymer deposition *Chem. Commun.* **46** 1317–9
- [46] Martinu L, Zabeida O and Klemberg-Sapieha J 2010 Plasma-enhanced chemical vapor deposition of functional coatings *Handbook of Deposition Technologies for Films and Coatings* ed P M Martin (Amsterdam: Elsevier) pp 392–465
- [47] d'Agostino R, Flamm D L and Auciello O 2012 *Plasma Deposition, Treatment, and Etching of Polymers: The Treatment and Etching of Polymers* (San Diego: Elsevier Science)
- [48] Manos D M and Flamm D L 1989 *Plasma Etching: An Introduction* (San Diego, CA: Academic Press)
- [49] Wertheimer M R, Martinu L and Liston E M 1996 *Handbook of Thin Film Process Technology* ed D Glocker and I Shah (Bristol: IOP Publishing)
- [50] Liston E, Martinu L and Wertheimer M 1993 Plasma surface modification of polymers for improved adhesion: a critical review *J. Adhes. Sci. Technol.* **7** 1091–127
- [51] Mittal K L and Pizzi A 1999 *Adhesion Promotion Techniques: Technological Applications* (Boca Raton, FL: CRC Press) (<https://doi.org/10.1201/9781482289879>)
- [52] Roth J R 2001 *Industrial Plasma Engineering* (Bristol: IOP Publishing) p 530
- [53] Hegemann D, Bülbül E, Hanselmann B, Schütz U, Amberg M and Gaiser S 2021 Plasma polymerization of hexamethyldisiloxane: revisited *Plasma Process. Polym.* **18** 2000176
- [54] Thiry D, Konstantinidis S, Cornil J and Snyders R 2016 Plasma diagnostics for the low-pressure plasma polymerization process: a critical review *Thin Solid Films* **606** 19–44
- [55] Manenschijn A and Goedheer W 1991 Angular ion and neutral energy distribution in a collisional rf sheath *J. Appl. Phys.* **69** 2923–30
- [56] Peter S, Graupner K, Grambole D and Richter F 2007 Comparative experimental analysis of the a-C:H deposition processes using CH<sub>4</sub> and C<sub>2</sub>H<sub>2</sub> as precursors *J. Appl. Phys.* **102** 053304
- [57] Lieberman M A and Lichtenberg A J 2005 *Principles of Plasma Discharges and Materials Processing* 2nd edn (Hoboken, NJ: Wiley)



- [58] Hegemann D 2014 Plasma polymer deposition and coatings on polymers *Comprehensive Materials Processing* vol 4, 1st edn, ed D Cameron (Amsterdam, NL: Elsevier Ltd) pp 201–28
- [59] Hegemann D and Gaiser S 2022 Plasma surface engineering for manmade soft materials: a review *J. Phys. D: Appl. Phys.* **55** 173002
- [60] Petrov I, Adibi F, Greene J, Hultman L and Sundgren J E 1993 Average energy deposited per atom: a universal parameter for describing ion-assisted film growth? *Appl. Phys. Lett.* **63** 36–38
- [61] Deutsch H and Schmidt M 1981 On the quantitative treatment of the growth rate of thin polymer films produced in glow discharges *Beiträge aus der Plasmaphysik* **21** 279–92
- [62] Thiry D, Reniers F and Snyders R 2019 A joint mechanistic description of plasma polymers synthesized at low and atmospheric pressure *Surface Modification of Polymers: Methods and Applications* ed J Pinson and D Thiry (New York: Wiley) pp 67–106
- [63] Hegemann D, Körner E, Blanchard N, Drabik M and Guimond S 2012 Densification of functional plasma polymers by momentum transfer during film growth *Appl. Phys. Lett.* **101** 211603
- [64] Ligot S, Bousser E, Cossement D, Klemberg-Sapieha J, Viville P, Dubois P and Snyders R 2015 Correlation between mechanical properties and cross-linking degree of ethyl lactate plasma polymer films *Plasma Process. Polym.* **12** 508–18
- [65] Zakrzewski Z and Moisan M 1995 Plasma sources using long linear microwave field applicators: main features, classification and modelling *Plasma Sources Sci. Technol.* **4** 379
- [66] Martinu L, Klemberg-Sapieha J, Küttel O, Raveh A and Wertheimer M 1994 Critical ion energy and ion flux in the growth of films by plasma-enhanced chemical-vapor deposition *J. Vac. Sci. Technol. A* **12** 1360–4
- [67] Moisan M, Barbeau C, Claude R, Ferreira C, Margot J, Paraszcak J, Sá A B, Sauvé G and Wertheimer M R 1991 Radio frequency or microwave plasma reactors? Factors determining the optimum frequency of operation *J. Vac. Sci. Technol. B* **9** 8–25
- [68] Martinu L, Klemberg-Sapieha J and Wertheimer M 1989 Dual-mode microwave/radio frequency plasma deposition of dielectric thin films *Appl. Phys. Lett.* **54** 2645–7
- [69] Klemberg-Sapieha J, Küttel O, Martinu L and Wertheimer M 1990 Dual microwave-rf plasma deposition of functional coatings *Thin Solid Films* **193** 965–72
- [70] Pomot C and Pelletier J 1992 *Microwave Excited Plasmas* ed M Moisan and J Pelletier (Amsterdam: Elsevier)
- [71] Lieberman M A and Lichtenberg A J 2005 *Principle of Plasma Discharge and Materials Processing* (New York: Wiley)
- [72] Coburn J and Kay E 1972 Positive-ion bombardment of substrates in rf diode glow discharge sputtering *J. Appl. Phys.* **43** 4965–71
- [73] Guimond S, Schütz U, Hanselmann B, Körner E and Hegemann D 2011 Influence of gas phase and surface reactions on plasma polymerization *Surf. Coat. Technol.* **205** S447–50
- [74] Thiry D, Vinx N, Damman P, Aparicio F J, Tessier P Y, Moerman D, Leclère P, Godfroid T, Desprez S and Snyders R 2020 The wrinkling concept applied to plasma-deposited polymer-like thin films: a promising method for the fabrication of flexible electrodes *Plasma Process. Polym.* **17** 2000119
- [75] Thiry D, Vinx N, Aparicio F J, Moerman D, Lazzaroni R, Cossement D and Snyders R 2019 An innovative approach for micro/nano structuring plasma polymer films *Thin Solid Films* **672** 26–32
- [76] Michelmore A, Steele D A, Whittle J D, Bradley J W and Short R D 2013 Nanoscale deposition of chemically functionalised films via plasma polymerisation *RSC Adv.* **3** 13540–57
- [77] Yasuda H 2005 *Luminous Chemical Vapor Deposition and Interface Engineering* (New York: Marcel Dekker)
- [78] Yasuda H 1985 Modification of polymer surfaces by plasma treatment and plasma polymerization *Polymer Wear and Its Control* (ACS Symposium Series) vol 287 (Elsevier Science) pp 89–102
- [79] Thiry D, Britun N, Konstantinidis S, Dauchot J-P, Guillaume M, Cornil J and Snyders R 2013 Experimental and theoretical study of the effect of the inductive-to-capacitive transition in propanethiol plasma polymer chemistry *J. Phys. Chem. C* **117** 9843–51
- [80] Friedrich J 2011 Mechanisms of plasma polymerization—reviewed from a chemical point of view *Plasma Process. Polym.* **8** 783–802
- [81] Hegemann D, Körner E, Albrecht K, Schütz U and Guimond S 2010 Growth mechanism of oxygen-containing functional plasma polymers *Plasma Process. Polym.* **7** 889–98
- [82] Merche D, Vandecasteele N and Reniers F 2012 Atmospheric plasmas for thin film deposition: a critical review *Thin Solid Films* **520** 4219–36
- [83] Choukurov A et al 2017 Advances and challenges in the field of plasma polymer nanoparticles *Beilstein J. Nanotechnol.* **8** 2002
- [84] Favia P 2004 Plasma deposition of fluoropolymer films in different glow discharges regimes *Plasma Polymer Films* ed H Bierderman (London: Imperial College Press) pp 46–47
- [85] Milella A, Palumbo F, Favia P, Cicala G and d'Agostino R 2004 Continuous and modulated deposition of fluorocarbon films from c-C4F8 plasmas *Plasma Process. Polym.* **1** 164–70
- [86] Ligot S, Thiry D, Cormier P A, Raynaud P, Dubois P and Snyders R 2015 *In situ* IR spectroscopy as a tool to better understand the growth mechanisms of plasma polymers thin films *Plasma Process. Polym.* **12** 1200–7
- [87] D'Agostino R, Cramarossa F, Fracassi F, Desimoni E, Sabbatini L, Zamboni P G and Caporiccio G 1986 Polymer film formation in C<sub>2</sub>F<sub>6</sub>-H<sub>2</sub> discharges *Thin Solid Films* **143** 163–75
- [88] Whittle J D, Steele D A and Short R D 2012 Reconciling the physical and chemical environments of plasma: a commentary on “mechanisms of plasma polymerisation—reviewed from a chemical point of view” *Plasma Process. Polym.* **9** 840–3
- [89] d'Agostino R and Palumbo F 2012 Comment on “Ion-assisted processes of polymerization in low-pressure plasmas” *Plasma Process. Polym.* **9** 844–9
- [90] Candan S, Beck A J, O'Toole L D, Short R, Goodyear A and Braithwaite S J N 1999 The role of ions in the continuous-wave plasma polymerisation of acrylic acid *Phys. Chem. Chem. Phys.* **1** 3117–21
- [91] Michelmore A, Bryant P M, Steele D A, Vasilev K, Bradley J W and Short R D 2011 Role of positive ions in determining the deposition rate and film chemistry of continuous wave hexamethyl disiloxane plasmas *Langmuir* **27** 11943–50
- [92] Michelmore A, Charles C, Boswell R W, Short R D and Whittle J D 2013 Defining plasma polymerization: new insight into what we should be measuring *ACS Appl. Mater. Interfaces* **5** 5387–91

- [93] Michelmore A, Gross-Kosche P, Al-Bataineh S A, Whittle J D and Short R D 2013 On the effect of monomer chemistry on growth mechanisms of nonfouling PEG-like plasma polymers *Langmuir* **29** 2595–601
- [94] Michelmore A, Steele D A, Robinson D E, Whittle J D and Short R D 2013 The link between mechanisms of deposition and the physico-chemical properties of plasma polymer films *Soft Matter* **9** 6167–75
- [95] Beck A J, Candan S, Short R D, Goodyear A and Braithwaite N S J 2001 The role of ions in the plasma polymerization of allylamine *J. Phys. Chem. B* **105** 5730–6
- [96] Michelmore A, Whittle J D, Bradley J W and Short R D 2016 Where physics meets chemistry: thin film deposition from reactive plasmas *Front. Chem. Sci. Eng.* **10** 441–58
- [97] Brookes P N, Fraser S, Short R D, Hanley L, Fuoco E, Roberts A and Hutton S 2001 The effect of ion energy on the chemistry of air-aged polymer films grown from the hyperthermal polyatomic ion  $\text{Si}_2\text{OMe}_5^+$  *J. Electron Spectrosc. Relat. Phenom.* **121** 281–97
- [98] Michelmore A, Whittle J D and Short R D 2015 The importance of ions in low pressure PECVD plasmas *Front. Phys.* **3** 3
- [99] d'Agostino R, Favia P, Förch R, Oehr C and Wertheimer M R 2010 *Views on Macroscopic Kinetics of Plasma Polymerisation* (Weinheim: Wiley)
- [100] Nisol B, Poleunis C, Bertrand P and Reniers F 2010 Poly (ethylene glycol) films deposited by atmospheric pressure plasma liquid deposition and atmospheric pressure plasma-enhanced chemical vapour deposition: process, chemical composition analysis and biocompatibility *Plasma Process. Polym.* **7** 715–25
- [101] Batan A, Nisol B, Kakaroglou A, De Graeve I, Van Assche G, Van Mele B, Terryn H and Reniers F 2013 The impact of double bonds in the APPECVD of acrylate-like precursors *Plasma Process. Polym.* **10** 857–63
- [102] Thiry D, Francq R, Cossement D, Guerin D, Vuillaume D and Snyders R 2013 Establishment of a derivatization method to quantify thiol function in sulfur-containing plasma polymer films *Langmuir* **29** 13183–9
- [103] Vinx N, Damman P, Leclère P, Bresson B, Fretigny C, Poleunis C, Delcorte A, Cossement D, Snyders R and Thiry D 2021 Investigating the relationship between the mechanical properties of plasma polymer-like thin films and their glass transition temperature *Soft Matter* **17** 10032–41
- [104] Haddow D B, France R M, Short R D, Bradley J W and Barton D 2000 A mass spectrometric and ion energy study of the continuous wave plasma polymerization of acrylic acid *Langmuir* **16** 5654–60
- [105] Voronin S, Alexander M and Bradley J 2006 Time-resolved mass and energy spectral investigation of a pulsed polymerising plasma struck in acrylic acid *Surf. Coat. Technol.* **201** 768–75
- [106] Denis L, Cossement D, Godfroid T, Renaux F, Bittencourt C, Snyders R and Hecq M 2009 Synthesis of allylamine plasma polymer films: correlation between plasma diagnostic and film characteristics *Plasma Process. Polym.* **6** 199–208
- [107] Denis L, Renaux F, Cossement D, Bittencourt C, Tuccitto N, Licciardello A, Hecq M and Snyders R 2011 Physico-chemical characterization of methyl isobutyrate-based plasma polymer films *Plasma Process. Polym.* **8** 127–37
- [108] Beck A J, Candan S, France R M, Jones F R and Short R D 1998 A mass spectral investigation of the RF plasmas of small organic compounds: an investigation of the plasma-phase reactions in the plasma deposition from allylamine *Plasma Polym.* **3** 97–114
- [109] Candan S 2002 Radio frequency-induced plasma polymerization of allyl alcohol and 1-propanol *Turk. J. Chem.* **26** 783–92
- [110] Fraser S, Short R D, Barton D and Bradley J W 2002 A multi-technique investigation of the pulsed plasma and plasma polymers of acrylic acid: millisecond pulse regime *J. Phys. Chem. B* **106** 5596–603
- [111] O'Toole L, Beck A J, Ameen A P, Jones F R and Short R D 1995 Radiofrequency-induced plasma polymerisation of propenoic acid and propanoic acid *J. Chem. Soc. Faraday Trans.* **91** 3907–12
- [112] Candan S, Beck A J, O'toole L and Short R D 1998 Effects of "processing parameters" in plasma deposition: acrylic acid revisited *J. Vac. Sci. Technol. A* **16** 1702–9
- [113] Ligot S, Guillaume M, Gerboux P, Thiry D, Renaux F, Cornil J, Dubois P and Snyders R 2014 Combining mass spectrometry diagnostic and density functional theory calculations for a better understanding of the plasma polymerization of ethyl lactate *J. Phys. Chem. B* **118** 4201–11
- [114] Denis L, Marsal P, Olivier Y, Godfroid T, Lazzaroni R, Hecq M, Cornil J and Snyders R 2010 Deposition of functional organic thin films by pulsed plasma polymerization: a joint theoretical and experimental study *Plasma Process. Polym.* **7** 172–81
- [115] Vandenebeele C, Buddhadasa M, Girard-Lauriault P-L and Snyders R 2016 Comparison between single monomer versus gas mixture for the deposition of primary amine-rich plasma polymers *Thin Solid Films* **630** 100–7
- [116] Thiry D, Francq R, Cossement D, Guillaume M, Cornil J and Snyders R 2014 A detailed description of the chemistry of thiol supporting plasma polymer films *Plasma Process. Polym.* **11** 606–15
- [117] Groenewoud L M H, Engbers G H M, Terlingen J G A, Wormeester H and Feijen J 2000 Pulsed plasma polymerization of thiophene *Langmuir* **16** 6278–86
- [118] Groenewoud L M H, Engbers G H M and Feijen J 2003 Plasma polymerization of thiophene derivatives *Langmuir* **19** 1368–74
- [119] Tsai C-H, Lee W-J, Chen C-Y, Tsai P-J, Fang G-C and Shih M 2003 Difference in conversions between dimethyl sulfide and methanethiol in a cold plasma environment *Plasma Chem. Plasma Process.* **23** 141–57
- [120] Kasperek E, Thiry D, Tavares J R, Wertheimer M R, Snyders R and Girard-Lauriault P-L 2018 Growth mechanisms of sulfur-rich plasma polymers: binary gas mixtures versus single precursor *Plasma Process. Polym.* **15** 1800036
- [121] Alexander M and Duc T 1998 The chemistry of deposits formed from acrylic acid plasmas *J. Mater. Chem.* **8** 937–43
- [122] Voronin S A, Zelzer M, Fotea C, Alexander M R and Bradley J W 2007 Pulsed and continuous wave acrylic acid radio frequency plasma deposits: plasma and surface chemistry *J. Phys. Chem. B* **111** 3419–29
- [123] Ligot S, Guillaume M, Raynaud P, Thiry D, Lemaur V, Silva T, Britun N, Cornil J, Dubois P and Snyders R 2015 Experimental and theoretical study of the plasma chemistry of ethyl lactate plasma polymerization discharges *Plasma Process. Polym.* **12** 405–15
- [124] Mathioudaki S, Vandenebeele C R, Tonneau R, Pflug A, Tennyson J and Lucas S 2020 Plasma polymerization of cyclopropylamine in a low-pressure cylindrical magnetron reactor: a PIC-MC study of the roles of ions and radicals *J. Vac. Sci. Technol. A* **38** 033003
- [125] Fauroux A, Pflug A and Lucas S 2021 Experimental and theoretical study of a magnetron DC-PECVD acetylene discharge: identification of the deposition precursors and

- film growth mechanisms *Surf. Coat. Technol.* **421** 127472
- [126] Brault P, Ji M, Sciacqua D, Poncin-Epaillard F, Berndt J and Kovacevic E 2022 Insight into acetylene plasma deposition using molecular dynamics simulations *Plasma Process. Polym.* **19** e2100103
- [127] Neyts E, Bogaerts A, Gijbels R, Benedikt J and Van De Sanden M 2004 Molecular dynamics simulations for the growth of diamond-like carbon films from low kinetic energy species *Diam. Relat. Mater.* **13** 1873–81
- [128] Neyts E, Bogaerts A and Van de Sanden M 2006 Effect of hydrogen on the growth of thin hydrogenated amorphous carbon films from thermal energy radicals *Appl. Phys. Lett.* **88** 141922
- [129] Neyts E, Bogaerts A and Van De Sanden M editors 2007 Reaction mechanisms and thin aC:H film growth from low energy hydrocarbon radicals *J. Phys.: Conf. Ser.* **80** 012034
- [130] Michlíček M, Hamaguchi S and Zajíčková L 2020 Molecular dynamics simulation of amine groups formation during plasma processing of polystyrene surfaces *Plasma Sources Sci. Technol.* **29** 105020
- [131] Barton D, Shard A G, Short R D and Bradley J W 2005 The effect of positive ion energy on plasma polymerization: a comparison between acrylic and propionic acids *J. Phys. Chem. B* **109** 3207–11
- [132] Alexander M R, Jones F R and Short R D 1997 Mass spectral investigation of the radio-frequency plasma deposition of hexamethyldisiloxane *J. Phys. Chem. B* **101** 3614–9
- [133] Alexander M, Jones F and Short R 1997 Radio-frequency hexamethyldisiloxane plasma deposition: a comparison of plasma- and deposit-chemistry *Plasma Polym.* **2** 277–300
- [134] O'Toole L, Short R D, Ameen A P and Jones F R 1995 Mass spectrometry of and deposition-rate measurements from radiofrequency-induced plasmas of methyl isobutyrate, methyl methacrylate and n-butyl methacrylate *J. Chem. Soc. Faraday Trans.* **91** 1363–70
- [135] Hazrati H D, Whittle J D and Vasilev K 2014 A mechanistic study of the plasma polymerization of ethanol *Plasma Process. Polym.* **11** 149–57
- [136] Saboohi S, Jasieniak M, Coad B R, Griesser H J, Short R D and Michelmore A 2015 Comparison of plasma polymerization under collisional and collision-less pressure regimes *J. Phys. Chem. B* **119** 15359–69
- [137] Ahmad J, Bazaka K, Whittle J D, Michelmore A and Jacob M V 2015 Structural characterization of  $\gamma$ -terpinene thin films using mass spectroscopy and x-ray photoelectron spectroscopy *Plasma Process. Polym.* **12** 1085–94
- [138] Mitu B, Satulu V and Dinescu G 2011 Mass spectrometry diagnostic during rf plasma polymerization of thiophene vapors *Rom. J. Phys.* **56** 120–5
- [139] Benedikt J 2010 Plasma-chemical reactions: low pressure acetylene plasmas *J. Phys. D: Appl. Phys.* **43** 043001
- [140] Moix F, McKay K, Walsh J L and Bradley J W 2015 Atmospheric-pressure plasma polymerization of acrylic acid: gas-phase ion chemistry *Plasma Process. Polym.* **12** 1400–9
- [141] Braithwaite N S J, Booth J and Cunge G 1996 A novel electrostatic probe method for ion flux measurements *Plasma Sources Sci. Technol.* **5** 677
- [142] Dhayal M and Bradley J W 2004 Using heated probes in plasma polymerising discharges *Surf. Coat. Technol.* **184** 116–22
- [143] Von Keudell A, Schwarz-Selinger T, Meier M and Jacob W 2000 Direct identification of the synergism between methyl radicals and atomic hydrogen during growth of amorphous hydrogenated carbon films *Appl. Phys. Lett.* **76** 676–8
- [144] Hopf C, Schwarz-Selinger T, Jacob W and von Keudell A 2000 Surface loss probabilities of hydrocarbon radicals on amorphous hydrogenated carbon film surfaces *J. Appl. Phys.* **87** 2719–25
- [145] Von Keudell A 2000 Surface processes during thin-film growth *Plasma Sources Sci. Technol.* **9** 455–67
- [146] Von Keudell A, Hopf C, Schwarz-Selinger T and Jacob W 1999 Surface loss probabilities of hydrocarbon radicals on amorphous hydrogenated carbon film surfaces: consequences for the formation of re-deposited layers in fusion experiments *Nucl. Fusion* **39** 1451
- [147] Von Keudell A, Meier M and Hopf C 2002 Growth mechanism of amorphous hydrogenated carbon *Diam. Relat. Mater.* **11** 969–75
- [148] Thiry D, De Vreese A, Renaux F, Colaux J L, Lucas S, Guinet Y, Paccou L, Bousser E and Snyders R 2016 Toward a better understanding of the influence of the hydrocarbon precursor on the mechanical properties of a-C:H coatings synthesized by a hybrid PECVD/PVD method *Plasma Process. Polym.* **13** 316–23
- [149] Robertson J 2002 Diamond-like amorphous carbon *Mater. Sci. Eng. R* **37** 129–281
- [150] Michlíček M, Blahová L, Dvořáková E, Nečas D and Zajíčková L 2021 Deposition penetration depth and sticking probability in plasma polymerization of cyclopropylamine *Appl. Surf. Sci.* **540** 147979
- [151] Asadian M, Onyshchenko I, Thiry D, Cools P, Declercq H, Snyders R, Morent R and De Geyter N 2019 Thiolation of polycaprolactone (PCL) nanofibers by inductively coupled plasma (ICP) polymerization: physical, chemical and biological properties *Appl. Surf. Sci.* **479** 942–52
- [152] Carette X *et al* 2021 Innovative one-shot paradigm to tune filler–polymer matrix interface properties by plasma polymer coating in osteosynthesis applications *ACS Appl. Bio Mater.* **4** 3067–78
- [153] Hegemann D, Lorusso E, Butron-Garcia M-I, Blanchard N, Rupper P, Favia P, Heuberger M and Vandenbossche M 2016 Suppression of hydrophobic recovery by plasma polymer films with vertical chemical gradients *Langmuir* **32** 651–4
- [154] Gengenbach T R and Griesser H J 1998 Deposition conditions influence the postdeposition oxidation of methyl methacrylate plasma polymer films *J. Polym. Sci. A* **36** 985–1000
- [155] Rupper P, Vandenbossche M, Bernard L, Hegemann D and Heuberger M 2017 Composition and stability of plasma polymer films exhibiting vertical chemical gradients *Langmuir* **33** 2340–52
- [156] Moisan M and Pelletier J 2012 *Physics of Collisional Plasmas* (Dordrecht, NL: Springer Science+Business Media)
- [157] Hegemann D 2023 Plasma activation mechanisms governed by the specific energy input: potential an perspectives *Plasma Process. Polym.* **20** e2300010
- [158] Hegemann D, Nisol B, Gaiser S, Watson S and Wertheimer M R 2019 Energy conversion efficiency in low- and atmospheric-pressure plasma polymerization processes with hydrocarbons *Phys. Chem. Chem. Phys.* **21** 8698–708
- [159] Pietanza L, Colonna G and Capitelli M 2020 Kinetics versus thermodynamics on CO<sub>2</sub> dissociation in high temperature microwave discharges *Plasma Sources Sci. Technol.* **29** 035022
- [160] van de Steeg A, Butterworth T, van den Bekerom D, Silva A, van de Sanden M and van Rooij G 2020 Plasma activation of N<sub>2</sub>, CH<sub>4</sub> and CO<sub>2</sub>: an assessment of the vibrational non-equilibrium time window *Plasma Sources Sci. Technol.* **29** 115001



- [161] Godyak V 2013 Electron energy distribution function control in gas discharge plasmas *Phys. Plasmas* **20** 101611
- [162] Bröcker L, Perlick G S and Klages C P 2020 Evidence of ionic film deposition from single-filament dielectric barrier discharges in Ar–HMDSO mixtures *Plasma Process. Polym.* **17** 2000129
- [163] Yasuda H and Hsu T 1977 Some aspects of plasma polymerization investigated by pulsed RF discharge *J. Polym. Sci. Polym. Chem. Ed.* **15** 81–97
- [164] Hegemann D, Brunner H and Oehr C 2001 Plasma treatment of polymers to generate stable, hydrophobic surfaces *Plasmas Polym.* **6** 221–35
- [165] Hegemann D, Hossain M M, Körner E and Balazs D J 2007 Macroscopic description of plasma polymerization *Plasma Process. Polym.* **4** 229–38
- [166] Creatore M, Barrell Y, Benedikt J and Van De Sanden M 2006 On the hexamethyldisiloxane dissociation paths in a remote Ar-fed expanding thermal plasma *Plasma Sources Sci. Technol.* **15** 421
- [167] Klages C P, Czerny A K, Philipp J, Becker M M and Loffhagen D 2017 DBD-based plasma polymerization from monomer-argon mixtures: analytical model of monomer reactions with excited argon species *Plasma Process. Polym.* **14** 1700081
- [168] Bülbül E, Hegemann D, Ataka K, Lehner S, Heberle J and Heuberger M 2021 Confined hydration in nanometer-graded plasma polymer films: insights from surface-enhanced infrared absorption spectroscopy *Surf. Interfaces* **23** 100922
- [169] Blanchard N E, Naik V V, Geue T, Kahle O, Hegemann D and Heuberger M 2015 Response of plasma-polymerized hexamethyldisiloxane films to aqueous environments *Langmuir* **31** 12944–53
- [170] Park S Y, Kim N, Kim U Y, Hong S I and Sasabe H 1990 Plasma polymerization of hexamethyldisilazane *Polym. J.* **22** 242–9
- [171] Rutscher A and Wagner H-E 1993 Chemical quasi-equilibria: a new concept in the description of reactive plasmas *Plasma Sources Sci. Technol.* **2** 279
- [172] Poll H-U and Schreiter S 1997 Problems of large scale deposition of thin plasma polymer films *Surf. Coat. Technol.* **93** 105–11
- [173] Truica-Marasescu F and Wertheimer M R 2008 Nitrogen-rich plasma-polymer films for biomedical applications *Plasma Process. Polym.* **5** 44–57
- [174] Veuillet M, Ploux L, Airoudj A, Gourbeyre Y, Gaudichet-Maurin E and Roucoules V 2017 Macroscopic control of DMAHEMA and HEMA plasma polymerization to tune the surface mechanical properties of hydrogel-like coatings *Plasma Process. Polym.* **14** 1600215
- [175] Bally-Le Gall F et al 2019 Poly (allylamine) plasma polymer coatings for an efficient retention of Ni (II) ions by ultrafiltration membranes *Plasma Process. Polym.* **16** 1800134
- [176] Jebali S, Airoudj A, Ferreira I, Hegemann D, Roucoules V and Gall F B L 2021 Unique combination of spatial and temporal control of maleic anhydride plasma polymerization *Plasma Process. Polym.* **18** e2000244
- [177] Zabeida O and Martinu L 1999 Ion energy distributions in pulsed large area microwave plasma *J. Appl. Phys.* **85** 6366–72
- [178] Zeuner M, Neumann H and Meichsner J 1997 Ion energy distributions in oxygen and argon in a pulsed mode RF discharge *Vacuum* **48** 443–7
- [179] Zabeida O, Hallil A, Wertheimer M and Martinu L 2000 Time-resolved measurements of ion energy distributions in dual-mode pulsed-microwave/radio frequency plasma *J. Appl. Phys.* **88** 635–42
- [180] Rosnagel S M, Cuomo J J and Westwood W D 1990 *Handbook of Plasma Processing Technology: Fundamentals, Etching, Deposition, and Surface Interactions* (Saddle River, NJ: Noyes Publications)
- [181] Cuomo J J, Rosnagel S M and Kaufman H R 1989 *Handbook of Ion Beam Processing Technology: Principles, Deposition, Film Modification and Synthesis* (Saddle River, NJ: Noyes Publications)
- [182] Movchan B A and Demchishin A V 1969 Structure and properties of thick condensates of nickel, tungsten, aluminum oxides, and zirconium dioxide in vacuum *Fiz. Metal. Metalloved.* **28** 653–60
- [183] Thornton J A 1974 Influence of apparatus geometry and deposition conditions on the structure and topography of thick sputtered coatings *J. Vac. Sci. Technol. A* **11** 666–70
- [184] Messier R, Giri A and Roy R 1984 Revised structure zone model for thin film physical structure *J. Vac. Sci. Technol. A* **2** 500–3
- [185] Anders A 2010 A structure zone diagram including plasma-based deposition and ion etching *Thin Solid Films* **518** 4087–90
- [186] Musil J 1992 *Proc. 9th Int. Symp. on Elementary Processes and Chemical Reactions in Low Temperature Plasma (Casta, Slovakia)* p177
- [187] Auciello O and Kelly R 1984 *Ion Bombardment Modification of Surfaces: Fundamentals and Applications* (Amsterdam: Elsevier Science Publishers)
- [188] Flory F R 1995 *Thin Films for Optical Systems* (New York: Taylor & Francis)
- [189] Klemberg-Sapieha J E, Oberste-Berghaus J, Martinu L, Blacker R, Stevenson I, Sadkhin G, Morton D et al 2004 Mechanical characteristics of optical coatings prepared by various techniques: a comparative study *Appl. Opt.* **43** 2670–9
- [190] Wertheimer M, Fozza A and Holländer A 1999 Industrial processing of polymers by low-pressure plasmas: the role of VUV radiation *Nucl. Instrum. Methods Phys. Res. B* **151** 65–75
- [191] Mort J and Jansen F 1986 *Plasma Deposited Thin Films* (Boca Raton, FL: CRC Press)
- [192] Lucovsky G, Mantini M, Srivastava J and Irene E 1987 Low-temperature growth of silicon dioxide films: a study of chemical bonding by ellipsometry and infrared spectroscopy *J. Vac. Sci. Technol. B* **5** 530–7
- [193] Xu Y-N and Ching W 1991 Calculation of ground-state and optical properties of boron nitrides in the hexagonal, cubic, and wurtzite structures *Phys. Rev. B* **44** 7787
- [194] Devine R and Marchand M 1993 Evidence for structural similarities between chemical vapor deposited and neutron irradiated SiO<sub>2</sub> *Appl. Phys. Lett.* **63** 619–21
- [195] Martin P J, Netterfield R P and Sainty W G 1984 Modification of the optical and structural properties of dielectric ZrO<sub>2</sub> films by ion-assisted deposition *J. Appl. Phys.* **55** 235–41
- [196] Han S M and Aydil E S 1996 Study of surface reactions during plasma enhanced chemical vapor deposition of SiO<sub>2</sub> from SiH<sub>4</sub>, O<sub>2</sub>, and Ar plasma *J. Vac. Sci. Technol. A* **14** 2062–70
- [197] Bertrand N, Drevillon B and Bulkin P 1998 *In situ* infrared ellipsometry study of the growth of plasma deposited silica thin films *J. Vac. Sci. Technol. A* **16** 63–71
- [198] Watanabe Y W Y and Shiratani M S M 1993 Growth kinetics and behavior of dust particles in silane plasmas *Jpn. J. Appl. Phys.* **32** 3074
- [199] Shamiryan D, Abell T, Iacopi F and Maex K 2004 Low-k dielectric materials *Mater. Today* **7** 34–39
- [200] Vallee C, Gouillet A, Nicolazo F, Granier A and Turban G 1997 *In situ* ellipsometry and infrared analysis of PECVD



- SiO<sub>2</sub> films deposited in an O<sub>2</sub>/TEOS helicon reactor *J. Non-Cryst. Solids* **216** 48–54
- [201] Robertson J 1991 Electronic structure of silicon nitride *Phil. Mag. B* **63** 47–77
- [202] Sanchez O, Aguilar M, Falcony C, Martinez-Duart J and Albella J 1996 SiO<sub>x</sub> N<sub>y</sub> films deposited by remote plasma enhanced chemical vapor deposition using SiCl<sub>4</sub> *J. Vac. Sci. Technol. A* **14** 2088–93
- [203] Fracassi F, d'Agostino R and Bruno G 1996 Plasma deposition of silicon nitride-like thin films from organosilicon precursors *Plasmas Polym.* **1** 3–16
- [204] Kildemo M, Bulkin P, Drévilion B and Hunderi O 1997 Real-time control by multiwavelength ellipsometry of plasma-deposited multilayers on glass by use of an incoherent-reflection model *Appl. Opt.* **36** 6352–9
- [205] Poitras D, Leroux P, Klemberg-Sapieha J E, Gujrathi S C and Martinu L 1996 Characterization of homogeneous and inhomogeneous Si-based optical coatings deposited in dual-frequency plasma *Opt. Eng.* **35** 2693–9
- [206] Vernhes R, Zabeida O, Klemberg-Sapieha J E and Martinu L 2004 Single-material inhomogeneous optical filters based on microstructural gradients in plasma-deposited silicon nitride *Appl. Opt.* **43** 97–103
- [207] Callard S, Gagnaire A and Joseph J 1997 Fabrication and characterization of graded refractive index silicon oxynitride thin films *J. Vac. Sci. Technol. A* **15** 2088–94
- [208] Tompkins H G, Gregory R B, Deal P W and Smith S M 1999 Analysis of silicon oxynitrides with spectroscopic ellipsometry and Auger spectroscopy, compared to analyses by Rutherford backscattering spectrometry and Fourier transform infrared spectroscopy *J. Vac. Sci. Technol. A* **17** 391–7
- [209] Klemberg-Sapieha J, Martinu L, Wertheimer M, Günther P, Schellin R, Thielemann C and Sessler G M 1996 Plasma deposition of low-stress electret films for electroacoustic and solar cell applications *J. Vac. Sci. Technol. A* **14** 2775–9
- [210] Ohring M 2001 *Materials Science of Thin Films* (Cambridge, MA: Elsevier Science) (<https://doi.org/10.1016/B978-0-12-524975-1.X5000-9>)
- [211] Lee Y H, Chan K K and Brady M J 1995 Plasma enhanced chemical vapor deposition of TiO<sub>2</sub> in microwave-radio frequency hybrid plasma reactor *J. Vac. Sci. Technol. A* **13** 596–601
- [212] Lee Y H 1998 A role of energetic ions in RF-biased PECVD of TiO<sub>2</sub> *Vacuum* **51** 503–9
- [213] Szymanowski H, Zabeida O, Klemberg-Sapieha J and Martinu L 2005 Optical properties and microstructure of plasma deposited Ta<sub>2</sub>O<sub>5</sub> and Nb<sub>2</sub>O<sub>5</sub> films *J. Vac. Sci. Technol. A* **23** 241–7
- [214] Patscheider J and Vepřek S 1992 Plasma-induced deposition of thin films of aluminum oxide *Plasma Chem. Plasma Process.* **12** 129–45
- [215] Arefi-Khonsari F, Hellegouarc'h F and Amouroux J 1998 Role of the bias voltage during the deposition of thin tin oxide films by plasma assisted chemical vapor deposition *J. Vac. Sci. Technol. A* **16** 2240–4
- [216] Lee J H, Kim D S and Lee Y H 1996 Room temperature deposition of silicon dioxide films by ion-assisted plasma enhanced chemical vapor deposition *J. Electrochem. Soc.* **143** 1443
- [217] Henley W and Sacks G 1997 Deposition of electrochromic tungsten oxide thin films by plasma-enhanced chemical vapor deposition *J. Electrochem. Soc.* **144** 1045
- [218] Seman M and Wolden C A 2003 Investigation of the role of plasma conditions on the deposition rate and electrochromic performance of tungsten oxide thin films *J. Vac. Sci. Technol. A* **21** 1927–33
- [219] Granqvist C G 2000 Electrochromic tungsten oxide films: review of progress 1993–1998 *Sol. Energy Mater. Sol. Cells* **60** 201–62
- [220] Poitras D, Larouche S and Martinu L 2002 Design and plasma deposition of dispersion-corrected multiband rugate filters *Appl. Opt.* **41** 5249–55
- [221] Bohling D, Coda M, Blacker R, Burton C, Gove R and Murphy P 2000 Abrasion resistant and optical thin film coatings for ophthalmic lenses *Proc. 43rd Annual Technical Conf. Society of Vacuum Coaters (Denver, CO, 15–20 April)* pp 222–9
- [222] Vernhes R 2006 Fabrication et analyse de revêtements de nitrure de silicium déposés par plasma pour de nouvelles applications optiques *PhD Thesis Ecole Polytechnique de Montréal, Montréal, QC*
- [223] Vernhes R, Klemberg-Sapieha J and Martinu L 2013 Fabrication and testing of nanoporous Si<sub>3</sub>N<sub>4</sub> optical filters for gas sensing applications *Sens. Actuators B* **185** 504–11
- [224] Clausing R E, Horton L L, Angus J C and Koidl P 2012 *Diamond and Diamond-like Films and Coatings* 1st edn (NATO Science Series B: 266) (New York, NY: Springer) (<https://doi.org/10.1007/978-1-4684-5967-8>)
- [225] Pouch J J and Alterovitz S A 1991 *Properties and Characterization of Amorphous Carbon Films* (Baech, Switzerland: Trans Tech Publications Limited)
- [226] d'Agostino R, Favia P and Fracassi F 1997 *Plasma Processing of Polymers* (Netherlands: Springer)
- [227] Raveh A, Martinu L, Gujrathi S, Klemberg-Sapieha J and Wertheimer M 1992 Structure-property relationships in dual-frequency plasma deposited hard aC: H films *Surf. Coat. Technol.* **53** 275–82
- [228] Martinu L 1995 Advances in diamond, diamond-like carbon and related film materials *Jemna Mehanika a Optika* **40** 186–9
- [229] Davis R F 1993 *Diamond Films and Coatings: Development, Properties and Applications* (Netherlands: Elsevier Science)
- [230] Pan L S and Kania D R 2013 *Diamond: Electronic Properties and Applications* (Springer US)
- [231] Feldman A et al 1995 *Applications of Diamond Films and Related Materials: 3rd Int. Conf.* (Gaithersburg, USA) (National Institute of Standards & Technology)
- [232] Biederman H 2004 *Plasma Polymer Films* (London: Imperial College Press) (<https://doi.org/10.1142/p336>)
- [233] Butoi C I, Mackie N M, Barnd J L, Fisher E R, Gamble L J and Castner D G 1999 Control of surface film composition and orientation with downstream PECVD of hexafluoropropylene oxide *Chem. Mater.* **11** 862–4
- [234] Zhang D and Kushner M J 2001 Investigations of surface reactions during C<sub>2</sub>F<sub>6</sub> plasma etching of SiO<sub>2</sub> with equipment and feature scale models *J. Vac. Sci. Technol. A* **19** 524–38
- [235] Biederman H 2004 *Introduction Plasma Polymer Films* ed H Biederman (London: Imperial College Press) pp 13–24
- [236] Kay E, Coburn J and Dilks A 1980 Plasma chemistry of fluorocarbons as related to plasma etching and plasma. *Plasma Chemistry III* (Top. Curr. Chem.) S Vepřek and M Venugopalan vol 94 pp 1–42
- [237] Badzian A, Badzian T, Roy R and Drawl W 1999 Silicon carbonitride, a new hard material and its relation to the confusion about 'harder than diamond' C<sub>3</sub>N<sub>4</sub> *Thin Solid Films* **354** 148–53
- [238] He Z, Carter G and Colligon J S 1996 Ion-assisted deposition of C N and Si C N films *Thin Solid Films* **283** 90–96
- [239] Wrobel A, Walkiewicz-Pietrzykowska A, Klemberg-Sapieha J, Hatanaka Y, Aoki T and Nakanishi Y 2002 Remote hydrogen plasma chemical vapor deposition of silicon-carbon thin-film materials from a

- hexamethyldisilane source: characterization of the process and the deposits *J. Appl. Polym. Sci.* **86** 1445–58
- [240] Jedrzejowski P, Cizek J, Amassian A, Klemberg-Sapieha J, Vlcek J and Martinu L 2004 Mechanical and optical properties of hard SiCN coatings prepared by PECVD *Thin Solid Films* **447** 201–7
- [241] Wang J, Ren Z, Hou Y, Yan X, Liu P, Zhang H, Zhang H-X and Guo J-J 2020 *New Carbon Mater.* **35** 193–208
- [242] Yi K, Liu D, Chen X, Yang J, Wei D, Liu Y and Wei D 2021 Plasma-enhanced chemical vapor deposition of two-dimensional materials for applications *Acc. Chem. Res.* **54** 1011–22
- [243] Dato A 2019 Graphene synthesized in atmospheric plasmas—a review *J. Mater. Res.* **34** 214–30
- [244] Rybin M, Pereyaslavtsev A, Vasilieva T, Myasnikov V, Sokolov I, Pavlova A, Obratsova E, Khomich A, Ralchenko V and Obratsova E 2016 Efficient nitrogen doping of graphene by plasma treatment *Carbon* **96** 196–202
- [245] Vepřek S 1999 The search for novel, superhard materials *J. Vac. Sci. Technol. A* **17** 2401–20
- [246] Voevodin A, O'neill J and Zabinski J 1999 Nanocomposite tribological coatings for aerospace applications *Surf. Coat. Technol.* **116** 36–45
- [247] Musil J 2000 Hard and superhard nanocomposite coatings *Surf. Coat. Technol.* **125** 322–30
- [248] Jedrzejowski P, Baloukas B, Klemberg-Sapieha J and Martinu L 2004 Optical characteristics and color of TiN/SiN 1.3 nanocomposite coatings *J. Vac. Sci. Technol. A* **22** 725–33
- [249] Hollek H 1999 *Surface Engineering: Science and Technology I* (San Diego CA, 28 February–4 March) ed A Kumar, Y W Chung, J J Moore and J W Smugeresky vol 207 (Minerals, Metals & Materials Society)
- [250] Cheng Y-T and Cheng C-M 1998 Relationships between hardness, elastic modulus, and the work of indentation *Appl. Phys. Lett.* **73** 614–6
- [251] Leyland A and Matthews A 2000 On the significance of the H/E ratio in wear control: a nanocomposite coating approach to optimised tribological behaviour *Wear* **246** 1–11
- [252] Galvan D, Pei Y and De Hosson J T M 2006 Deformation and failure mechanism of nano-composite coatings under nano-indentation *Surf. Coat. Technol.* **200** 6718–26
- [253] Hassani S, Klemberg-Sapieha J E, Bielawski M, Beres W, Martinu L and Balazinski M 2008 Design of hard coating architecture for the optimization of erosion resistance *Wear* **265** 879–87
- [254] Oliver W C and Pharr G M 1992 An improved technique for determining hardness and elastic modulus using load and displacement sensing indentation experiments *J. Mater. Res.* **7** 1564–83
- [255] Vepřek S and Argon A S 2001 Mechanical properties of superhard nanocomposites *Surf. Coat. Technol.* **146** 175–82
- [256] Patscheider J, Zehnder T and Diserens M 2001 Structure–performance relations in nanocomposite coatings *Surf. Coat. Technol.* **146** 201–8
- [257] Jedrzejowski P, Klemberg-Sapieha J and Martinu L 2003 Relationship between the mechanical properties and the microstructure of nanocomposite TiN/SiN<sub>1.3</sub> coatings prepared by low temperature plasma enhanced chemical vapor deposition *Thin Solid Films* **426** 150–9
- [258] Jedrzejowski P, Klemberg-Sapieha J and Martinu L 2004 Quaternary hard nanocomposite TiC<sub>x</sub>Ny/SiCN coatings prepared by plasma enhanced chemical vapor deposition *Thin Solid Films* **466** 189–96
- [259] Hultman L, Bareño J, Flink A, Söderberg H, Larsson K, Petrova V, Odén M, Greene J E and Petrov I 2007 Interface structure in superhard TiN-SiN nanolaminates and nanocomposites: film growth experiments and *ab initio* calculations *Phys. Rev. B* **75** 155437
- [260] Nouvellon C, Belchi R, Libralesso L, Douhéret O, Lazzaroni R, Snyders R and Thiry D 2017 WC/C:H films synthesized by an hybrid reactive magnetron sputtering/plasma enhanced chemical vapor deposition process: an alternative to Cr (VI) based hard chromium plating *Thin Solid Films* **630** 79–85
- [261] Houska J, Klemberg-Sapieha J and Martinu L 2009 Atomistic simulations of the characteristics of TiSiN nanocomposites of various compositions *Surf. Coat. Technol.* **203** 3348–55
- [262] Guruvenket S, Li D, Klemberg-Sapieha J, Martinu L and Szpunar J 2009 Mechanical and tribological properties of duplex treated TiN, nc-TiN/a-SiN<sub>x</sub> and nc-TiCN/a-SiCN coatings deposited on 410 low alloy stainless steel *Surf. Coat. Technol.* **203** 2905–11
- [263] Hassani S, Bielawski M, Beres W, Martinu L, Balazinski M and Klemberg-Sapieha J 2008 Predictive tools for the design of erosion resistant coatings *Surf. Coat. Technol.* **203** 204–10
- [264] Zabeida O, Vernhes R, Poirié T, Chiarotto S, Scherer K, Schmitt T and Martinu L 2013 Hybrid organic-inorganic optical films deposited by ion beam assisted CVD *Optical Interference Coatings* (Washington, DC: Optica Publishing Group) p ThA.4
- [265] Caron M, Zabeida O, Klemberg-Sapieha J E and Martinu L 2017 Stability and performance of organic-inorganic thin films on polymer substrates *Surf. Coat. Technol.* **314** 131–8
- [266] Shelemin A, Zabeida O, Klemberg-Sapieha J-E and Martinu L 2021 Ion beam assisted chemical vapor deposition of hybrid coatings—process diagnostics and mechanisms *J. Vac. Sci. Technol. A* **39** 063003
- [267] Muhl S and Pérez A 2015 The use of hollow cathodes in deposition processes: a critical review *Thin Solid Films* **579** 174–98
- [268] Xu Y, Li L, Luo S, Lu Q, Gu J, Lei N and Huo C 2017 Self-enhanced plasma discharge effect in the deposition of diamond-like carbon films on the inner surface of slender tube *Appl. Surf. Sci.* **393** 467–73
- [269] Kilicaslan A, Zabeida O, Bousser E, Schmitt T, Klemberg-Sapieha J and Martinu L 2019 Hard titanium nitride coating deposition inside narrow tubes using pulsed DC PECVD processes *Surf. Coat. Technol.* **377** 124894
- [270] Profijt H, Potts S, Van de Sanden M and Kessels W 2011 Plasma-assisted atomic layer deposition: basics, opportunities, and challenges *J. Vac. Sci. Technol. A* **29** 050801
- [271] Knoops H C, Faraz T, Arts K and Kessels W M 2019 Status and prospects of plasma-assisted atomic layer deposition *J. Vac. Sci. Technol. A* **37** 030902
- [272] Lamarre J-M, Billard F, Kerboua C H, Lequime M, Roorda S and Martinu L 2008 Anisotropic nonlinear optical absorption of gold nanorods in a silica matrix *Opt. Commun.* **281** 331–40
- [273] Alvarez Barragan A, Ilawe N V, Zhong L, Wong B M and Mangolini L 2017 A non-thermal plasma route to plasmonic TiN nanoparticles *J. Phys. Chem. C* **121** 2316–22
- [274] Guruvenket S, Andrie S, Simon M, Johnson K W and Sailer R A 2012 Atmospheric-pressure plasma-enhanced chemical vapor deposition of a-SiCN: H films: role of precursors on the film growth and properties *ACS Appl. Mater. Interfaces* **4** 5293–9
- [275] Levasseur O, Stafford L, Gherardi N, Naudé N, Blanchard V, Blanchet P, Riedl B and Sarkissian A 2012 Deposition of hydrophobic functional groups on wood surfaces using

- atmospheric-pressure dielectric barrier discharge in helium-hexamethyldisiloxane gas mixtures *Plasma Process. Polym.* **9** 1168–75
- [276] Zhang X, Chen K-S and Spearing S M 2003 Thermo-mechanical behavior of thick PECVD oxide films for power MEMS applications *Sens. Actuators A* **103** 263–70
- [277] Perrin J, Schmitt J, Hollenstein C, Howling A and Sansonnens L 2000 The physics of plasma-enhanced chemical vapour deposition for large-area coating: industrial application to flat panel displays and solar cells *Plasma Phys. Control. Fusion* **42** B353
- [278] Late D J, Liu B, Matte H R, Dravid V P and Rao C 2012 Hysteresis in single-layer MoS<sub>2</sub> field effect transistors *ACS Nano* **6** 5635–41
- [279] Yeh C-T, Chu S-M, Louh T, Yang L-W, Yang T and Chen K-C 2015 Capacitance density and breakdown voltage improvement by optimizing the PECVD dielectric film characteristics in metal insulator metal capacitors *2015 Joint e-Manufacturing and Design Collaboration Symp. (Emdc) & 2015 Int. Symp. on Semiconductor Manufacturing (ISSM) (Taipei, Taiwan, 2–3 September 2015)* (IEEE) pp 1–4 (available at: <https://ieeexplore.ieee.org/document/7328900>)
- [280] Peri B, Borah B and Dash R K 2015 Effect of RF power and gas flow ratio on the growth and morphology of the PECVD SiC thin films for MEMS applications *Bull. Mater. Sci.* **38** 1105–12
- [281] Kolawole F O, Kolawole S K, Varela L B, Owa A F, Ramirez M A and Tschiptschin A P 2020 Diamond-like carbon (DLC) coatings for automobile applications *Engineering Applications of Diamond* ed A Mallik (London: IntechOpen) (<https://doi.org/10.5772/intechopen.95063>)
- [282] Mitterer C, Holler F, Reitberger D, Badisch E, Stoiber M, Lugmair C, Nöbauer R, Müller T and Kullmer R 2003 Industrial applications of PACVD hard coatings *Surf. Coat. Technol.* **163** 716–22
- [283] Hegemann D 2006 Plasma polymerization and its applications in textiles *Indian J. Fibre Text. Res.* **31** 99
- [284] Steele D and Short R D 2010 *Applications of Plasma Polymerization in Biomaterials* (Weinheim: Wiley)
- [285] Vasilev K, Griesser S S and Griesser H J 2011 Antibacterial surfaces and coatings produced by plasma techniques *Plasma Process. Polym.* **8** 1010–23
- [286] Aziz G, Ghobeira R, Morent R and De Geyter N 2018 Plasma polymerization for tissue engineering purposes *Recent Research in Polymerization* N Cankaya (London: IntechOpen) (<https://doi.org/10.5772/intechopen.72293>)
- [287] Chen Z, Bachhuka A, Wei F, Wang X, Liu G, Vasilev K and Xiao Y 2017 Nanotopography-based strategy for the precise manipulation of osteoimmunomodulation in bone regeneration *Nanoscale* **9** 18129–52
- [288] Hegemann D, Indutnyi I, Zajíčková L, Makhneva E, Farka Z, Ushenin Y and Vandenbossche M 2018 Stable, nanometer-thick oxygen-containing plasma polymer films suited for enhanced biosensing *Plasma Process. Polym.* **15** 1800090
- [289] de Oliveira J C, Airoudj A, Kunemann P, Bally-Le Gall F and Roucoules V 2021 Mechanical properties of plasma polymer films: a review *SN Appl. Sci.* **3** 656